ENERGY SYSTEM DESIGN AND OPERATION OF HYDROGEN FUELLED SHIPS

H_2

FOIVOS PANAGIOTIS MYLONOPOULOS

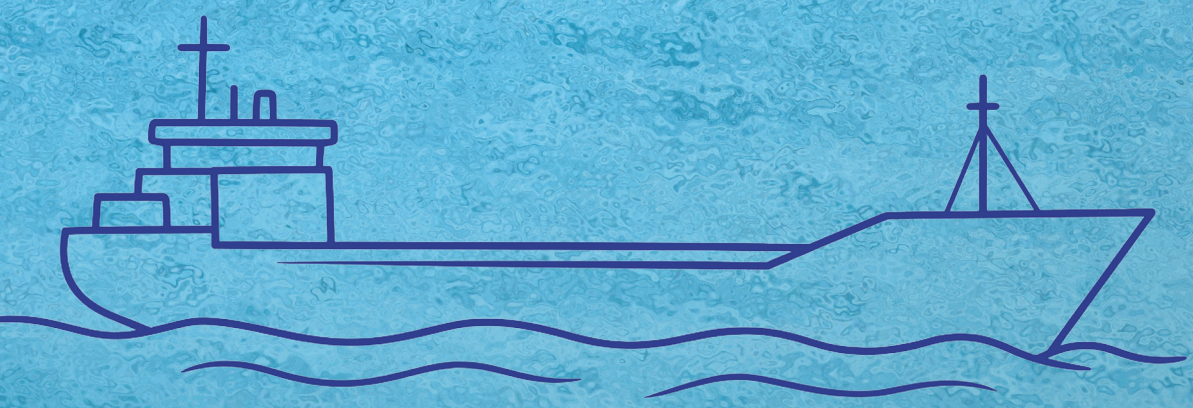

ENERGY SYSTEM DESIGN AND OPERATION OF HYDROGEN FUELLED SHIPS

FOIVOS PANAGIOTIS MYLONOPOULOS

ENERGY SYSTEM DESIGN AND OPERATION OF HYDROGEN FUELLED SHIPS

Dissertation

for the purpose of obtaining the degree of doctor
at Delft University of Technology
by the authority of the Rector Magnificus,
Prof.dr.ir. H. Bijl,
chair of the Board of Doctorates
to be defended publicly on
Monday, 1 June 2026, 17:30

BY

Foivos Panagiotis MYLONOPOULOS

This dissertation has been approved by the promotors.

Composition of the doctoral committee:

Rector Magnificus	chairperson
Dr.ing. A. Coraddu	Delft University of Technology, promotor
Dr.ir. H. Polinder	Delft University of Technology, promotor

Independent members:

Prof.dr.ir. W. de Jong	Delft University of Technology
Dr.ir. P. de Vos	Delft University of Technology
Prof.dr. A. Buonomano	University of Naples Federico II, Italy
Prof.dr.ir. T. Hofman	Eindhoven University of Technology
Dr.ir. U. Shipurkar	MARIN
Prof.dr.ir. B.J. Boersma	Delft University of Technology, *reserve member*

This research is part of the SH2IPDRIVE project (Sustainable Hydrogen Integrated Propulsion Drives). The project is funded by the Netherlands Enterprise Agency (RVO: Rijksdienst voor Ondernemend Nederland) under the grant number MOB21013 through the RDM regulation of the Ministry of Economic Affairs and Climate Policy.

SH2IPDRIVE partners: FutureProofShipping, ConcordiaDamen, Van Dam Shipping, Defense Materiel Organization, Cryovat, H2 Circular Fuel, H2 Fuel, H2 Storage, Van Halteren Technologies, Harborn, Holland Shipyards Group, Koedood, MARIN, Nedstack, Rivermaas B.V., Royal IHC, Royalroos, Shell, Mana Engineering, TNO, TU Eindhoven, Encontech B.V, University of Twente, University of Amsterdam, Voyex.

Printed by: Ridderprint
Typesetting: LaTeX

ISBN/EAN: 978-94-6518-314-5

An electronic version of this dissertation is available at: http://repository.tudelft.nl

ENERGY SYSTEM DESIGN AND OPERATION OF HYDROGEN FUELLED SHIPS

FOIVOS PANAGIOTIS
MYLONOPOULOS

SUMMARY

The maritime sector faces growing pressure to decarbonize, driven by increasingly stringent regulations and long-term climate targets. Among zero-emission propulsion options, hydrogen fuel cell–battery-electric systems have emerged as promising solutions, particularly for short-sea shipping. However, their large-scale adoption remains limited due to high fuel and investment costs, insufficient infrastructure, safety considerations, and significant uncertainty regarding lifetime economic performance.

A key challenge in hydrogen-fuelled ship design is the strong coupling between energy system sizing, operational strategies, and external influences such as weather and market conditions. In the literature, these aspects are often treated separately, focusing either on control of fixed designs or on system sizing under simplified operating assumptions, which can lead to economically suboptimal or operationally infeasible solutions. This thesis addresses this gap by developing a unified design-operation optimization framework that minimizes lifetime cost while accounting for technical, operational, and regulatory constraints under realistic operating conditions.

This thesis focuses on conceptually retrofitted cargo vessels, where conventional diesel propulsion is replaced by a fuel cell-battery electric configuration. Lifetime performance is evaluated using a techno-economic framework based on a Net Present Value (NPV)-based cost formulation, which captures capital expenses, operational costs, component degradation, and replacement over the remaining service life of the vessel. The framework is used to compare the diesel baseline and hydrogen retrofitted configurations in terms of system design and lifetime cost under consistent operational assumptions.

The proposed methodology combines physics-based component models with advanced optimization techniques. Fuel cells and batteries are modeled using realistic efficiency and degradation characteristics, while ship resistance, power demand, and operational constraints are derived from measured vessel data. A real-time, low-pass filter-based energy management strategy is first developed to distribute power between fuel cells and batteries for a fixed system design, enabling a realistic assessment of fuel consumption and degradation under varying operating conditions. Building on this, a simultaneous design-operation optimization framework is formulated, allowing component sizing, system topology, and power distribution to be optimized jointly within a single lifetime cost minimization problem.

A key methodological contribution is the development of a representative operating profile synthesis technique. Large-scale operational datasets, covering multiple routes and sailing conditions, are reduced to a single representative profile using a probability-based approach, preserving fuel consumption and component

degradation within acceptable thresholds. This enables accurate and computationally efficient lifetime cost optimization without relying on large datasets or overly simplified profiles and deterministic load assumptions.

The optimization framework incorporates ship stability and feasibility constraints, including component placement, tank arrangement, trim, and vertical center of gravity limits, ensuring that optimized solutions are technically feasible and compliant with naval architecture requirements. In addition, weather-driven operational variability and navigation safety constraints are considered by modifying ship speed and power demand under different metocean conditions, including safety-driven speed reductions required to mitigate navigation risks. This allows assessing how adverse weather, added resistance, and safety-related speed reductions influence required system capacities and lifetime cost.

The results demonstrate that lifetime fuel cost is the dominant contributor to the economic performance of hydrogen-fuelled ships, making fuel price assumptions a critical driver for retrofit feasibility. The lifetime cost comparison between the original and the retrofitted design shows that hydrogen retrofit may be more cost-effective than the diesel baseline under scenarios with significantly reduced hydrogen prices and increased carbon taxation. Fuel cells act as the primary energy source, while batteries are optimally sized for low-load support and peak shaving operations. Oversizing either component was shown to increase lifetime cost, since additional capital expenses outweigh efficiency gains. From a design perspective, the main engine room components of the diesel and hydrogen configurations were found to be comparable in terms of volume and weight, whereas hydrogen storage introduces challenges in terms of space, integration, and safety. The stability analysis, for the retrofitted design, highlights that hydrogen tank placement and ballast requirements have a dominant influence on vessel stability, while engine room components have a comparatively minor effect for the considered cargo vessel. Weather variability is shown to significantly affect power profiles and required system capacities, indicating that neglecting environmental effects can lead to non-robust design decisions and unreliable lifetime cost outcomes.

Overall, this thesis demonstrates that economically and technically viable hydrogen ship designs require a holistic approach that couples system design, operation, stability, and environmental uncertainty within a unified lifetime optimization framework. The developed framework provides a robust foundation for informed decision-making in the transition toward zero-emission shipping.

SAMENVATTING

De maritieme sector staat onder druk om te verduurzamen dankzij de steeds strengere regelgeving en ambitieuzere klimaatdoelstellingen. Systemen gebaseerd op een combinatie van waterstof brandstofcellen, batterijen en een elektrische aandrijving zijn een van de veelbelovende oplossingen "zero-emission" scheepvaart, zeker voor de kustvaart. Grootschalige toepassing van deze systemen blijft echter uit, mede dankzij hoge brandstof- en investeringskosten, gebrekkige infrastructuur, veiligheidsoverwegingen en onzekerheid over de economische prestaties en levensduur.

Een belangrijke uitdaging bij het ontwerpen van waterstof-aangedreven schepen, is de sterke relatie tussen de dimensionering van het energiesysteem, aansturingsstrategieën, degradatie en externe invloeden zoals weers- en marktomstandigheden. In de literatuur worden deze aspecten vaak los van elkaar benaderd, waarin men ofwel focust op het regelsysteem voor één ontwerp, ofwel op systeemdimensionering onder vereenvoudigde operationele aannames, wat kan leiden tot economisch suboptimale of operationeel onuitvoerbare oplossingen. Dit proefschrift richt zich op dit vraagstuk, door een geïntegreerd ontwerp-operatie-optimalisatiekader te ontwikkelen dat de levensduurkosten minimaliseert, terwijl technische, operationele en randvoorwaarden vanuit regelgeving worden meegenomen onder consistente en realistische operationele omstandigheden.

Dit proefschrift onderzoekt conceptueel omgebouwde vrachtschepen, waarbij conventionele dieselvoortstuwing wordt vervangen door een hybride brandstofcel-batterij-configuratie. De prestaties worden gedurende de levensduur geëvalueerd met behulp van een techno-economisch kader. Het kader is gebaseerd op de netto constante waarde ("Net Present Value"), waarin kapitaaluitgaven, operationele uitgaven, componentdegradatie en vervanging gedurende de resterende levensduur van het schip worden meegenomen. Het kader wordt gebruikt om het referentie scenario van een dieselconfiguratie te vergelijken met een omgebouwde waterstofconfiguraties. De vergelijking richt zich op het systeemontwerp en levensduurkosten bij gangbaar gebruik.

De voorgestelde methode combineert fysische componentmodellen met geavanceerde optimalisatietechnieken. Brandstofcellen en batterijen worden gemodelleerd met realistische efficiëntie- en degradatiekarakteristieken, terwijl scheepsweerstand, vermogensvraag en operationele randvoorwaarden worden afgeleid uit gemeten scheepsdata. Eerst wordt een real-time energiebeheerstrategie ontwikkeld op basis van een laagdoorlaatfilter, daarmee wordt het vermogen verdeeld tussen brandstofcellen en batterijen voor een vast systeemontwerp. Dit maakt een realistische beoordeling van brandstofverbruik en degradatie onder variërende operationele omstandigheden mogelijk. Gelijktijdig wordt een ontwerp-gebruik-optimalisatiekader

geformuleerd, waarin componentdimensionering, systeemtopologie en vermogensverdeling gezamenlijk worden geoptimaliseerd binnen één enkel levensduurkosten-minimalisatie-probleem.

Een belangrijke methodologische bijdrage is de ontwikkeling van een representatieve techniek voor het synthetiseren van operationele profielen. Grootschalige operationele datasets, die meerdere routes en vaaromstandigheden omvatten, worden met behulp van een op waarschijnlijkheid gebaseerde aanpak gereduceerd tot één representatief profiel, waarbij het brandstofverbruik en de componentdegradatie binnen acceptabele grenzen blijven. Dit maakt nauwkeurige en rekenkundig efficiënte optimalisatie van de levensduurkosten mogelijk zonder afhankelijk te zijn van grote datasets of te sterk vereenvoudigde profielen en deterministische aannames over de belasting.

Het optimalisatiekader omvat stabiliteits- en haalbaarheidsbeperkingen van het schip, waaronder componentplaatsing, tankconfiguratie, trim en grenzen voor het verticale zwaartepunt, zodat de geoptimaliseerde oplossingen technisch uitvoerbaar zijn en voldoen aan de eisen van de scheepsbouwkunde. Daarnaast worden weersafhankelijke variabiliteit en navigatieveiligheidsbeperkingen meegenomen door de scheepssnelheid en vermogensvraag aan te passen onder verschillende meteorologische en oceanografische (“metocean”) omstandigheden, inclusief veiligheid gerelateerde snelheidsvermindering die nodig is om navigatierisico’s te beperken. Dit maakt het mogelijk om te beoordelen hoe ongunstige weersomstandigheden, extra weerstand en veiligheid gerelateerde snelheidsreducties de vereiste systeemcapaciteiten en levensduurkosten beïnvloeden.

De resultaten tonen aan dat de levensduurkosten van brandstof de dominante bijdrage leveren aan de economische prestaties van waterstof-aangedreven schepen, waardoor aannames over de brandstofprijs een cruciale factor zijn voor de haalbaarheid van retrofit-oplossingen. De vergelijking van levensduurkosten tussen het oorspronkelijke diesel ontwerp en het omgebouwde waterstof ontwerp laat zien dat een waterstof retrofit kosteneffectiever kan zijn dan de dieselreferentie onder scenario’s met aanzienlijk verlaagde waterstofprijzen en verhoogde koolstofbelasting. Brandstofcellen fungeren als primaire energiebron, terwijl batterijen optimaal worden gedimensioneerd voor ondersteuning bij lage belasting en voor piekafvlakking. Aangetoond wordt dat overdimensionering van een van beide componenten leidt tot hogere levensduurkosten, aangezien extra kapitaalkosten zwaarder wegen dan efficiëntiewinsten. Vanuit ontwerpperspectief blijken de hoofdcomponenten in de machinekamer van de diesel- en waterstofconfiguraties vergelijkbaar te zijn wat betreft volume en gewicht, terwijl waterstofopslag uitdagingen met zich meebrengt op het gebied van ruimte, integratie en veiligheid. De stabiliteitsanalyse van het omgebouwde ontwerp laat zien dat de plaatsing van waterstoftanks en ballastvereisten een dominante invloed hebben op de scheepsstabiliteit, terwijl de machinekamercomponenten voor het hier bestudeerde vrachtschip een relatief geringe invloed hebben. Verder blijkt dat weersvariabiliteit een aanzienlijke invloed heeft op vermogensprofielen en vereiste systeemcapaciteiten, wat aangeeft dat het negeren van omgevingsinvloeden kan leiden tot niet-robuuste ontwerpbeslissingen en onbetrouwbare levensduurkosten- resultaten.

Alles overziend toont dit proefschrift aan dat economisch en technisch haalbare waterstofscheepsontwerpen een holistische benadering vereisen waarin systeemont-

werp, gebruik, stabiliteit en omgevingsonzekerheid worden gekoppeld binnen één uniform levensduuroptimalisatiekader. Het ontwikkelde kader biedt een robuuste basis voor weloverwogen besluitvorming in de transitie naar emissievrije scheepvaart.

CONTENTS

LIST OF FIGURES

LIST OF TABLES

SYMBOLS

Symbol	Description
Latin Symbols	
a	Coefficient for the quadratic term of fuel cell efficiency curve
A_{XV}	Transverse projected area of the vessel exposed to wind
b	Coefficient for the linear term of fuel cell efficiency curve
$b_{\text{batt,replace}}$	Binary variable for battery replacement
$b_{\text{FC,replace}}$	Binary variable for fuel cell replacement
b_{h2}	boil-off factor
B	Ship breadth
c	Coefficient for the constant term of fuel cell efficiency curve
C_{AA}	Wind resistance coefficient
$C_{\text{batt,replace}}$	Battery replacement cost
$C_{\text{FC,replace}}$	Fuel cell replacement cost
C_{h_2}	Green hydrogen price
C_{system}	System cost per unit
$C_{\text{system,maint}}$	System maintenance cost
C_{tank}	Tank cost per unit mass of stored hydrogen
C_{rate}	Battery C-rate
d	Fuel cell degradation factor
$D_{\text{LH}_2\text{,tank}}$	Diameter of the hydrogen tank
d_{r}	Ship's mean draft
dF	Annual increase in fuel consumption due to degradation
dV_{high}	Fuel cell voltage reduction due to operation at high power levels
dV_{low}	Fuel cell voltage reduction due to operation at low power levels
dV_{ramp}	Fuel cell voltage reduction due to load variations
dV_{start}	Fuel cell voltage reduction due to start/stop
dV_{total}	Total fuel cell voltage reduction until replacement
$E_{\text{batt,rated}}$	Rated energy capacity of the battery
F_{annual}	Annual fuel consumption
F_{FC}	Fuel consumption of a single fuel cell stack

Symbol	Description
F_{total}	Total fuel consumption of all fuel cells for a single voyage
$f_{\text{margin,tank}}$	LH_2 tank margin factor for sizing
FSM	Free surface moment
g	Gravitational acceleration
GG'	Virtual rise in vertical center of gravity
GM	Metacentric height
GZ	Righting lever
h_s	Significant wave height
I_{tank}	Transverse moment of inertia of a tank
$k_{e\text{-}m}$	Energy-to-mass conversion coefficient
KM	Keel-to-metacenter distance
L	Ship length
LCB	Longitudinal center of buoyancy
LCG	Longitudinal center of gravity
$L_{\text{LH}_2\text{,tank}}$	Length of the hydrogen tank
MCT	Moment to change trim
N_{batt}	Number of batteries
$N_{\text{batt,conv}}$	Number of battery converters
N_{FC}	Number of fuel cells
$N_{\text{FC,conv}}$	Number of fuel cell converters
$N_{\text{trips,annual}}$	Number of annual trips
$N_{\text{trips,refuel}}$	Number of trips before refuelling
P_{batt}	Battery power output
P_{demand}	Propulsive power demand
P_{diesel}	Original diesel engine power output
P_{FC}	Fuel cell power output
$P_{\text{system,rated}}$	Rated system power
r	Discount rate
R_{calm}	Calm water resistance
R_{wave}	Added wave resistance
R_{wind}	Added wind resistance
R_t	Total ship resistance
SoC_{batt}	State of charge of the battery
t	Time index
T	Remaining years of the vessel after retrofitting
T_E	Wave encounter period
T_w	Wave period

Symbol	Description
T_N	Natural roll period
V_{cell}	Actual cell operating voltage
$V_{\text{cell,nominal}}$	Nominal cell voltage
$V_{\text{reversible}}$	Theoretical reversible cell voltage under ideal conditions
VCG	Vertical center of gravity
$V_{\text{LH}_2\text{,tank}}$	Volume of the hydrogen tank
v_{spec}	Volumetric specification of the hydrogen tank
V_s	Ship speed in knots
$V_{s,\text{ms}}$	Ship speed in meters per second
V_{TW}	True wind speed
V_{WR}	Relative wind velocity
$W_{\text{LH}_2\text{,tank}}$	Weight of the hydrogen tank
w_{spec}	Gravimetric specification of the hydrogen tank
w	Weight of each system
x	Longitudinal position measured from the aft perpendicular
X_d	Maximum added wave resistance
y	Transverse position measured from the centerline
Y_{replace}	Number of years until fuel cell replacement
z	Vertical position measured from the keel

Greek Symbols

α	Relative wave direction
α_{high}	Fuel cell degradation coefficient at high-power operation
α_{low}	Fuel cell degradation coefficient at low-power operation
Δt	Time step
ΔV_{ramp}	Fuel cell degradation coefficient for load variations
ΔV_{start}	Fuel cell degradation coefficient for fuel cell start/stop
δ_{start}	Binary variable for fuel cell start/stop
η_{conv}	Efficiency of converter
η_{FC}	Fuel cell efficiency
η_{gb}	Gearbox efficiency
η_{inv}	Inverter efficiency
η_{m}	Propulsion motor efficiency
η_{t}	Total propulsive efficiency
ρ	Liquid density
ρ_A	Air density
φ	Heeling angle
ψ_{WR}	Relative wind direction

ACRONYMS

AC	Alternating Current
CAPEX	Capital Expenses
CII	Carbon Intensity Indicator
CO	Carbon Monoxide
CO_2	Carbon Dioxide
DC	Direct Current
DoD	Depth of Discharge
ECMS	Equivalent Consumption Minimization Strategy
EEXI	Energy Efficiency Existing Ship Index
EMS	Energy Management Strategy
ETS	Emissions Trading System
EU	European Union
GA	Genetic Algorithm
GOA	Grasshopper Optimization Algorithm
GWO	Grey Wolf Optimizer
GHG	Greenhouse Gas
IMO	International Maritime Organization
KPI	Key Performance Indicator
LFP	Lithium iron phosphate
LH_2	Liquefied Hydrogen
LNG	Liquefied Natural Gas
LPF	Low Pass Filter
MFO	Moth Flame Optimizer
MGO	Marine Gas Oil
MI(N)LP	Mixed Integer (Non)linear Programming
(MO)PSO	(Multi Objective) Particle Swarm Optimization
MPC	Model Predictive Control
NO_x	Nitrogen Oxides
NPV	Net Present Value
NSGA	Non-dominated Sorting Genetic Algorithm
OPEX	Operational Expenses

PEM	Proton Exchange Membrane
PI	Proportional Integral
PMS	Power Management Strategy
RDP	Ramer Douglas Peucker
RPM	Revolutions per minute
RQ	Research Question
SoC	State of Charge
SoH	State of Health
SQP	Sequential Quadratic Programming
SO_x	Sulphur Oxides

1

INTRODUCTION

This chapter introduces the technological and methodological background of the thesis and motivates integrated design and operation optimization of hydrogen-based ship energy systems within current maritime decarbonization efforts. The key contribution of this thesis is the development of a unified lifetime techno-economic framework that integrates system design and operation, power profile analysis and synthesis, component degradation, system topology and ship stability constraints, and weather-driven operational variability.

The chapter is organized as follows: Section 1.1 reviews emissions and regulations in the maritime industry, and examines the role of hydrogen in energy transition. Section 1.2 introduces the main objective of this thesis. Section 1.3 discusses the key challenges. Section 1.4 presents the problem statement and research questions. Section 1.5 briefly discusses the proposed approach to tackle the challenges and answer the research questions, and summarizes the main scientific contributions. Section 1.6 outlines the thesis structure.

1.1 MOTIVATION FOR ZERO-EMISSION SHIPPING

The shipping industry is facing increasing regulatory and societal pressure to decarbonize, driven by the climate risks associated with a continued reliance on fossil fuels. Approximately 90% of global trade volume is transported by ships [1], most of which are powered by diesel engines that emit harmful gases such as carbon dioxide (CO_2), carbon monoxide (CO), nitrogen oxides (NO_x), sulfur oxides (SO_x), and particulate matter (PM). The shipping sector is responsible for about 3% of global greenhouse gas (GHG) emissions. If no countermeasures are taken, this percentage may increase to 17% by 2050 [2]. Thus, the International Maritime Organization (IMO) targets at least a 20% reduction in total GHG emissions by 2030 and 70% by 2040, relative to 2008 levels, on a pathway to net-zero around 2050 [3].

To monitor near-term progress, the IMO has introduced two additional measures: the Energy Efficiency Existing Ship Index (EEXI), which is a technical standard requiring existing ships to meet a minimum energy efficiency level, and the Carbon

Intensity Indicator (CII), which is an operational metric aimed at reducing the annual carbon footprint of vessels [4]. In parallel, regional measures are tightening as the EU extends its Emissions Trading System (EU ETS) to shipping, assigning a carbon price to CO_2 emitted on voyages between EU ports.

The increasingly stringent regulatory targets necessitate the deployment of zero-emission propulsion technologies for both retrofit and newbuilt vessels. IMO envisages the uptake of zero-emission fuels and systems to reach up to 10% of the energy used in international shipping by 2030 [3]. Achieving the emissions targets requires accelerated investments in alternative fuels and power systems to deliver more energy-efficient and environmentally sustainable ships [3].

Hydrogen is among the most promising alternative fuel solutions. It is abundant in nature and, when used in fuel cells, can enable zero tank-to-wake CO_2 emissions, with lifecycle (well-to-wake) emissions depending on the production pathway. Its wider adoption depends mainly on fuel storage solutions, bunkering infrastructure, safety frameworks, and total lifetime cost. The applicability of hydrogen-based ship systems remains limited due to the low technical maturity, limited availability of low-cost green hydrogen, high investment costs, and insufficient infrastructure. Hybrid electric configurations with hydrogen fuel cells as the main power source, supported by batteries, are most applicable for short-range operations in proximity to recharging and refueling infrastructure. Compared to conventional diesel-mechanical propulsion systems, fuel cell–battery-electric configurations offer lower emissions, operational flexibility, and redundancy in case of component failures [5]. Despite these advantages, there remains limited understanding of how fuel cell–battery-electric systems should be optimally designed and operated over a vessel's lifetime when realistic operational profiles, component degradation, system placement and ship stability constraints, and economic uncertainties are jointly considered.

1.2 THESIS OBJECTIVE

The objective of this PhD thesis is to develop a unified techno-economic lifetime cost optimization framework for fuel cell–battery-electric ship energy systems. In this context, 'unified' refers to the simultaneous consideration of system design (component sizing and topology), operational strategies (power sharing and control) and lifetime economics within a single optimization framework. The focus is on system integration for conceptually retrofitted vessels, where conventional diesel propulsion is replaced by a fuel cell–battery-electric configuration. The main goal is to provide quantitative insight into the design and operation of hydrogen fuelled propulsion systems from a lifetime cost perspective, accounting for capital and operational expenses, degradation and replacement costs, and the volumetric and gravimetric implications of alternative designs. Lifetime cost is expressed using a Net Present Value (NPV)-based formulation, which discounts future operational and component replacement expenses to their present economic value, enabling realistic cost estimation.

A simultaneous system design and operation optimization framework is developed to determine the optimal component capacities and power distribution between the fuel cells and batteries. Such combined design-operation optimization is essential because sizing decisions and operational strategies are strongly coupled.

Treating them separately may lead to suboptimal or infeasible solutions [6]. The developed lifetime cost optimization framework integrates physics-based models, component degradation, system topology and ship stability constraints, representative operating profile synthesis methods considering different sailing routes, and weather-driven speed variability.

This PhD thesis is part of the SH2IPDRIVE (Sustainable Hydrogen Integrated Propulsion Drives) project which consists of universities, companies, and research institutes in the Netherlands, aiming to accelerate the transition to zero-emission shipping. The main goal of the project is to develop safe, scalable, and cost-effective solutions for hydrogen-fuelled vessels. The project's research covers five key areas: i) system integration (addressed in this thesis), ii) bunkering and hydrogen storage, iii) power density and lifetime of fuel cells, iv) hydrogen carriers and v) safety.

1.3 KEY CHALLENGES

While numerous studies address individual aspects of ship energy system design or operation, existing approaches typically treat these elements in isolation, limiting their applicability to complex, real-world hydrogen-based systems. System integration, ensuring efficient interaction among powertrain components, is vital for overall vessel performance.

The design space of the optimization problem is multi-dimensional with many feasible propulsion system configurations. Hence, classical design approaches are likely to fail, as design choices (sizing, topology, placement) interact with operation (control, power management) and lifetime economics. This makes it challenging to ensure optimality for the integrated powertrain.

Holistic design and lifetime operation frameworks for ship energy systems, developed in this thesis, are inherently complex, as they are influenced by many factors, including:

- **Operational variability, weather and navigation safety**:
  Power profiles vary across areas, routes and metocean conditions over time. Operating speed limits may need to be enforced to mitigate navigation risks such as surf-riding, resonance and successive high-wave attacks.

- **Economic uncertainty**:
  Long-term volatility in hydrogen prices, carbon pricing, and capital costs of emerging technologies introduces significant uncertainty into lifetime cost assessments.

- **Lifetime technical evolution**:
  System degradation and replacements, liquid hydrogen (LH_2) storage boil-off losses, and post-retrofit powertrain efficiency changes that affect the required power demand.

- **Feasibility constraints**:
  Ship stability (e.g., vertical center of gravity, trim), space/placement rules, and class/regulatory limits must hold to avoid infeasible design solutions.

- **Computational complexity**:
  Mixed-integer, nonlinear, nonconvex, and combinatorial problem structure.

In summary, the main challenge addressed in this thesis is the development of a coupled design–operation optimization that captures technical, operational, economic, and external influences within a single lifetime cost framework, while remaining computationally efficient and physically realistic.

1.4 PROBLEM STATEMENT AND RESEARCH QUESTIONS

This thesis answers the following problem statement:

How can the energy systems of hydrogen-fuelled ships be designed and operated from a lifetime cost perspective, under realistic operational and regulatory constraints?

This problem statement leads to the following Research Questions (RQs), each addressed in a specific thesis chapter. These RQs are formulated based on the knowledge gaps identified in Chapter 2, where a detailed literature review on optimization of ship energy systems is presented.

- **RQ1**: What methods, solvers, and objective functions are used for modeling and optimization of hydrogen-based and hybrid ship energy systems? (Chapter 2)

- **RQ2**: How can the design and lifetime cost implications of retrofitting a diesel fuelled ship to a hydrogen fuel cell-battery configuration be quantified under varying economic scenarios? (Chapter 3)

- **RQ3**: How can a single representative operating profile be synthesized from multiple routes and operating conditions, enabling accurate and computationally efficient lifetime cost optimization? (Chapter 4)

- **RQ4**: How can the energy system of a hydrogen fuelled vessel be optimally designed, from a system sizing and topology perspective, considering ship stability and safety constraints? (Chapter 4)

- **RQ5**: How can the impacts of weather variability and navigation risks on the ship power profiles, required system capacities, and lifetime cost be assessed? (Chapter 5)

1.5 PROPOSED APPROACH AND SCIENTIFIC CONTRIBUTIONS

A brief description of the methodology followed in this PhD thesis to answer the problem statement is presented in this section.

A diesel-based general cargo ship is conceptually retrofitted to a fuel cell–battery-electric version. The main energy systems (fuel cells, batteries) are modeled using physics-based equations with well-defined input-output relations [7]. Lifetime cost is calculated via NPV under varying operational expenses (OPEX) and capital expenses (CAPEX), including progressive degradation and replacements, and compared against the diesel baseline design in terms of system volume and weight. Power sharing between fuel cells and batteries is addressed first, for a fixed system design using a real-time Low-Pass Filter (LPF) Energy Management Strategy (EMS). Subsequently, a probability-based downsampling approach is employed to generate a single representative operating profile that preserves similar fuel consumption and fuel cell degradation to the annual operational data, enabling accurate and computationally-efficient lifetime cost optimization. This representative profile is used within a simultaneous system sizing and operation optimization framework, solved using a specialized Mixed-Integer Nonlinear Programming (MINLP) solver (SCIP), to manage computational complexity and ensure high-quality solutions. System placement and ship stability constraints (e.g., trim, vertical center of gravity) are incorporated into the optimization framework to ensure feasibility of the resulting energy system design. Weather variability and navigation safety constraints (surf-riding, resonance and successive high-wave attack impacts) are incorporated to assess how power profile variability affects required system capacities and total lifetime cost.

In summary, in this thesis, physics-based models, built on established engineering equations, are applied to represent the ship energy system performance. Realistic operational measurements (e.g., speed, power, heading, weather conditions) and design data (e.g., ship particulars and stability data, machinery specifications) are used as input to the model. Thus, the framework combines realistic data with a physics-based core, ensuring both interpretability and consistency with physical laws, while reflecting actual operating scenarios.

The main scientific contributions of this PhD thesis address RQ1-RQ5, and are summarized below:

- A systematic and structured review of optimization methods for hydrogen-based and hybrid ship energy systems, utilizing a novel classification that distinguishes between design, control and combined design-control approaches.
- A unified lifetime techno-economic framework for evaluating diesel-to-hydrogen ship retrofits, integrating component degradation, fuel price uncertainty, and volumetric and gravimetric implications.
- Development and implementation of a probability-based downsampling method to generate a representative power profile from annual measurements, enabling accurate and computationally-efficient lifetime cost optimization.
- Development of a holistic framework for combined system design and operation optimization of MINLP problems, including system topology and ship stability constraints.
- Assessment of the impact of weather variability and navigation safety constraints on speed and power profiles, energy system sizing and lifetime cost.

1.6 THESIS STRUCTURE

The remainder of the thesis is organized as follows: Chapter 2 reviews the state-of-the-art optimization approaches for ship energy systems to identify the literature gaps, which are addressed in the following chapters. Chapter 3 provides insight into the design and lifetime cost implications of retrofitting a diesel-fuelled cargo ship to a fuel cell–battery-electric version, using a LPF EMS. Chapter 4 presents a probability-based power profile synthesis method to derive a representative profile from multi-route operational data, and develops a holistic framework for the optimal sizing, topology, and operation of ship energy systems to minimize the total lifetime cost, while accounting for vessel stability regulations. Chapter 5 includes the effects of weather variability and navigation risks on power profiles, energy system sizing, and lifetime cost minimization. Chapter 6 summarizes the findings of the thesis, addressing each research question, and suggests directions for future research. Chapter 2 - Chapter 5 are published journal papers that can be reviewed as independent chapters, while collectively contributing to the overarching methodological framework and research questions of the thesis.

An overview of the thesis structure is illustrated in Fig. 1.1.

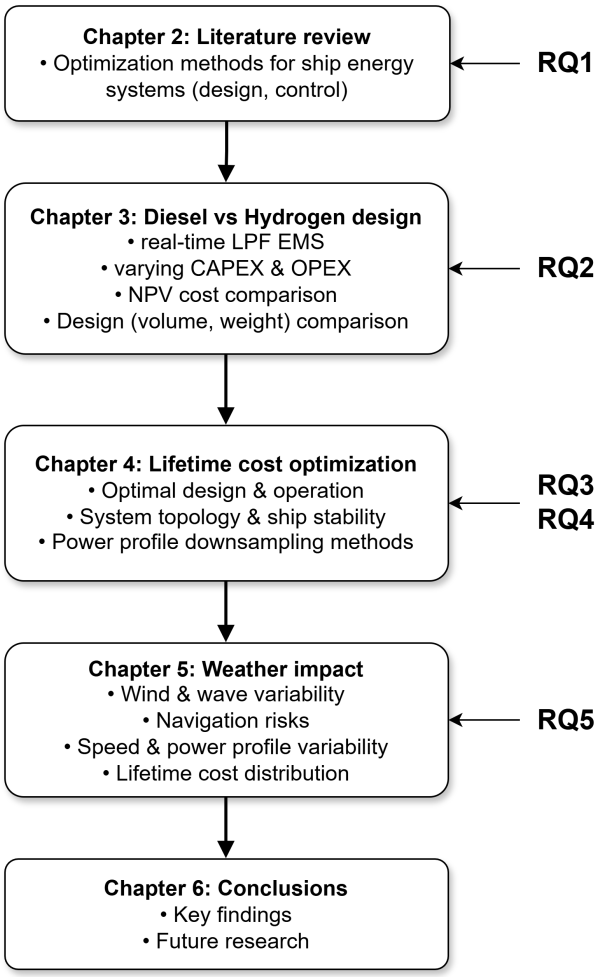

Figure 1.1: Thesis structure

2

LITERATURE REVIEW

This chapter is partly reproduced from Mylonopoulos et al. [8]

In this Chapter, the studies that are relevant to the optimization of ship energy systems will be discussed in terms of objective functions, methods/algorithms, and key results. There will be a division in a) optimal design (topology and sizing) in Section 2.1, b) optimal control in Section 2.2, and c) combined optimal design and control studies in Section 2.3. Concluding remarks, summarizing the literature review gaps are presented in Section 2.4.

2.1 OPTIMAL DESIGN STUDIES

In this section, the studies focus on optimizing the system capacities and powertrain configurations, without optimizing the power distribution or the system control parameters.

Wu and Bucknall [9] presented a multi-objective optimization for a hydrogen-hybrid ferry. Deterministic Dynamic Programming was used to select the component sizes and yield the optimal performance in terms of operational expenses and emissions, for an averaged operating profile (normalized from route data). With the proposed approach and propulsion system, a life-cycle emission reduction of at least 65% could be achieved, compared to the original diesel-based systems. Ganjian et al. [10] used a Genetic Algorithm (GA) to determine the optimal fuel cell and battery sizes for a fishing vessel, with system mass, volume, investment cost, and electrical safety, each optimized separately in independent runs. The Mayfly algorithm was also implemented to benchmark the GA results, showing comparable performance across the evaluated cases. The study focused on component sizing, without including fuel and degradation costs, and without optimizing the time-varying power distribution between fuel cells and batteries.

Vieira et al. [11] proposed a configuration optimization for a retrofitted hybrid platform supply vessel, to minimize carbon emissions and battery degradation. The HOMER software, that implements a proprietary derivative-free approach, was used to optimize the topology of the powertrain, considering uncertainties in power demand. Two scenarios were considered by scaling the baseline power profile by

±10% across all timesteps: one profile fixed at +10% and another fixed at -10%. These two variations of the power profile may not fully capture the operational and environmental uncertainties that occur under real sailing conditions. A 10% reduction of carbon dioxide emissions was obtained in the configuration with main and auxiliary generators, a 3 MW battery pack, and a 250 kW fuel cell system. Vasilikis et al. [12] proposed an optimization framework for sizing of hybrid ship energy systems, under operational and environmental uncertainty. Probability distributions of actual sailing profiles were used to represent realistic operating conditions. The energy management strategy was a controller consisting of two tasks: propulsion mode selection and generator load allocation, without co-optimizing the power distribution between diesel gensets and batteries. A multi-start scheme, combining GA and interior-point approach, was used to solve the multi-objective Mixed Integer Nonlinear Programming (MINLP) problem for an ocean patrol vessel. The optimization objectives included CAPEX, OPEX, carbon intensity and total system weight. Results showed that increasing electric motor sizes could reduce OPEX by 11%.

Zhu et al. [13] presented an optimal design study for a diesel-battery hybrid vessel to reduce fuel consumption, lifecycle costs and emissions. The Pareto solutions of the Non-dominated Sorting Genetic Algorithm-II (NSGA-II) and the Multi-Objective Particle Swarm Optimization (MOPSO) algorithm were compared in terms of space and quality criteria, and it was demonstrated that the NSGA-II provided more solutions which were less-distributed in space. The same authors in [14] presented a multi-objective design optimization, using the NSGA-II, for an anchor handling tug supply vessel, to minimize diesel consumption and emissions. Rule-based control strategies for power splitting, and hardware-in-the-loop tests for model validations were used in both studies [13], [14]. The experiments demonstrated that the multi-objective optimization results were closer to the ideal point compared to the single-objective optimizations with focus either on fuel consumption or emissions.

Lan et al. [15] combined the NSGA-II and the MOPSO algorithm to obtain the optimal sizes for solar panels, diesel generators, and batteries of a hybrid tanker, to minimize capital expenses, fuel costs and onboard emissions. Through a sensitivity analysis, it was demonstrated that the local time and the time zones had the largest effects on the efficiency of the photovoltaic panels. Wang et al. [16] used the NSGA-II to select the optimal component sizes of an unmanned patrol boat with sail-assisted systems, solar panels, and batteries, to reduce the total cost and emissions. The optimal design was compared to a configuration without photovoltaic arrays. Reduced emissions and lifecycle costs were obtained. Both studies [15], [16] illustrate the use of multi-objective evolutionary algorithms to size hybrid ship systems where photovoltaic panels and wind-assisted devices are auxiliary energy sources to reduce fuel consumption and emissions of conventional diesel generators.

Zhan et al. [17] used the NSGA-II to select the optimal component capacities for a retrofitted diesel electric trailing suction hopper dredger. The optimimization aimed to reduce fuel consumption and system weight, achieving up to 10% improvement compared to the original diesel mechanical configuration. The battery SoC was constrained between 40% and 90%, and the study focused on design-level trade-offs for the hybrid configuration, without including any cost-related considerations. Zhu

and Li [18] used the NSGA-II to determine the optimal component sizes for a hybrid electric catamaran, with scalable electrical systems, to reduce energy consumption and emissions. About 10% reductions in emissions and energy consumption were observed compared to the conventional diesel mechanical version of the vessel.

Wang et al. [19] proposed a multi-objective design optimization using NSGA-II for a battery hybrid polar cruise ship, to minimize diesel consumption, lifecycle costs, and maximize the battery usage onboard. Compared to the original diesel electric version, the retrofitted system presented a 38% increase of annual time in pure electric mode, with almost the same fuel consumption, but with 8% higher lifecycle costs. Nivolianiti et al. [20] presented a techno-economic analysis for diesel-battery-solar hybrid short-sea passenger ships. Different energy storage configurations and battery types were examined to minimize lifecycle costs and emissions. Load following and cycle charging were considered as predefined dispatch strategies for energy management. Different optimization algorithms were compared, including GA, Grasshopper Optimization Algorithm (GOA), Grey Wolf Optimizer (GWO) and Moth-flame Optimizer (MFO), highlighting the robust performance of GOA across all evaluated cases.

Valera-Garcia and Atutxa-Lekue [21] presented a design optimization study using the NSGA-II for a hybrid offshore support vessel, investigating both DC and AC configurations. The total costs including capital and operational expenses were reduced, and spinning reserve was imposed as a safety constraint to reduce blackout probability. The focus was on selecting the most economical power system architecture, without addressing long-term operational behavior and power profile variability.

Dolatabadi and Mohammadi-Ivatloo [22] presented an optimal sizing study for a hybrid solar-diesel-battery system of an oil tanker, using a MINLP algorithm for different operating modes and power requirements. The aim was to reduce fuel and maintenance costs. Uncertainty in solar radiation was modeled using Monte Carlo simulations, and risk metrics such as variance and expected shortfall were quantified using a conditional value-at-risk approach. The study focused on cost- and risk-oriented system sizing under renewable energy uncertainty, without addressing operational optimization strategies or system integration aspects.

Kistner et al. [23] optimized the design of a decentralized AC-based power system, consisting of Liquefied Natural Gas (LNG)-fueled solid oxide fuel cells and batteries, with the objectives of reducing capital and fuel costs, and waste power. A rule-based control strategy was implemented for power distribution, and an ant colony optimization algorithm was used to select the optimal onboard locations of the fuel cell units. This spatial distribution enhanced fault-tolerance and system reliability by ensuring continued power availability under potential component malfunctions. Cardenas et al. [24] used a parametric sweeping approach to investigate the trade-off between cost/fuel savings, and battery lifetime for a hybrid marine vessel. Different battery capacities and operating modes were evaluated, and it was demonstrated that 80% of the maximum cost savings could be achieved when the battery was used only in spinning reserve mode. The study focused on battery sizing using fixed operational strategies based on strategic loading and spinning reserve operation.

The optimization objectives and methods/algorithms used in the optimal design studies are summarized in Table 2.1.

Table 2.1: Optimal design studies.

Ref.	Optimization Objectives	Methods/Algorithms
[9]	Operational expenses, emissions.	Deterministic Dynamic Programming.
[10]	System mass, volume, capital cost, electrical safety.	GA, Mayfly algorithm .
[11]	Carbon emissions, battery degradations.	Derivative-free approach.
[12]	Capital and operational costs, system weight, carbon intensity.	GA-interior point multi-start method
[13], [14]	Diesel consumption, emissions.	NSGA-II.
[15]	Capital and fuel costs, onboard emissions.	NSGA-II and MOPSO.
[16]	Total cost, emissions.	NSGA-II.
[17]	System weight, fuel consumption.	NSGA-II.
[18]	Energy consumption, emissions.	NSGA-II.
[19]	Diesel consumption, lifecycle costs, battery usage.	NSGA-II.
[20]	Lifecycle costs, emissions.	GA, GWO, GOA, MFO
[21]	Capital and operational expenses.	NSGA-II.
[22]	Fuel and maintenance costs.	MINLP.
[23]	Capital and fuel costs, waste power.	Ant colony algorithm.
[24]	Cost savings, battery lifetime.	Brute-force method.

2.2 OPTIMAL CONTROL STUDIES

In this section, the studies focus on optimizing the system control and power distribution parameters, for fixed system topology and component capacities. The Energy Management Strategy (EMS) coordinates the operation of the hybrid power system by determining how the load is shared across the fuel cells, batteries, diesel generators and other onboard components. EMS can be categorized into rule-based or optimization-based methods. The studies below fall into one of these categories.

Sun et al. [25] formulated the energy management problem of a fuel cell-battery hybrid ship as a convex formulation, to be solved by the optimizers using the MOSEK with CVX package. The objective was to optimally split the power between the batteries and the fuel cells in order to reduce the fuel and the degradation costs of the fuel cells over the sailing profile. The simulation results demonstrated that incorporating aging cost into the EMS leads to improved long-term performance of

the fuel cell. Han et al. [26] developed a rule-based EMS for a fuel cell-battery hybrid boat, consisting of operating states defined by battery SoC and propulsion load. The EMS assigns fuel cell and battery power according to predefined rules and selects the operating state dynamically to maintain efficient operation. Simplified component models and ideal gas equations were used to reduce computational complexity. The performance of the power system was evaluated using real operating data from a small fuel cell-powered boat.

Mitropoulou et al. [27] developed an optimal EMS for a naval ship with hybrid power supply and hybrid propulsion, using the Nelder Mead direct search algorithm to balance fuel and maintenance costs, noise, and infrared signature. The control strategy can adapt to different mission profiles. Grid losses and battery degradation during charging were not considered. The proposed method provided improved solutions compared to the rule-based start point of the search, and it can be an effective method for multi-objective non convex problems. Xiang and Yang [28] presented a two-layer multi-objective optimization strategy for a diesel electric fishing boat, where the inner layer applies the Equivalent Consumption Minimization Strategy (ECMS) with mode switching to reduce energy consumption, while the outer layer uses an ant colony algorithm to tune the equivalent factor of the ECMS and maintain the battery SoC close to a target value. The proposed strategy was compared with traditional and rule based ECMS, and achieved fuel consumption reductions of up to 12%.

Dall'Armi et al. [29] formulated a degradation-aware operational optimization for a fuel cell-battery hybrid ship propulsion system using a MILP model solved with Gurobi. The optimization determined the optimal power split between fuel cells and batteries to minimize hydrogen consumption and components' degradation. The results showed that including progressive aging effects can increase the lifetime of the fuel cells and batteries up to 185% compared to an optimization that neglects degradation. Zhang et al. [30] proposed a real time EMS, which combined ECMS and a filter-based control strategy. The Sequential Quadratic Programming (SQP) algorithm was implemented to maximize efficiency and minimize the degradation of batteries and fuel cells. The proposed approach provided smoother responses for the batteries and fuel cells, and increased energy efficiency by 5-7% compared to the rule-based and wavelet-based control strategies. Bassam et al. [31] presented a multi-scheme EMS for a hydrogen fuel cell-battery passenger ship, in which several predefined control strategies were switched during operation based on propulsion load and battery SoC to minimize total energy consumption. The results demonstrated that energy savings of up to 8% could be achieved compared to applying each of the four strategies (ECMS, Charge-Depleting Charge-Sustaining, Classical Proportional Integral and state-based EMS) independently.

Hein et al. [32] proposed a joint voyage planning and EMS optimization framework for a fuel cell-battery hybrid system. The study aimed to reduce fuel consumption and battery degradation by optimizing the route and ship speed using dynamic programming, and allocating power through a multi-objective MILP dispatch solved with an augmented ε-constraint method and a reactive strategy to handle load uncertainty. The results demonstrate how sea-state-aware routing and the operating characteristics of the power supply systems affect propulsion demand, power distribution, and operational robustness. Shang et al. [33] proposed a multi-

objective framework for a diesel-battery hybrid ship that jointly optimizes cruising speed, generator scheduling and battery operation to minimize diesel consumption and emissions. The optimal control problem was solved using the NSGA-II. The results demonstrated that integrating voyage speed decisions and battery dispatch with generator scheduling improves fuel consumption and emission performance compared to fixed-voyage generation scheduling. Both studies [32],[33] considered fixed system sizes in their analyses.

In a few studies, data-driven machine learning methods have been used for the optimal control of ship energy systems. Wu et al. [34] developed a deep reinforcement learning-based EMS for a fuel cell-battery hybrid ferry, using a Double Deep Q-Network to determine optimal fuel cell power under uncertain load profiles. It was demonstrated that the proposed approach could mitigate the function overestimates in stochastic environments and provide lower cost results by 5.5% and in a shorter time by 93.8%, compared to the Double Q-learning agent in state space without function approximations presented in [35]. In [36], an optimal ECMS for a generator-battery hybrid ship system was used to generate rule-based training data for an artificial neural network to improve energy efficiency and reduce fuel consumption. A Bayesian regularization approach was applied during neural network training to minimize the error between the ECMS-derived outputs and network predictions.

Optimal Power Management Strategies (PMS) were presented in [37] and [38] using PSO algorithms to minimize operational expenses, while satisfying the emission constraints, for hybrid electric vessels. In [38], the fuzzy based PSO algorithm provided faster convergence and better performance than the traditional PSO and Dynamic Programming methods. Fuzzy logic EMS were also implemented in [39] and [40] for real-time control of fuel cell-battery hybrid systems, with [39] reporting energy consumption reductions of up to 14% compared to traditional rule-based EMS.

Kopka et al. [41] presented an offline optimal energy management framework for a fuel cell-battery hybrid ship using dynamic programming to minimize fuel consumption and fuel cell degradation for a given load profile. Both simultaneous on-off switching of all modules and selective switching strategies were investigated. The results demonstrated that optimizing the on-off switching of fuel cell stacks can significantly reduce degradation with only marginal effects on fuel consumption. The same authors in [42] developed a distributed Model Predictive Control (MPC) strategy to minimize hydrogen consumption and fuel cell degradation, using load forecasting. The results showed that the proposed distributed approach achieved similar cost performance to a centralized MPC (all modules optimized by a single controller), while being more scalable and better suited to modular energy system architectures. Furthermore, the study demonstrated that increasing the prediction horizon (e.g., beyond 15 minutes) leads to further reductions in operational cost, highlighting the importance of accurate load forecasting. Loffler et al. [43] presented a nonlinear MPC-based EMS with mixed integer decision variables for a dual fuel vessel, coordinating diesel generators, fuel cells and batteries to minimize operational fuel cost using predicted load profiles. When compared with rule-based and instantaneous optimization strategies [44], the proposed MPC achieved superior

fuel-cost performance and demonstrated additional savings by utilizing future demand information.

The optimization objectives and methods/algorithms used in the optimal control studies are summarized in Table 2.2.

Table 2.2: Optimal control studies.

Ref.	Optimization Objectives	Methods/Algorithms
[25]	Fuel and degradation costs of fuel cells.	Convex solvers, rule based EMS.
[26]	Efficiency of propulsion system.	Rule-based EMS.
[27]	Fuel and maintenance costs, noise.	Nelder–Mead algorithm.
[28]	Energy consumption, battery SoC deviation from target value.	ECMS—inner layer; ant colony algorithm—outer layer.
[29]	Fuel consumption, battery and fuel cell degradation.	MILP solved with Gurobi.
[30]	System efficiency, battery and fuel cell degradation.	ECMS and filter-based strategy; SQP algorithm.
[31]	Energy consumption.	Multi-scheme EMS—four schemes switched during operation.
[32]	Fuel consumption, battery degradation.	Dynamic Programming, augmented ε-constraint, reactive dispatch.
[33]	Fuel consumption, emissions.	NSGA-II.
[34], [35]	Operational cost.	Double Deep Q-Network, Double Q-learning.
[36]	Energy efficiency, diesel consumption.	ECMS, neural network with Bayesian regularization.
[37], [38]	Operational expenses.	PMS using PSO algorithms.
[39], [40]	Energy consumption.	Fuzzy-logic EMS.
[41]	Fuel consumption, fuel cell degradation.	Dynamic Programming.
[42]	Hydrogen cost, degradation cost.	MPC.
[43]	Fuel cost.	MPC.
[44]	Fuel cost and emissions.	ECMS.

2.3 COMBINED OPTIMAL DESIGN AND OPTIMAL CONTROL STUDIES

In this section, the studies that analyze combined optimal design and optimal control for ship energy systems are presented.

Wang et al. [45] developed a nested plant and control design architecture for a hydrogen-hybrid vessel. In the external optimization layer, NSGA-II was used to reduce capital expenses, operational costs, and emissions, by varying the sizes of the components. In the inner layer, a MILP algorithm was used to select the optimal control strategy. For an emission-free target, the fuel cells were sized based on load-leveling, the batteries covered the maximum demand and transient load fluctuations, and the diesel generators were used only for emergency purposes. Dall'Armi et al. [46] presented a coupled health-conscious optimization using a MILP algorithm and Monte Carlo analysis (Gurobi solver), to consider the long-time uncertainties related to fuel cell and battery capital expenses, and hydrogen fuel costs. A sensitivity analysis demonstrated that the hydrogen cost was the most influential parameter in the cost function. The optimal topologies and sizes of components were validated using the approach presented in [47].

Pivetta et al. [47] presented a multi-objective design and operation optimization strategy. The MILP algorithm was used to minimize fuel cell degradation, daily operational costs, and capital expenses. It was demonstrated that the strategy could be adapted to different hydrogen hybrid vessel sizes. In [48] a PSO algorithm was implemented for the component sizing, to reduce fuel consumption, and a fuzzy logic controller was utilized for optimally splitting the energy between the diesel generators and the batteries. The proposed fuzzy-PSO method reduced fuel consumption up to 40%, compared to the original conventional boat.

Wu and Bucknall [49] presented an optimal design and control study using a genetic algorithm in the external layer to minimize emissions and fuel costs, and Dynamic Programming in the inner layer for the optimal EMS. It was highlighted that even if hydrogen is produced by steam reforming of natural gas, the well-to-propeller emissions can be reduced by more than 25% for the considered case study. Zhu et al. [50] proposed a bi-level optimization using the MOPSO algorithm for component sizing in the upper layer, and a modified adaptive ECMS for control at the lower level. The aim was to find the best compromise between emissions, fuel consumption, and Net Present Cost including investment costs, operational expenses, and battery replacement costs. The results were validated experimentally with hardware-in-the-loop approaches, demonstrating that the bi-level optimization outperformed the two single-level (upper and lower) in terms of convergence to the optimal solutions. Emissions were reduced by 3-7% and the Net Present Cost by 11-14%, with the multi-objective bi-level approach.

Balsamo et al. [51] formulated an optimization problem for a battery-supercapacitor semi-active hybrid system, using the Ritz method. It was demonstrated that the peak current values could be reduced up to 40%. Letafat et al. [52] presented an optimal design and control study for a hydrogen hybrid ferry using the Improved Sine Cosine Algorithm with Harmony Search. The approach yielded a small cost reduction up to 2% compared to a rule-based EMS.

Chen et al. [53] introduced a modified equivalent circuit battery degradation and semi-empirical life prediction model for the optimal design (sizing) and optimal EMS

of a hybrid electric propulsion system. Experimental data were used for building the model. An error of 13% was observed in the validation stage. Hofman et al. [54] presented a system-level optimization study, using convex and Mixed Integer solvers, for the simultaneous sizing of the batteries and system control. The simplification of the problem, from non-linear to convex, led to a simulation convergence in around 8 minutes. Durgaprasad et al. [55] developed a scenario-based MILP framework, solved with Gurobi, to co-optimize battery sizing and powerplant scheduling for hybrid vessels, showing that optimal scheduling improves the economic use of battery throughput across fuel-price and operational scenarios. The same authors in another study [56], also solved with Gurobi, analyzed 24 battery-use strategies across seven vessel types and proposed a chemistry-selection decision tree, indicating that lithium titanate oxide and nickel manganese cobalt batteries are preferable for high-power applications whereas lithium iron phosphate batteries are advantageous for energy-dense operating profiles.

Chen et al. [57] presented a novel approach, based on Support Vector Machine and frequency control for the joint optimization of the sizing of the battery supercapacitor hybrid system and the EMS, using the Whale Algorithm. The proposed approach decreased the power fluctuations by 44% compared to the traditional fixed-filter rule-based EMS. Si et al. [58] proposed a configuration optimization combining fuzzy rules and a quantum artificial bee colony algorithm, to reduce the total cost, but also increase the reliability and components' lifetime. An optimal EMS was also developed using the Quantum PSO algorithm to maximize clear energy utilization.

The results from the combined optimal design and optimal control studies are summarized in Table 2.3.

Table 2.3: Combined optimal design and control studies.

Ref.	Optimization Objectives	Methods/Algorithms
[45]	Operational and capital costs, emissions.	NSGA-II in the external layer; MILP in the inner layer.
[46]	Costs and degradation of components.	MILP algorithm and Monte Carlo analysis (Gurobi).
[47]	Operational and capital costs, fuel cell degradation.	MILP solved with Gurobi.
[48]	Fuel consumption.	PSO algorithm and fuzzy-logic controller.
[49]	Fuel costs, emissions.	GA—outer layer; Dynamic Programming—inner layer.
[50]	Emissions, fuel consumption, net present cost.	MOPSO at upper level; modified adaptive ECMS at lower level.
[51]	Battery degradation.	Ritz Method.
[52]	Operating costs and capital expenses.	Improved Sine Cosine Algorithm with Harmony Search.
[53]	Lifecycle cost, battery degradation.	Battery degradation and semi-empirical life prediction model.
[54]	Capital and operating costs.	Convex and Mixed-Integer solvers/algorithms.
[55], [56]	Capital and operating costs.	MILP solved with Gurobi.
[57]	Battery degradation, energy efficiency.	Support Vector Machine; Whale algorithm.
[58]	Total cost, reliability, and lifetime of components.	Fuzzy rules and a quantum artificial bee colony algorithm; Quantum PSO algorithm.

2.4 LITERATURE REVIEW CONCLUSIONS

This chapter summarized the state-of-the-art approaches for optimization of ship energy systems in terms of design, control and combined design-control optimization. The main optimization objectives and the optimization methods, algorithms and EMS used in each study were reviewed.

Most studies used physics-based component models. The most frequently used optimization techniques were the NSGA-II, MOPSO and MILP formulations. The most frequent optimization objectives were fuel costs and emissions, especially for diesel-battery hybrid ships. For fuel cell-battery systems research focused primarily on optimizing EMS parameters rather than system design or topology.

The key gaps identified from the literature review are summarized below:

- **Lifetime techno-economic assessment is not systematically addressed.** Only a few studies jointly optimize CAPEX, OPEX, and lifetime replacement costs, and comprehensive analyses under varying economic scenarios and retrofit constraints remain limited.
- **Limited hydrogen retrofit investigation for cargo vessels.** Existing research rarely evaluates retrofitting cargo vessels with hybrid hydrogen–battery systems, accounting for multiple realistic power profiles, robust real-time EMS, and the influence of system sizing and operational constraints.
- **Integrated design–operation optimization for hydrogen-powered ship energy systems remains limited.** Most studies optimize EMS for a predetermined design, while only a few works address the co-optimization of energy-system topology, component sizing, and operation within a unified framework.
- **Stability, safety, and operational feasibility constraints are often neglected.** Ship energy systems are commonly optimized without considering navigation safety, vessel stability limits, or real-world feasibility constraints, which may lead to designs that are impractical or unsafe under realistic maritime missions.
- **Model simplifications may reduce solution quality.** To reduce computational complexity, optimization problems are frequently linearized or relaxed to MILP formulations. These simplifications may lead to suboptimal sizing or EMS outcomes.
- **Operating uncertainty is insufficiently captured.** Many studies evaluate designs or EMS strategies under a single simplified, averaged or insufficiently representative load profile, which may lead to under- or overestimation of economic outcomes when future speed, weather, power demand or mission conditions are uncertain.
- **Weather-driven speed and safety considerations are rarely addressed.** Holistic frameworks integrating weather-induced speed variability, safety-related speed adjustments, and lifetime cost optimization have not been fully developed.

Although many studies conduct multi-objective optimization and analyze trade-offs between emissions, degradation, and cost, shipowners and operators ultimately select a single design and EMS strategy, and the practical decision is based on the total lifetime cost subject to volume and weight constraints. There is a need for holistic, real-world frameworks that move beyond generic trade-off exploration and deliver one economical design-operation solution under realistic uncertainty.

Overall the literature indicates a clear need for combined, holistic optimization frameworks that jointly consider sizing, control, stability, safety, weather variability,

uncertainty, degradation, and lifetime cost, delivering feasible and economically optimal energy system designs for real maritime applications.

3

DESIGN AND COST IMPLICATIONS OF RETROFITTING: DIESEL TO HYDROGEN

This chapter is reproduced from Mylonopoulos et al. [59]

ABSTRACT

Fuel cell-battery electric drivetrains are attractive alternatives to reduce the shipping emissions. This research focuses on emission-free cargo vessels and provides insight on the design, lifetime operation and costs of hydrogen-hybrid systems, which require further research for increased utilization. A representative round trip is created by analysing one-year operational data, based on load ramps and power frequency. A low-pass filter controller is employed for power distribution. For the lifetime cost analysis, 14 scenarios with varying capital and operational expenses were considered. The Net Present Value of the retrofitted fuel cell-battery propulsion system can be up to $ 2.2 million lower or up to $ 18.8 million higher than the original diesel mechanical configuration, highly dependent on the costs of green hydrogen and carbon taxes. The main propulsion system weights and volumes of the two versions are comparable, but the hydrogen tank (68 tons, 193 m^3) poses significant design and safety challenges.

3.1 INTRODUCTION

Approximately 90% of the world's goods are transported by marine vessels, most of which are powered by diesel engines, which emit harmful exhaust gases such as carbon dioxide (CO_2) and monoxide [1]. The shipping industry is responsible for 3% of global emissions but this percentage may increase exponentially in the next few years without drastic changes in the utilized fuels and power systems of ships [2]. Cargo vessels including bulk carriers, containerships and oil tankers represent 85–90% of the world's merchant fleet according to [60]. General cargo vessels are a subcategory of merchant ships and they are usually short sea vessels operating between countries in proximity to urban areas. Hence, reducing the environmental footprint of such ships is crucial.

The International Maritime Organization (IMO) envisages a 40% reduction in carbon emissions by 2030 (compared to 2008) and until this period the goal is to cover 5–10% of the required global shipping energy by alternative fuels (e.g., hydrogen, methanol, ammonia) and power sources (e.g., fuel cells, batteries, solar panels, wind turbines) [3]. The emissions should be reduced by 70–80% until 2040, and the ultimate maritime goal is to reach net-zero well-to-wake emissions by 2050. The adoption and increasing utilization of green fuels and systems will be crucial to adhere to the strict regulatory requirements and achieve the maritime emission targets.

Hydrogen fuel cells and lithium-ion batteries are among the most attractive zero-emission alternatives to conventional diesel propulsion systems for short sea cargo vessels [5], [61]. Fuel cells and batteries have low energy density, so they can be used for ships with short sailing distances near refuelling and recharging infrastructures. Despite the safety concerns associated with the explosiveness of hydrogen and the fire risks of batteries, there has been an increasing interest in these new technologies as these hazards can be mitigated by implementing appropriate risk control options [62]. Hybrid configurations with fuel cells and batteries as power supply sources eliminate the dynamic limitations of pure hydrogen-based systems and the weight limitations of pure battery-electric propulsion [5].

Different studies have focused on the design and operation of hybrid ship energy systems. A comprehensive review on modelling and optimization of the power and propulsion components is presented in [8]. The focus of this literature review section is on the design and operation of ship power systems that utilize alternative energy sources, with a particular emphasis on fuel cells and batteries.

Ganjian et al. [10] presented an optimal design analysis for a fuel cell-battery hybrid fishing vessel to minimize system mass, volume, costs and improve electrical safety. A genetic algorithm was used to optimize separately each objective function. The degradation and the replacement costs of the components were not included in the optimization analysis. Vieira et al. [11] optimized the configuration of a hybrid platform supply vessel with fuel cells, diesel gensets and batteries to reduce the CO_2 emissions. However, the total costs were not included in the analysis. Wang et al. [45] proposed a nested design and control optimization for a similar type of hybrid system with [11], but including the capital and operational costs in the objective functions. The degradation of batteries and fuel cells was not included in the two studies [11], [45]. Wu and Bucknall [9] presented a two-layer optimization for a

fuel cell-battery driven ferry incorporating the degradation effects, for an averaged simplified load profile. The focus of this study was on the estimation of emissions reduction after retrofitting. Bassam et al. [63] developed an improved Proportional Integral (PI) controller to reduce the fuel cell consumption and degradation. The controller was tuned to satisfy the specific input conditions of the given power profile. The same authors in [31] developed a multi-scheme control strategy that could switch between different energy management approaches during the a-priori predicted power profile, based on battery SoC and power demand. However, the online adjustment of control strategies due to unpredicted operating conditions was not demonstrated.

The above studies [10], [11], [45], [9], [63], [31] focus on global optimization and do not include real-time controllers. A limitation of such approaches is that they typically rely on a-priori knowledge of the operating profile, which may not be fully realistic under variable operating conditions. Some research works that utilize online control approaches are listed below.

In [39], [40] fuzzy logic controllers were used to optimize fuel cell-driven ships with hybrid energy storage systems, in terms of efficiency and components' degradation. The implemented strategies are rule-based, so they rely on human experience and engineering knowledge. Si et al. [58] also implemented fuzzy rules, but combined with an artificial bee colony algorithm to optimize the design of a bulk carrier consisting of wind turbines, solar panels, fuel cells, batteries and diesel gensets. The practical challenges of integrating all these systems into one design were not discussed. Fan et al. [64] presented a robustly coordinated two-stage control approach for the power splitting between fuel cells, batteries and diesel gensets. Pre- and intra-voyage information (based on short term prediction) were utilized to reduce the operational costs and emissions.

The above studies [10], [11], [45], [9], [63], [31], [39], [40], [58], [64] include optimization problems which do not take into account the design, lifetime performance and cost uncertainties of retrofitting. The remainder of the literature section focuses on studies that consider the systems' (fuel cells and batteries) lifecycle performance and/or costs.

Zhu et al. [13] optimized a diesel-battery hybrid ship system using a genetic algorithm and a rule-based controller to minimize the annual fuel consumption, emissions, and lifecycle costs, considering a single power profile. The diesel tank and converter investment costs, and the maintenance costs of the components were not considered. Furthermore, there was no degradation model for the estimation of battery lifetime and its replacement cost. A battery cycling degradation model was presented by Chen et al. [53] for the minimization of lifecycle costs of a diesel genset-battery hybrid passenger vessel. The genset model equations, the battery calendar aging effects and the fuel prices were not discussed. Wang and Li [65] presented a lifecycle optimization problem for a battery hybrid energy storage system, considering the design cost and lifetime of batteries and supercapacitors. However, the investment costs of other systems such as engines, converters, tanks, motors, and the fuel and maintenance costs were not considered in the economic analysis.

Bassam et al. [66] optimized the sizes of a hydrogen-hybrid ferry using a PI controller considering Capital Expenses (CAPEX), Operational Expenses (OPEX),

maintenance and replacement costs. There were no battery and fuel cell degradation models. The components were replaced at their expected end of life, provided by the manufacturer. The implemented controller is not real-time, so it cannot adapt to varying operating conditions due to uncertainties and disturbances. Its parameters have been tuned to satisfy the specific conditions of a given power profile, which represents a key limitation of global optimization approaches, as it may restrict their ability to adapt to varying and uncertain operating conditions. Dall'armi et al. [29] used a Mixed Integer Linear Programming (MILP) algorithm, for the optimal sizing problem, to minimize the fuel consumption and degradation, focusing on the lifetime performance and the progressive ageing of fuel cells and batteries. Fixed fuel and component prices were considered for the cost analysis. Dall'armi et al. [46] extended the previous work [29] by utilizing the MonteCarlo analysis to account for uncertainties related to hydrogen, fuel cell and battery costs. In both studies [29], [46] a single power profile was used as input to the optimization frameworks. The original and the retrofitted versions were not compared in terms of design, lifetime operation and costs. Moreover, these are global optimization studies in which the operating profiles are assumed to be known in advance, without real-time controller capabilities. Zhang et al. [30] developed an online real-time controller combining the Equivalent Consumption Minimization Strategy (ECMS) and a filter-based approach to maximize the power plant efficiency and minimize the fuel cell and battery degradation of a passenger ship. Chen et al. [57] optimized the size and control of a fuel cell-battery-supercapacitor hybrid system, using a controller combining support vector machine and low-pass filter, to minimize energy losses, bus voltage fluctuations and battery degradation. In both studies [30], [57] the impact of the design and control solutions on the lifetime costs were not discussed, since the focus was on the technical objectives.

Lagemann et al. [67] presented a study for the selection of the optimal power systems and fuels in terms of lifecycle costs and emissions, considering the potential retrofits along the lifetime of the case vessel. Methanol, ammonia, hydrogen and liquefied natural gas were among the fuels that were compared, but hybrid configurations were not considered due to the constraint that the algorithm can select only one compatible fuel and power system option. Uncertainties in fuel costs and carbon emission prices were included in the authors' extended work in [68]. In both studies [67], [68] a high-level approach was used for the system design and operation. There was no discussion about the configurations and the control of the systems that can have a significant impact on the estimation of the lifetime costs.

There have been a few studies that focus on the techno-economic feasibility and lifecycle assessment of fuel cell and battery powered vessels.

Al-Falahi et al. [69] presented a lifetime techno-economic study for a retrofitted fully battery powered ferry. The packs were sized based on the Depth of Discharge (DoD) and the maximum load. The calendar aging effects were not considered, and the cycling degradation was estimated assuming the battery operates at 80% DoD over its lifetime, for a single profile. Furthermore, the retrofitting implications in terms of overall weight and volume changes were not discussed. Wang et al. [70] presented a lifecycle emission and cost assessment for two ferries, a tug and a trawler, that were conceptually retrofitted with hydrogen engines. This study did not discuss the uncertainties associated with the low technological system maturity,

the required retrofitting changes, and the design and cost specifications of the rest of the energy systems.

Inal et al. [71] presented a lifecycle emission and cost assessment case study for a retrofitted hydrogen-fuelled general cargo vessel, and compared the results to the original diesel version. The tank placement onboard and the replacement of the fuel cell stacks were not considered. It was assumed that the fuel cells can last for 15 years and cover the load fluctuations without hybridization with batteries. Furthermore, fixed fuel and component prices were considered for the economic analysis. Karvounis et al. [72] presented a lifecycle emission and cost assessment using hydrogen and ammonia as substitute fuels for marine engines, but without discussing the practicality and feasibility of retrofitting considering the design constraints (weight, volume, costs) and the low system technical maturity. In both case studies of short sea cargo vessels [71], [72] a single power profile was considered. Trillos et al. [73] demonstrated that a fuel cell-battery passenger ferry could reduce the well-to-wake emissions by 89% compared to the diesel-hybrid version. This study focused on environmental and health aspects such as emissions, maritime ecotoxicity and human carcinogenic toxicity. The impact of the design decisions on the lifetime costs was not discussed.

Overall, the studies that perform a lifecycle emission and cost assessment do not discuss the control strategies and lifetime operation of the systems.

The main outcomes and gaps from the literature review are summarized below:

- There is a gap in the literature for retrofitting studies of cargo vessels with hydrogen fuel cells and batteries, considering the impact of multiple power profiles on system sizing and control, using a robust real-time controller. Most studies focus on developing control approaches and sizing methods tailored to specific applications with a single (simplified) power profile.
- There is a lack of comprehensive design, lifetime operation and cost analyses under varying economic scenarios, especially for hydrogen-based ship energy systems.
- To the best of the authors' knowledge, there is no study that considers all the following: the degradation effects of both fuel cells and batteries (combined cycling and calendar aging), the replacement periods and costs, and the tank sizing based on the lifetime increase in fuel consumption.

The focus of this research is on the design and operation of emission-free cargo ships. A diesel-mechanical vessel is retrofitted with hydrogen fuel cells and lithium-ion batteries to reduce its environmental footprint. A representative round trip is selected for the analysis. The power distribution between the fuel cells and batteries, and the system sizes are obtained using a real-time low-pass filter controller. The fuel consumption, system weights and volumes, components' degradation, and lifetime costs of the retrofitted fuel cell-battery propulsion system are estimated and compared to the conventional diesel mechanical version. This chapter provides insight on the design and operation of hydrogen hybrid cargo vessels, for the research community, shipowners and vessel operators regarding the implications and uncertainties of such retrofitting.

To summarize, the novelty of this chapter is threefold:

- Proposal of a method for the selection of representative ship power profiles.
- A detailed methodology including system design, sizing, real-time control, lifecycle operation, and net present value analysis of a ship propulsion system for varying OPEX and CAPEX.
- Estimation of fuel cell degradation, combined battery cycling and calendar aging, component replacement costs, and the impact of degradation on tank sizing.

The rest of this chapter is organised as follows: In Section 3.2, the case study details for the vessel and the retrofitted hydrogen-based energy system are presented. In Section 3.3, the proposed methodology for the design, operation and cost analysis is described. The results from the analysis and the simulations are discussed in Section 3.4. Finally, the concluding remarks are presented in Section 3.5.

3.2 CASE STUDY

In this section, the case vessel details and the retrofitted hydrogen-based energy system characteristics are discussed.

The case ship is a diesel mechanical general cargo ship 90 m long, 12.5 m wide and it carries 3638 tons of cargo [74]. It is retrofitted with hydrogen fuel cells and batteries as the power supply components to minimize the onboard emissions. The vessel does not have a fixed load profile and schedule since it sails between different countries, mainly in the Baltic and the North Sea.

The original version has a direct-drive diesel mechanical system with a main engine of 1.8 MW (oversized system), and a controllable pitch propeller. In the new hydrogen-based version, the engine is replaced by two Alternating Current (AC) variable speed electric motors on the same shaft, connected to a fixed pitch propeller. The number and types of fuel cells and batteries will be determined after employing the real-time control strategy, which will be discussed in Section 3.3.2. After discussions with the vessel operators, an emergency/standby diesel generator (800 kW) is included in the considered case study to ensure system reliability in case hydrogen is not available at the right place or quantity. The original and the retrofitted design will be discussed in more detail in Section 3.4.5.

3.3 METHODOLOGY

A flowchart of the methodology proposed in this chapter for the design, operation, and cost analysis is shown in Fig. 3.1. In Step 1, the power profiles of the vessel, considering one-year operational data, are analyzed in terms of load ramps and power frequency distribution, to select a representative round trip. Then in Step 2, the fuel cells are sized based on the maximum power demand of the vessel. In Step 3, a real-time low-pass filter based control strategy is implemented to distribute the power between the components. The batteries are iteratively sized until the power balance and SoC constraints are satisfied for all the profiles of the round trip. The obtained fuel cell and battery power distributions are used as input to calculate the degradation of the components in Steps 4 and 5. Finally, in Step 6,

the lifetime system costs are estimated following a sensitivity analysis for varying operational and capital costs. The retrofitted energy system is compared to the original configuration in terms of design and lifetime costs. The methodology is explained in detail in Section 3.3.1 - Section 3.3.5.

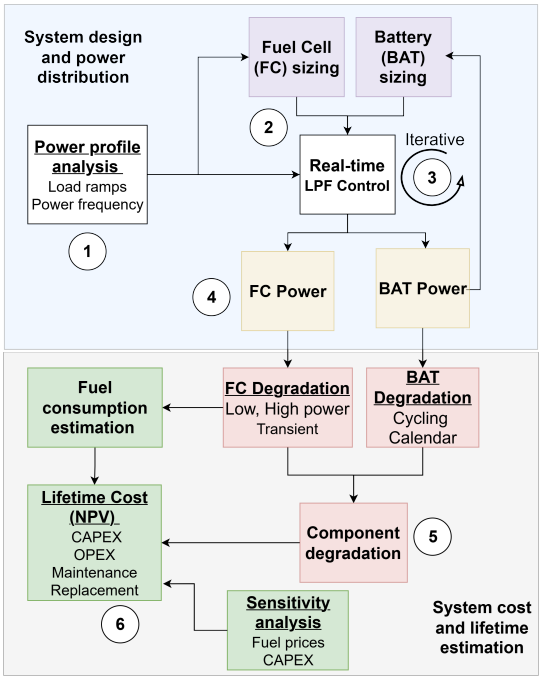

Figure 3.1: Flowchart for the design, operation and cost analysis

The following assumptions are considered in this chapter:

- Only the propulsive power demand of the vessel is considered, with a sampling interval of 5 min, without any auxiliary loads and systems such as filters, cooling, and safety equipment. For the original diesel-based vessel, shaft generator data indicate that conventional auxiliary electrical demand is on the order of 3-4% of propulsion power across the operating dataset, suggesting a relatively small contribution compared to propulsion demand. This should be interpreted as an indicative and partial proxy for auxiliary demand, as it may not capture all onboard consumers and does not represent additional loads associated with the hydrogen-based system, such as thermal management and balance-of-plant components. For this reason, auxiliary loads are not included in the model to avoid inconsistent representation.
- For the cost analysis, it is assumed that the hydrogen-based version is refuelled with green hydrogen that is always available. This is an optimistic assumption since there are certain challenges that need to be addressed for wide availability of green hydrogen such as: high production cost and limited existing infrastructure including storage systems, distribution and transportation

networks. The stringent environmental regulations, and the price drop and development of renewable systems (e.g., wind and solar) are expected to enhance the economics of green hydrogen production in the future [75]. Regarding the fuel storage equipment, various methods such as salt caverns and hydrogen carriers are investigated to store large amounts of fuel [75]. The produced green hydrogen may be in remote locations or far away from the ship, so there might be a need for a large pipeline network or intermodal fuel tank transportation (e.g., trucks, trains) as part of the supply chain network [76].

- The vessel, after retrofitting, has a remaining lifetime of 20 years, and it operates in the same round trip.
- Only the fuel cells and the batteries require replacement during the 20-year period.
- The recycling of the components and their residual cost values at the end of the vessel's lifetime are not considered.

3.3.1 *Analysis of power profiles*

All the power profiles (one-year data) of the case vessel are analyzed in terms of frequency of power and load ramps. Compared to the one-year data, the representative round trip is selected such that the vessel operates for a similar percentage of the sample data at the same power ranges (e.g., 100–200 kW, 500–600 kW) and has a similar percentage of fluctuations at various load ramps (e.g., 5–10% $\Delta kW/\Delta t$). A few profiles were chosen for the round trip to reduce the computational burden, but they still have an accurate representation of actual ship voyages. The power distribution is an important key performance indicator for more accurate lifetime fuel consumption estimation, and the load ramps are critical for the estimation of fuel cell degradation.

The selected round trip should include the most power demanding operating conditions for fuel cell sizing, the most energy intensive fluctuations for battery sizing, and the longest profile with the highest fuel consumption for tank sizing.

3.3.2 *Real-time low-pass filter-based controller*

The case vessel does not have a fixed power profile and schedule, so a robustly coordinated real-time control strategy that can be implemented to different power profiles is necessary. In this study, robustness of the controller refers to its ability to maintain stable and feasible operation without retuning under varying operating conditions, including changes in power demand, load transients, and operating modes (e.g., manoeuvring, cruising), while respecting system constraints. Fuzzy-logic rule-based approaches can be simple and effective but they rely on human expertise, and according to [30] they can be highly dependent on specific power profiles and operating conditions, so they are not selected for this study. Some possible real-time control approaches that can be used are: ECMS, Model Predictive Control (MPC), or Artificial Intelligent (AI) methods. The studies that use ECMS usually focus on fuel consumption minimization, neglecting other objectives such as

the degradation of components [30]. Moreover, the controller might face challenges adapting to unpredictable sailing profiles due to incorrect real-time tuning of the equivalence factors. MPC approaches can be used in dynamic simulations to predict future states and optimize the system's operation at every time step, but they usually require high fidelity models and significant computational time. Furthermore, the creation of a robust controller can be challenging due to the disturbances and uncertainties [77]. AI methods can also be used to predict future operating states but they may require a large amount of data and resources to produce accurate, physically-consistent and interpretable results [8]. Predictive methods can be beneficial in scenarios where significant battery charging and discharging is required (e.g., peak shaving functions), as they enable prior charging to ensure the power and energy demand constraints are satisfied.

In this chapter, a filter-based control approach is selected due to its simplicity in terms of implementation, robustness under different operating conditions, and low computational complexity. The developed low-pass filter-based real-time controller for operation is shown in Fig. 3.2. The generic fuel cell, battery, and converter models from Simulink are used for the analysis. The DC bus voltage is controlled by a PI controller at 1000 V. The low-frequency current is delivered by the fuel cells and the high-frequency current by the batteries. The lower the time constant in the low-pass filter, the faster the fuel cells respond to load changes and thus degrade. The battery SoC is also controlled around 50% with a P controller to reduce its degradation. The saturation blocks are used to ensure that the current limits for the components are not exceeded. Overall, this low-pass filter control approach provides at low complexity and computational requirements: real-time operation for different power profiles, controllability of fuel cell and battery operation for reduced fuel consumption or components' degradation, and stable DC bus system voltage. The robustness of the controller contributes directly to the robustness of the integrated system, as stable and constraint-compliant operation across varying profiles ensures that component limits are not violated and degradation mechanisms remain within the modeled assumptions. More details about the models and the control strategy are discussed in the authors' previous work [74].

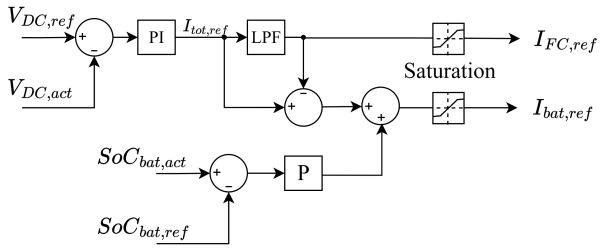

Figure 3.2: Real-time low-pass filter controller

The battery power is estimated by subtracting the fuel cell power from the load demand. The energy capacity is estimated considering a C-rate equal to 1. For each profile of the round trip, the power supplied by the fuel cells and the batteries

should be equal to the load demand at each time step, and the battery SoC should remain between 20% and 80% for the selected low pass filter time constant. If one of the conditions is not satisfied, the battery size should be modified. Then, the battery components can be selected, and the fuel consumption for one round trip can be calculated using the Simulink model, as presented in [74], for the considered fuel cell stacks [78].

In the proposed control strategy, the battery is used for smoothing the load experienced by the fuel cells and for providing ramp support. For such battery functions, it can be simple and effective to use a low-pass filter control strategy [30], [57].

3.3.3 *Degradation of fuel cells and batteries*

Fuel cell degradation at chemical scale may affect different parts such as the membrane and the electrodes. The reactant humidity, temperature, stoichiometry and flow rates are critical operating factors for the efficiency and durability of the fuel cell stacks. Low relative humidity or high temperature can lead to structural dissolution of the membrane [79]. Low reactants' flow rates and low relative humidity may lead to the formation of radicals which can cause platinum dissolution and carbon support corrosion in the catalyst layer. Those lead to impedance rise and thus voltage decay for the cells [79]. The carbon support corrosion can also lead to active surface area loss (for reactions) or conductivity loss which also result in voltage drop.

The focus of this study is on the degradation of fuel cells based on their operating power levels. It is defined as the voltage drop of a single cell at constant current output, assuming that the reduction of voltage is the same across all the cells of each stack [29], [46].

The total degradation is measured in microvolts (μV), and it is a summation of the voltage drops due to transient loading, start/stop cycles, low power operation (<10% P_{max}), and high-power operation (>90% P_{max}), where P_{max} is the rated power of the fuel cell stacks [80].

The degradation of the fuel cells is described by Eq. (3.1) - Eq. (3.5). It is assumed that all fuel cells operate at the same power level, and there is no individual control or switching on/off during manoeuvring and cruising phases.

$$dV_{\text{ramp}}(t{+}1) = \left| P_{\text{FC}}(t) - P_{\text{FC}}(t{+}1) \right| \Delta V_{\text{ramp}} \tag{3.1}$$

$$dV_{\text{start}}(t) = \delta_{\text{start}}(t)\, \Delta V_{\text{start}} \tag{3.2}$$

$$dV_{\text{low}}(t) = \begin{cases} a_{\text{low}} \dfrac{0.1\, P_{\text{max}} - P_{\text{FC}}}{0.1\, P_{\text{max}}} \Delta t & \text{if } P_{\text{FC}} < 0.1\, P_{\text{max}} \\ 0 & \text{otherwise} \end{cases} \tag{3.3}$$

$$dV_{\text{high}}(t) = \begin{cases} a_{\text{high}} \dfrac{P_{\text{FC}} - 0.9\, P_{\text{max}}}{0.1\, P_{\text{max}}} \Delta t & \text{if } P_{\text{FC}} > 0.9\, P_{\text{max}} \\ 0 & \text{otherwise} \end{cases} \tag{3.4}$$

$$dV_{\text{total}}(t) = dV_{\text{ramp}}(t) + dV_{\text{start}}(t) + dV_{\text{low}}(t) + dV_{\text{high}}(t) \quad (\mu\text{V}) \tag{3.5}$$

where $dV_{\text{ramp}}(t)$ is the voltage reduction due to load variations and is proportional to the transient coefficient ΔV_{ramp}. In Eq. (3.2), $dV_{\text{start}}(t)$ is the voltage reduction due to start/stop, proportional to ΔV_{start}; the binary variable $\delta_{\text{start}}(t) \in \{0,1\}$ indicates whether the fuel cell is off/on, respectively. Eq. (3.3) and Eq. (3.4) model degradation during low- and high-power operation. The values of the fuel cell degradation parameters are shown in Table 3.1.

Table 3.1: Values for fuel cell degradation parameters.

Parameter	Value/Unit
ΔV_{ramp}	0.4185 μV/ ΔkW [81]
ΔV_{start}	23.91 μV/cycle [29]
a_{low}	10.17 μV/hour [82]
a_{high}	11.74 μV/hour [82]

The degradation effects within the operating range of 10-90% load are captured through the transient degradation term in Eq. (3.1), which depends on the magnitude of power variation. However, it does not explicitly account for the steepness of the ramp rate, which may influence degradation in practical applications. Furthermore, degradation model parameters are derived from automotive fuel cell data and may not fully represent degradation behaviour under maritime operating conditions, which can differ in terms of load profiles and dynamics. For this reason, the degradation and lifetime estimation are compared with manufacturer-provided lifetime data to ensure a realistic representation of fuel cell performance.

The batteries degrade due to cycling and calendar aging. The critical lithium-ion battery aging factors are the DoD, temperature and C-rate. High DoD can lead to structural disordering and thus loss of active material or lithium inventory which lead to cell capacity drop [79]. The temperature effect is considered only for calendar aging in this study. High temperatures can lead to binder decomposition and contact loss in the anode side. These can cause conductivity loss and impedance rise, leading to power or capacity fade [79]. The effect of C-rate on battery degradation is not analyzed in this study. However, high C-rates can lead to particle cracking, lithium plating or structural disordering [79].

For cycling aging, the rainflow counting algorithm is used to estimate the number of cycles for each profile at a specific DoD [83]. The equivalent cycles are calculated as shown in Eq. (3.6).

$$\text{EC} = \sum_{j=1}^{n} \frac{\text{cycle range}_j \cdot \text{cycle number}_j}{\text{DoD}} \tag{3.6}$$

where j indexes each measured half-cycle or full cycle. The cycle range (SoC range) is multiplied by the number of cycles for each measured half or full cycle obtained from the rainflow counting algorithm. The DoD is the difference between the maximum and minimum SoC for each profile. The capacity loss due to cycling aging is defined as a percentage from the ratio between the measured equivalent

cycles and the maximum number of cycles at the specific DoD, based on the battery datasheet [84].

A calendar-aging prediction model was developed by Ali et al. [85] to estimate the battery degradation when it is not operated, as a function of storage temperature, SoC, and idling time, and is given by Eq. (3.7).

$$\text{Idling Degradation} = a_1\, e^{a_2\,\text{SoC}} \cdot b_1\, e^{b_2/T_s} \cdot t^{c_1}. \tag{3.7}$$

where a_1, a_2, b_1, b_2, and c_1 are fitting parameters for lithium-ion batteries. These parameters have been obtained from experiments for different chemistries [85]. Lithium-iron-phosphate (LFP) batteries are selected due to their superior safety, long cycle life, deep discharge capability, and thermal stability, making them well-suited for maritime applications. The SoC ranges from 0 to 1; T_s is the storage temperature in Kelvin; and t is the idling time (e.g., in days). The LFP battery is assumed to be stored at 50% SoC and 25 °C for 36 days at the end of each year when the system is not in operation.

3.3.4 *Lifecycle costs of the energy systems*

The Net Present Value (NPV) includes the CAPEX and the OPEX, and represents the total discounted cost, as no revenues are considered, over the 20 years of the remaining vessel's lifetime. It is calculated as shown in Eq. (3.8) for both versions (diesel, hydrogen). A sensitivity analysis is performed for varying fuel prices, carbon taxes, and CAPEX of fuel cells and batteries.

$$\text{NPV} = \text{CAPEX} + \sum_{k=1}^{20} \frac{\text{OPEX}_k}{(1+r)^k} \tag{3.8}$$

where k is the number of years, and r is the discount rate which is assumed to be 5% based on [68], [86], [87]. The OPEX includes fuel costs, hydrogen liquefaction, carbon tax costs (only for the diesel-based version), maintenance and component replacement costs. The CAPEX includes the initial investment for the propulsion systems and the storage tanks.

3.3.5 *Design and cost comparison with the diesel mechanical version*

The retrofitted hydrogen-hybrid version is compared to the original diesel mechanical system in terms of lifecycle costs and system design, to investigate the implications of the conversion of the propulsion system. The weights and volumes of the components of the two versions are compared. Design recommendations are also provided for the new fuel cell-battery hybrid configuration.

3.4 RESULTS AND DISCUSSION

In this section, the results from the analysis and the simulations are presented and discussed.

3.4.1 *Profile analysis results: load ramps and frequency of power*

The data of the propulsive power demand of the original diesel mechanical version is analyzed. The selected round trip from the one-year data should have a similar percentage of the same power ranges and load variations (ramps). The results from the power frequency analysis are shown in Table 3.2 and summarized in Table 3.3. The sum of the percentages is equal to 100% for each case. As shown in Table 3.2, the vessel operates 11.9% of the total one-year sample data between 500 and 600 kW, and 13.4% of the samples of the selected round trip at the same power range. In Table 3.3, the results are summarized, and it is shown that the representative round trip is very similar to the one-year data, considering power ranges of 500 kW.

Table 3.2: Frequency of power (detailed).

Power range (kW)	One-year data	Selected round trip
0–100	0.8%	0.6%
101–200	6.1%	5.5%
201–300	2.1%	2.5%
301–400	2.1%	2.6%
401–500	3.4%	3.2%
501–600	11.9%	13.4%
601–700	16.6%	21.2%
701–800	21.4%	29.7%
801–900	21.2%	9.1%
901–1000	9.5%	6.1%
1001–1100	1.7%	1.0%
1101–1200	2.7%	4.4%
1201–1300	0.5%	0.7%
1301–1400	0.0%	0.0%

Table 3.3: Frequency of power (summarized).

Power range (kW)	One-year data	Selected round trip
0–500	14.5%	14.3%
501–1000	80.6%	79.5%
1001–1500	4.9%	6.2%

The load fluctuation results are shown in Table 3.4. The sum of the percentages is equal to 100% for each case. The ramps cover both positive and negative power changes for each interval. It is shown that the representative round trip is very similar to the one-year data in terms of percentages of load fluctuations. As expected

for a general cargo vessel, about 88.5% of the total load changes are in the range of 0–5% ΔkW/Δt (time step of 5 minutes), which indicates that most of the time the vessel operates at almost constant power levels with small fluctuations.

Table 3.4: Load fluctuations (ramps).

(±) ΔkW/Δt	One-year data	Selected round trip
0–5%	88.5%	88.4%
5–10%	2.9%	2.7%
10–15%	1.5%	1.5%
15–20%	1.1%	1.1%
>20%	6.0%	6.3%

The selected round trip is shown in Fig. 3.3. It consists of 11 single trips, with the vessel sailing between the Netherlands, Finland, Sweden, Lithuania, and Belgium. The ship starts its first voyage from Dordrecht, Netherlands and ends the last voyage, after 47 days, at the same location. After each voyage, the vessel stays at the port for 1–2.5 days, based on the actual data, for hydrogen refuelling and/or cargo operations. It is assumed that there are appropriate risk control options that enable simultaneous bunkering and cargo loading/unloading, if necessary [62]. According to [88], it takes around 1 h to refill 1 ton of liquefied hydrogen (LH_2) through direct refuelling by trailers. This option can be more cost-effective and flexible than refuelling with fixed bunkering infrastructure, especially at the early stages of operation [88]. The round trip (consisting of 11 single sequential trips/power profiles) is repeated 7 times per year.

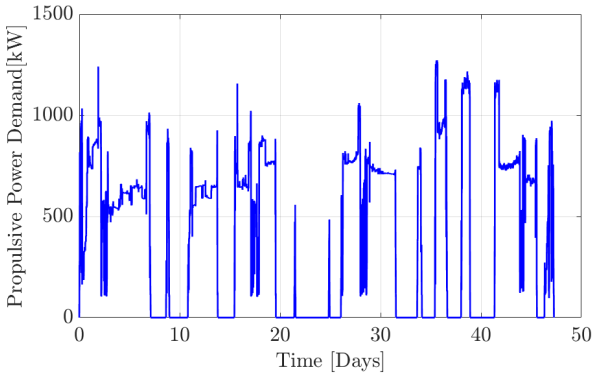

Figure 3.3: Selected round trip

3.4.2 *Real-time low-pass filter control strategy results*

The maximum required propulsive power of the round trip is 1230 kW (Fig. 3.3), but an additional 10% margin is considered for uncertainties in power profiles due

to extreme wind and wave conditions. Hence, the total installed fuel cell power is 1350 kW, covered by 9 efficient and compact fuel cells of 150 kW each [78].

The time constant in the low pass filter is set to 10 min such that the fuel cells slowly react to load changes, with power data sampled every 5 min in the load demand profiles. Hence, the fuel cells slowly follow the power demand for all the profiles, and when fast transients are required, the batteries are used. One profile with a large interval of almost constant power, and one purely manoeuvring profile, with high fluctuations, are shown in Fig. 3.4 and Fig. 3.6 respectively. The battery SoC is shown in Fig. 3.5 and Fig. 3.7 respectively for both profiles.

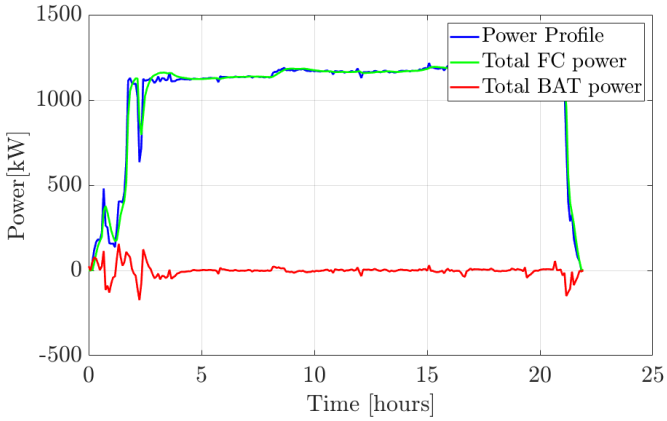

Figure 3.4: Constant power profile — power distribution.

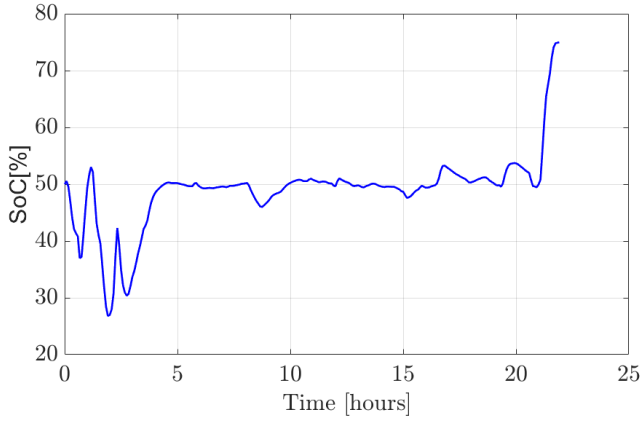

Figure 3.5: Constant power profile — battery SoC.

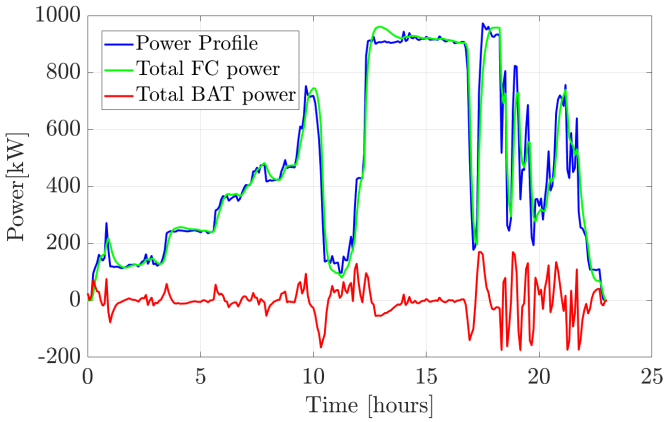

Figure 3.6: Manoeuvring power profile — power distribution.

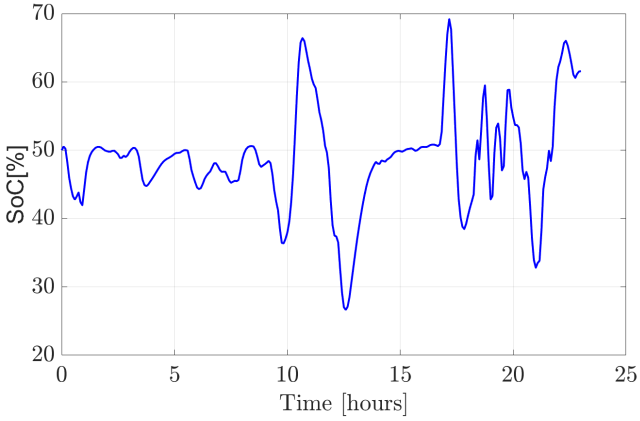

Figure 3.7: Manoeuvring power profile — battery SoC.

For the constant power profile Fig. 3.4, the battery power is close to zero for most of the time during the cruising mode of operation, since there are no significant load fluctuations.

In Fig. 3.7, for the manoeuvring profile, the battery operates between 25 and 70% SoC, with more fluctuations. At some intervals, the fuel cell power exceeds the load demand since the batteries need to be charged. This behavior is feasible in hybrid configurations. However, operating the fuel cells above the instantaneous load demand may increase degradation. In practice, this is managed by operating the fuel cells within preferred reguions to balance efficiency and lifetime. The P controller (Fig. 3.2) tries to reduce the gap between the actual SoC and the reference value which is 50%. For all profiles, the SoC at the end of the voyage is equal or greater than 50% (initial value), to avoid shore charging due to safety risks related

to fire and explosion, and uncertainties related to infrastructure and electricity availability.

After analysing all 11 profiles of the round trip, the average DoD is equal to 41.3% for the two battery racks of 100 kW, 100 kWh each [84]. Two batteries are installed for active redundancy, and their sizes are selected so that they operate in the recommended SoC range of 20–80% which results in low cycling aging [84]. The power balance and SoC constraints are satisfied for all the profiles of the round trip. The batteries are mainly used for load smoothing and ramp support in all operating conditions.

To verify the power distribution results of the developed Simulink model and the low-pass filter controller, a simple moving average control strategy, with the same time constant, was developed in MATLAB.

For the moving average controller, the fuel consumption is estimated as shown in Eq. (3.9).

$$F_{FC}(t) = a \cdot P_{FC}^2(t) + b \cdot P_{FC}(t) + c \tag{3.9}$$

where $F_{FC}(t)$ is the fuel consumption of the fuel cell as a function of time, $P_{FC}(t)$ is the power of the fuel cell as a function of time, and a, b, and c are the quadratic function coefficients based on the actual curve from the manufacturer's datasheet [78].

As a sanity check, the fuel consumption difference between the two models is less than 1% for all the profiles of the round trip.

3.4.3 *Lifetime fuel consumption and degradation of components*

The hydrogen consumption is estimated for each voyage of the round trip based on Eq. (3.9). The journey from Dordrecht (Netherlands) to Finland is the longest in duration (170 h) and it requires the largest amount of hydrogen onboard (5.6 tons). This power profile will determine the required size of the LH_2 tank, but an increased consumption due to fuel cell degradation by the end of life of the components, and an additional margin of 15% for spare capacity due to hull fouling and other operational uncertainties need to be considered [89].

The State of Health (SoH) of the components is estimated based on [29], considering the cumulative voltage drop of the fuel cells and the capacity loss of the batteries. The cell voltage drop is calculated based on Eq. (3.5), and when it is reduced by 15% from a reference value of 0.95 V, the stack needs to be replaced [29]. The maximum fuel cell power at the beginning of life is 175 kW, and the rated power is 150 kW, which corresponds to the end-of-life condition of the stack [29]. Similarly, the battery is replaced when the capacity is reduced by 20% from its maximum value [29], [46]. The SoH graph of the components is shown Fig. 3.8.

The fuel cells are replaced every 4.92 years or 26,300 operational hours, which is very close to the design life provided by the stack's manufacturer (25,000 h) [78]. The low and high-power fuel cell operating regions are limited, and there are no startup/shutdown cycles during manoeuvring and cruising. A single startup/shutdown cycle is considered per voyage, corresponding to fuel cell operation between departure and arrival. The transient loads have the biggest impact on the total

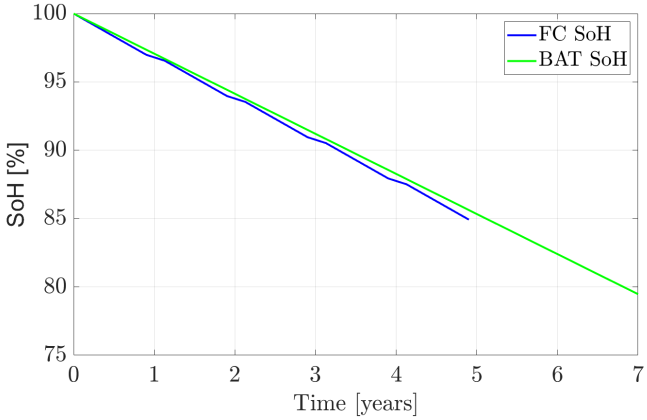

Figure 3.8: SoH of fuel cells and batteries

fuel cell degradation. A breakdown of the degradation contributions shows that transient operation accounts for approximately 86.5% of the total degradation, while low-power and high-power operation contribute 5.7% and 1.2% respectively, and startup/shutdown cycles account for 6.4%. At the end of each year, during the period the vessel is in idle condition, there is no fuel cell degradation. The batteries are replaced every 6.83 years. The annual capacity lost is 2.93% (0.96% due to cycling aging, and 1.97% due to calendar aging).

The progressive increase in hydrogen consumption due to fuel cell degradation (Fig. 3.9) has been estimated, as a function of voltage drop, based on [29]. After the first round trip, the hydrogen consumption is 24.2 tons, and at the end of life of the fuel cells after 4.9 years, the round trip consumption is 24.5% higher.

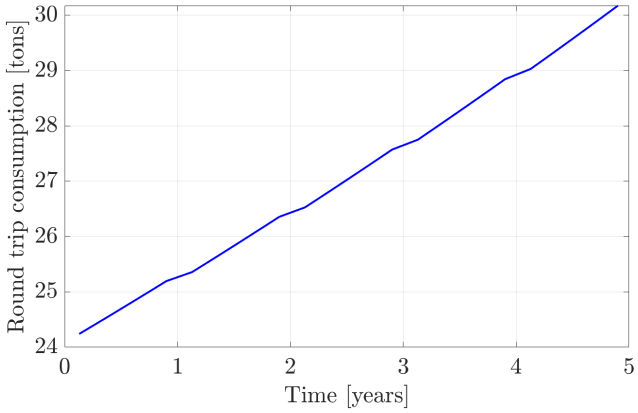

Figure 3.9: Hydrogen consumption increase due to fuel cell degradation

To size the hydrogen tank, an additional 15% spare capacity is considered due to various parameters that increase fuel consumption such as hull fouling, boil-off, thermal tank expansion etc. [89]. The LH_2 tank is sized, considering the total margin of 39.5% (24.5 + 15), to contain the 7.8 tons required for the longest voyage with the highest fuel consumption. Hence, considering the gravimetric and volumetric specifications of a cryogenic cylindrical storage tank [88], the LH_2 tank weighs 68 tons, and its volume is 193 m^3.

The fuel consumption of the main propulsion engine in the original diesel-based version was measured with onboard sensors, and the data was provided by the vessel operators. The increase of diesel consumption over time due to the wear and fouling of the main engine parts is shown in Fig. 3.10. The drops in diesel consumption are due to the periodic maintenance of the engine components, as described in [90]. It is assumed that the engine can last for 20 years (about 100,000 operating hours), without replacement, for short sea cargo vessels [91]. The Marine Gas Oil (MGO) tank is sized following a similar process with the LH_2 tank. The required volume of the MGO tank is 38 m^3, and it should carry 33.2 tons MGO, considering the longest profile and the required margins.

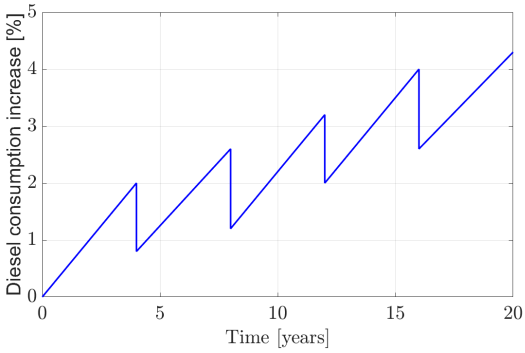

Figure 3.10: Diesel consumption increase due to wear and fouling of the main engine parts based on [90]

3.4.4 *NPV results for varying CAPEX and OPEX*

In this subsection, the NPV analysis is presented for varying fuel costs, carbon taxes, and CAPEX of the fuel cells and batteries.

The CAPEX, maintenance and replacement costs for the propulsion systems of the two versions are presented in Table 3.5. The average cost values are used, when there are two or more references for a specific component, for higher reliability in the prices.

Table 3.5: Fixed system costs.

Systems	CAPEX	Maintenance	Replacement
Fuel cell	1014 $/kW [92], [93], [94], [95], [96]	1% CAPEX [94]	50% CAPEX [94]
Battery	492 $/kWh [11], [93], [97]	0.5 $/kW/a [93]	CAPEX *Assumption*
Converter	216 $/kW [86], [89], [93]	2.6 $/kW/a [86], [93]	Not replaced [89]
Motor	133.5 $/kW [86], [93]	1.3 $/kW/a [86]	Not replaced [89]
LH_2 tank	233 $/kg H_2 [66], [98], [99]	Not considered	Not replaced [73], [89], [99]
Standby diesel generator	350 $/kW [93]	Not operated	Not replaced [73], [87], [97]
Diesel engine	289 $/kW [45], [86], [87], [93], [97]	5.2 $/kW/a [93]	Not replaced [73], [87], [97]
MGO tank	1.1 $/kg MGO [91], [97]	Not considered	Not replaced

The maintenance costs of the components are uncertain parameters and they have been approximated based on the available literature, since they depend on the way of operation of the systems. It is also assumed for the cost analysis that the efficiency curve of the fuel cell stacks does not improve over time. In a future work, given that more data will be available regarding the long-term operation and further development of fuel cells, the sensitivity analysis can be improved by considering variable maintenance costs and efficiency improvements over time.

The fuel cells are compact containerized solutions that include the stack, its balance of plants, control and monitoring systems, and an integrated DC-DC converter [78]. Their replacement costs are 50% CAPEX because only the degradable components (cells) are replaced periodically when the voltage has dropped by 15% [94]. The rest of the systems (piping, control, monitoring, sensors, vents etc.) inside the stack are non-wearable balance of plant components that are assumed to last 20 years with proper regular maintenance, without requiring replacement [89]. The process of replacing a degraded stack takes a few hours, so it can take place overnight without the need to take the ship out of service [89].

The batteries require very little maintenance over their lifetime, and the whole rack is replaced after 7 years of operation. They can be operated continuously without requiring to be switched off for extensive maintenance, as required for diesel generators. The rest of the propulsion components of both versions do not require replacement, since with regular maintenance they can last until the end of life of the vessel.

For the fuel cells and the LFP batteries, variable CAPEX has also been considered based on [92] and [100] respectively, as shown in Fig. 3.11, to account for CAPEX uncertainty, since these components have low technological maturity levels compared to the rest of the propulsion systems. The capital cost predictions of fuel cells and batteries are provided until 2029. For the LFP batteries it is assumed that C-rate equals 1. After 2030 (until 2044), it is assumed that the CAPEX remains constant for both components at 600 and 224 $/kW respectively [101].

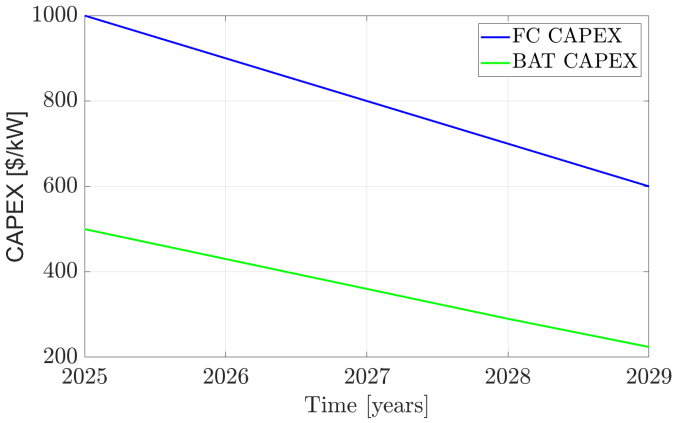

Figure 3.11: Variable CAPEX of fuel cells and batteries

A sensitivity analysis has been performed for different fuel costs (green hydrogen and MGO), and carbon taxes. In this study, only green hydrogen has been considered, to minimize the well-to-wake emissions. Four different scenarios, based on literature values, have been considered for its price: a) constant value at 4 $/kg, b) constant value at 6$/kg, c) constant value at 8$/kg, and d) variable fuel cost based on predictions of PwC, from 2025 to 2044 [66], [68], [102], [103]. For MGO, two different scenarios have been considered. Either its price is constant at today's value (0.73 $/kg) for 20 years (averaged from [87], [97], [104]), or there is a linear increase over time, as predicted by DNV classification society [86]. The variable fuel price scenarios for green hydrogen and MGO are shown in Fig. 3.12.

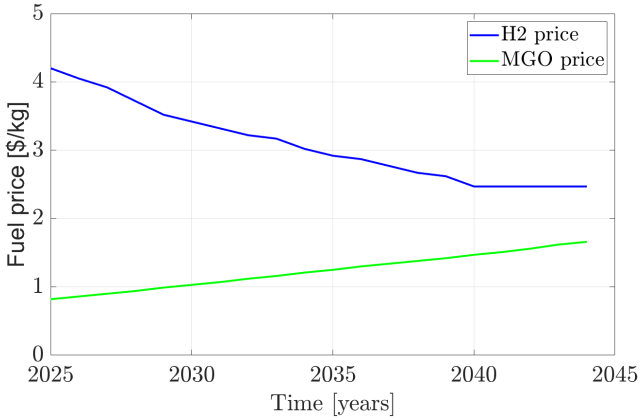

Figure 3.12: Variable green hydrogen and MGO prices until 2044

In Fig. 3.12, the average price over time from the five countries of operation, i.e., Netherlands, Finland, Sweden, Lithuania, and Belgium, has been considered. The Netherlands and Belgium have the lowest green hydrogen prices, and the two Scandinavian countries the highest price over the 20 years. In 2025, it is predicted from PwC [103], that the price of green hydrogen in the Netherlands will be 72% lower than in Finland. This indicates that it might be more cost-effective to refuel hydrogen from either the Netherlands or Belgium, if possible. Considering the low technological maturity of the systems/infrastructure and the potentially limited amount of available green hydrogen, it is recommended to refuel the tank to its limit when there is available quantity at the ports, especially at the early stages of operation, due to the high uncertainty.

Different scenarios have also been considered for carbon tax costs. The implementation of carbon taxes acts as an incentive to reduce emissions by penalising the use of fossil fuels. The implementation of carbon taxes for ships with Gross Tonnage (GT) above 5000 m^3 is expected start in 2025 based on the European Union Emission Trading System (EU ETS) [105]. The case general cargo vessel sails under a Dutch flag around countries of the EU, and it has a GT less than 5000 m^3. For such ships it is uncertain if and when the carbon taxes will be applied [105], [106]. Hence, three different tax cost scenarios have been considered: a) no carbon tax, b) constant carbon tax at 85 \$/ton CO_2 over 20 years [105], and c) a variable carbon tax with linear increase, based on PwC predictions [107]. In the last scenario, there is an average carbon tax of 175\$/ton CO_2, which can have a significant impact on achieving the maritime decarbonization goals, as stated in [108]. An emission factor of 3 ton CO_2/ton MGO has been considered in this study based on [72], [109].

Hydrogen needs to be liquefied to be stored at the cryogenic tank at the required temperature and pressure conditions. The cost to liquefy hydrogen is assumed to be 1\$/kg based on [110]. The transportation cost has not been considered in this study.

The NPV results for the 8 scenarios of the hydrogen-based version, and the 6 scenarios of the diesel-based version are shown in Table 3.6.

Table 3.6: NPV results for the two versions.

Hydrogen-based version — Scenarios	Total NPV ($)
1. Fixed CAPEX, 4 $/kg	17 624 606
2. Fixed CAPEX, 6 $/kg	22 332 508
3. Fixed CAPEX, 8 $/kg	27 040 410
4. Fixed CAPEX, PwC H_2 price	15 817 129
5. Variable CAPEX, 4 $/kg	17 062 684
6. Variable CAPEX, 6 $/kg	21 770 586
7. Variable CAPEX, 8 $/kg	26 478 489
8. Variable CAPEX, PwC H_2	15 255 207
Diesel-based version	
9. 0.735 $/kg, no carbon tax	8 198 714
10. DNV MGO prices, no tax	12 608 312
11. 0.735 $/kg, fixed tax ($85/ton CO_2)	10 815 923
12. DNV MGO prices, fixed tax	15 225 522
13. 0.735 $/kg, variable tax (PwC)	13 086 068
14. DNV MGO prices, variable tax	17 495 667

The Fixed CAPEX scenarios are for constant investment costs of all the components, including fuel cells and batteries, over 20 years, based on the prices of 2025. The variable CAPEX scenarios consider the cases that the prices of fuel cells and batteries drop until 2029 and then remain constant (Fig. 3.11). For the diesel-based version, either a fixed fuel cost is considered (0.73$/kg MGO) or a variable price based on DNV predictions (Fig. 3.12). Based on current prices of fuels, components, and carbon taxes (Scenarios 1, 11), the retrofitted hydrogen-based propulsion system has a NPV of $17.62 million, and the original diesel-based version has a NPV of $10.81 million, which is 38.6% less expensive. A more realistic scenario based on the cost predictions and future developments is the following: green hydrogen price declines, MGO prices increases, carbon tax cost increases, CAPEX of fuel cells and batteries decrease (Scenarios 8, 14). As shown in these two scenarios, the NPV of the diesel-based version is 12.8% higher than the hydrogen-based propulsion system, which indicates that the retrofitted version may be more cost-effective from a long-time perspective, if the price trends evolve as expected. In the worst-case scenario of the sensitivity analysis, the NPV of the hydrogen-based version can be up to $18.8 million higher than the original diesel-based system (Scenarios 3, 9), in case hydrogen is not widely used as a fuel in the future.

3.4.5 *Design recommendations and comparison with the diesel-based version*

In the hydrogen-based design, there are 9 fuel cells of 150 kW for propulsion, and an additional 10th stack for passive redundancy [111].

The total battery power and energy of the two racks are 200 kW and 200 kWh respectively. Each power supply component has its DC-DC converter. There are 2 × 710 kW inverters (690V) and 2 × 675 kW induction motors from ABB [112], [113]. The main diesel engine from Wartsila [114] in the original configuration can be used as a standby generator, with fewer cylinders, in the new fuel cell-battery propulsion system, as discussed in Section 3.2. The weights and volumes of the main components of the two version are shown in Table 3.7.

Table 3.7: Propulsion system weights and volumes

Systems	**Weight (kg)**	**Volume (m^3)**
Fuel cell stacks	3195	5.35
Battery racks	2090	1.58
Inverters	126	0.11
Motors	7740	10.12
Diesel Engine	11 600	15.53

The fuel cell stack includes the integrated DC-DC converter and the balance of plant components. The main propulsion system weights and volumes of the two versions are comparable, but the onboard placement of the hydrogen tank (68 tons, 193 m^3) poses significant design and safety challenges, as it will be discussed below in more detail. The total system weight and volume of the hydrogen-based propulsion system is 13,151 kg and 17.16 m^3 respectively, which is only 1.5 tons heavier and occupies around 1.6 m^3 more space than the main engine in the original diesel-based version.

The accommodation space is below the bridge at the aft of the vessel. The engine room is located right below the accommodation area. It is expected that the propulsion and auxiliary systems of the new hydrogen-based version will fit the existing engine room space (465 m^3), without requiring any change in the dimensions of the vessel, or the cargo carrying capacity. There are five cargo holds ahead of the superstructure. The foredeck is at the bow of the ship.

There are a few possible locations for the LH_2 tank onboard: a) engine room, b) sideways to the bridge, c) in place of one cargo hold at the upper deck, d) foredeck. It is important to note that there should also be an extra margin for the tank connection space, which contains valves, piping, safety systems, and vaporizers.

Placing the tank below the main deck is not recommended by regulations, since in case of damage, any leakage should not be contained in enclosed spaces, to reduce explosion risks [62], [115].

In the existing design, there is no space at the side of the bridge. Hence, if the tank is to be placed there, the superstructure design should be modified, the tank should be protected from side collisions, the superstructure should be protected from explosions, and ideally the tank should be located more than 20% of the breadth of the vessel from the sides [115]. It is also important to ensure that there is no heat ingress from the accommodation space below the bridge.

Another option is to remove one of the cargo holds and place the tank at its position at the top deck. However, this is not a desired option for shipowners since a certain amount of cargo and thus income is lost. It can also pose a risk in case of crane operation during loading and unloading cargo from adjacent cargo holds.

Placing the tank at the foredeck could also be a possible option if there are no violations of stability criteria. Some other risks that arise are large piping distances and a high number of connecting points that increase the risk of failure and leakage, frontal collision, and reduced visibility from the bridge.

A final option is to change the dimensions of the vessel, but this is not realistic for the 17-year-old case ship. However, it is a design recommendation for similar types of new-built vessels.

Overall, from the design analysis it is shown that retrofitting hydrogen-based ship systems can be challenging in terms of volume, weight and safety due to the large and heavy fuel tank, and the stringent regulatory requirements compared to the diesel setup. In this retrofitting study, the placement of the main propulsion equipment in the existing engine room space did not pose any space or weight issues. However, it is important to follow the safety guidelines of class societies for a detailed design analysis regarding the placement of the equipment in fuel cell and battery rooms. On the other hand, a newbuild ship would be optimized to accommodate the special design and safety requirements of the electrical and fuel systems, without constraints imposed by the existing vessel structure, but at higher CAPEX and lead times compared to a retrofit.

Fuel cell-battery hybrid systems offer modularity and scalability advantages since they can be used for various ship types (retrofits or newbuilds) and energy demand levels by adjusting the number of the required modules and configurations, depending on the application. The developed model and control strategy can be used for different ship types with similar load profile characteristics, where the battery is used alongside the fuel cell for load smoothing. The same models and controller can also be used for vessels requiring other battery functions such as peak shaving by adjusting the low-pass filter time constant.

3.5 CONCLUSION

This chapter presented a lifetime design, operation, and cost analysis for the propulsion system of a retrofitted cargo vessel with hydrogen fuel cells and batteries. A representative round trip was created by analysing one-year operational data based on the frequency of power distribution and the load ramps. A low-pass filter based real-time controller was employed to distribute the power between the components, by satisfying the energy balance and battery SoC constraint. The batteries were used mainly for ramp support, with an average DoD of 41.3%. The fuel cell degradation was estimated based on a stack voltage degradation model and for the battery degradation, both cycling and calendar aging were considered. The fuel cells require replacement every 5 years, and the batteries every 7 years.

The LH2 tank (68 tons, 193 m^3) was sized based on the most fuel demanding profile, considering the increased consumption due to component deteriorations, and a 15% spare capacity. Its onboard placement poses significant design and safety challenges, associated with the weight distribution, volume requirements, and explosion

risks. The lifetime costs of the energy systems were estimated following a sensitivity analysis with 14 scenarios of varying CAPEX and OPEX. The green hydrogen price and the carbon tax costs had the biggest impact on the NPV value. If the CAPEX and OPEX remain constant over 20 years, the NPV of the retrofitted hydrogen-based version is 38.6% higher than the original diesel-based propulsion system. Based on future predictions that green hydrogen price and fuel cell CAPEX drop, while MGO price and carbon taxes increase, it is possible that the retrofitted propulsion system can be more cost-effective, from a lifetime perspective, by $2.24 million.

4

DESIGN AND LIFETIME COST OPTIMIZATION INCLUDING STABILITY CONSTRAINTS

This chapter is reproduced from Mylonopoulos et al. [116]

ABSTRACT

Low total lifetime cost is essential for the adoption of zero-emission ship energy systems, which must meet operational power demands while complying with onboard safety regulations. However, many studies rely on a simplified, averaged or insufficiently representative load profile and treat system design, operation, and integration feasibility separately, which can distort lifetime cost assessments and result in practically infeasible retrofit concepts. This study investigates how a hydrogen-based ship energy system can be optimally sized, operated, and arranged onboard to minimize total lifetime cost while satisfying operational constraints and stability requirements for a general cargo vessel retrofit. A representative power profile is synthesized from one year of operational data using a probability-based downsampling method and then used in a mixed-integer nonlinear lifetime cost optimization with discrete placement and ballast decisions, solved using the SCIP solver. The optimal retrofit comprises 1.4 MW of fuel cells, 180 kWh of batteries, and a 146 m^3 liquefied hydrogen (LH_2) tank, requires 171 t of ballast to satisfy trim and vertical stability constraints, and is primarily driven by fuel costs, which account for 74% of the total lifetime cost. Overall, the results indicate that the viability of hydrogen-based ship retrofits primarily depends on LH_2 storage integration constraints and hydrogen price assumptions, and that the proposed framework provides a practical basis for lifetime cost assessment of feasible retrofit designs.

4.1 INTRODUCTION

4.1.1 *Background*

The International Maritime Organization (IMO) has imposed stringent regulations to reduce shipping emissions [2]. In the short term, carbon emissions must be reduced by 40% by 2030 and by at least 70% by 2040, relative to 2008 levels [3]. The adoption of green fuels and novel energy systems for both newbuilds and retrofits is a key driver in achieving the maritime emission targets. Hydrogen fuel cells and lithium-ion batteries are promising zero-emission alternatives to drive the maritime energy transition, especially for short-sea operations near refuelling and recharging infrastructure [60], [61].

The applicability of hydrogen-based ship systems remains limited due to the low technical maturity, limited availability of cheap green hydrogen, high investment costs, and insufficient infrastructure. This study aims to accelerate the maritime energy transition by providing insights into the optimal design and operation of ship energy systems integrating hydrogen fuel cells and batteries. The focus is on retrofitting existing vessels and optimizing system topology and operation from a holistic perspective considering operational needs, lifetime cost, and ship stability.

4.1.2 *Literature review*

A comprehensive review of methods for the design and control of energy systems is provided in [8], emphasizing the importance of integrating design and operational considerations in optimization problems.

Several studies reduce computational complexity by adopting linear or mixed-integer linear formulations and using simplified or averaged power profiles. Bassam et al. [66] conducted a system sizing optimization for a passenger ferry, evaluating various fuel cell-battery combinations to minimize the total energy system cost. Power distribution was managed using a proportional-integral controller, without optimizing the operational parameters. The analysis was based on a single profile with an extended period of nearly constant power output, rather than a representative sailing cycle derived from the operational data. Pivetta et al. [47] applied a Mixed Integer Linear Programming (MILP) algorithm to optimize daily costs and fuel cell degradation for three passenger vessels of different sizes, with battery degradation incorporated as a constraint. Dall'armi et al. [29] used the same algorithm, for an optimal design and operation study, aiming to minimize the fuel consumption and degradation of both fuel cells and batteries in one of the three passenger vessels, with a focus on the progressive aging of the power supply systems. In [47] and [29], the system weight and volume were set as optimization constraints, considering that the combined system weight and volume of the retrofitted components (fuel cells, batteries, tank) would be lower than those of the original diesel engine. The same authors extended their work in [46] by incorporating uncertainties related to fuel and component costs, without considering the impact of different power profiles on the results. As noted in [66], [29], hydrogen consumption had the most significant influence on the optimal solution. In [47], [29], [46] a hierarchical objective approach was used, with linear objective functions to simplify the optimization process. Simil-

arly in [25], a non-convex bi-objective optimal control problem was transformed into a convex framework to facilitate computation using MOSEK optimization software.

Many studies optimize control/energy management parameters for fixed system designs. Zhang et al. [30] applied a real-time equivalent consumption minimization strategy to enhance the system efficiency and reduce the fuel cell and battery degradation. Supercapacitors were integrated to handle high transient loads. The fuel cells were sized to meet the average load demand, while the power distribution between the supercapacitors and the batteries was managed using a high-pass filter. Several other studies [26], [31], [63] have also optimized energy management strategies for fuel cell-battery hybrid powertrains with fixed design parameters. In [39], [40] supercapacitors were integrated into hybrid energy storage systems to improve system efficiency and reduce battery degradation using fuzzy logic controllers. Fan et al. [64] proposed a control strategy for optimal power coordination, leveraging pre-voyage and intra-voyage information to minimize the costs and emissions. This optimization problem was solved in two stages using the column and constraint generation algorithm.

A few studies have presented combined energy system design and control optimization, but without considering the impact of system placement onboard and the effects of different system arrangements on ship stability. Vieira et al. [11] optimized the system configuration and operation of a hybrid platform supply vessel to minimize carbon emissions by varying the sizes of the components. Wang et al. [45] conducted a nested design and control optimization for a fixed number of diesel gensets, fuel cells and batteries, allowing for variable rated capacities. A MILP algorithm was used in the inner layer for the operation optimization and a genetic algorithm in the outer layer for the design optimization. Various system topologies were analyzed based on low, medium, and high emission reduction targets. Similarly, Wu and Bucknall [9] implemented a two-layer optimization using deterministic dynamic programming. Their study focused on lifetime emission reduction after retrofitting a diesel-mechanical coastal ferry with hydrogen fuel cells and batteries. The analysis was based on a simplified averaged power profile. Si et al. [58] combined fuzzy logic rules with the artificial bee colony algorithm to optimize the design and operation of a bulk carrier integrating photovoltaic panels, fuel cells, batteries, wind turbines, and diesel generators. This study did not provide a detailed discussion of the practical challenges associated with weight, volume, integration, safety, and reliability when incorporating multiple energy systems into a single design. Chen et al. [57] proposed a sizing and energy management optimization framework for a hydrogen-fueled vessel with a hybrid energy storage system using a support vector machine and frequency control. The weighted sum method prioritized energy efficiency, followed by battery degradation, with bus voltage fluctuations assigned the lowest importance. This study did not explore different pareto front solutions across a wide range of weighting coefficients. Ganjian et al. [10] conducted an optimal design study for a fishing boat powered by hydrogen fuel cells and batteries. As claimed, this was the first study to use volume as an objective function. The interactions between different objectives (electrical safety, cost, and volume) were not considered, as each was solved independently using single-objective formulations.

4.1.3 *Literature gaps*

The key findings and gaps identified in the literature review are summarized below:

- Few studies have explored the combined optimization of system design and operation for ship energy systems, particularly from a holistic perspective. Most research focuses on optimizing energy management strategies for a predetermined (fixed) design.
- Ship stability and system placement constraints are often overlooked and not integrated into energy system optimization models, which may lead to infeasible design solutions. In ship retrofits, trim and vertical stability constraints are particularly critical.
- To reduce computational complexity, ship energy system optimization problems are frequently simplified into linear, quadratic, or mixed-integer linear formulations. However, these relaxations and simplifications may lead to suboptimal solutions.
- Many studies rely on simplified, smoothed, averaged, arbitrarily selected or insufficiently representative power profiles for optimization, which may distort lifetime cost assessments.
- Few studies optimize energy system total lifetime cost, despite this being a crucial factor for shipowners' decision-making.

4.1.4 *Research focus and key contributions*

The focus of this research is on the optimal energy system design and operation of a general cargo vessel from a holistic perspective. The original diesel mechanical propulsion system of the ship is conceptually replaced by a hydrogen-hybrid powertrain to reduce emissions. A probability-based downsampling approach is used to generate a representative power profile in terms of fuel consumption and fuel cell degradation, based on the annual propulsion data. The power and propulsion systems are optimized to minimize the total lifetime cost including fuel, capital and system replacement costs, while ensuring compliance with the safety and ship stability constraints. The optimization is a Mixed Integer, Nonlinear Programming (MINLP) problem incorporating binary decision variables and combinatorial aspects, and is solved using a specialized MIP solver. Overall, this study provides a holistic framework for the optimal design and operation of ships with novel energy systems, aligning operational needs, lifetime cost efficiency, and regulatory requirements.

The key contributions of this chapter are summarized below:

- Development of a holistic framework for the optimal topology and operation of ship energy systems, minimizing total lifetime costs while considering operational requirements and vessel stability regulations.
- Formulation of a global optimization framework to solve complex MINLP problems for ship energy systems, utilizing a specialized MIP solver to efficiently handle computational complexity and ensure high-quality solutions.

- Development and implementation of a probability-based downsampling method to generate a representative power profile from annual measurements, enabling computationally-efficient lifetime cost optimization while preserving fuel consumption and fuel cell degradation estimates within an acceptable threshold.

The remainder of this chapter is structured as follows: Section 4.2 introduces the case vessel and its powerplant components. Section 4.3 presents the methodology for optimal system topology and operation, incorporating stability constraints. Section 4.4 presents and discusses the optimization results. Finally, Section 4.5 provides concluding remarks and recommendations for future research directions.

4.2 CASE STUDY

The case vessel is a short-sea general cargo ship operating primarily in the Baltic and North Sea, without a fixed route or schedule. Its length is 90 meters and its breadth is 12.5 meters [59], [74]. The original diesel-powered configuration has a mechanical propulsion system with a single oversized 1800 kW main engine and a controllable pitch propeller (direct drive without gearbox). In this study, the vessel is conceptually retrofitted with proton exchange membrane fuel cells and lithium iron phosphate batteries to reduce its environmental footprint. Fuel cells and batteries generate electricity which is supplied to the Direct Current (DC) bus via DC/DC converters. Excess fuel cell power can be used to charge the batteries onboard. After the DC distribution system, the electric current is converted to Alternating Current (AC) through inverters, delivering power to the propulsion motors that drive the ship's propeller through a reduction gearbox. The focus of this study is to determine the optimal total capacities of fuel cells and batteries, along with the optimal power distribution between these sources, to minimize the total lifetime cost, while ensuring compliance with regulatory requirements for equipment placement and ship stability.

4.3 METHODOLOGY

Fig. 4.1 presents a flowchart illustrating the proposed methodology for this chapter. The methodology is divided into two main steps:

- Step 1: The onboard measured power demand data of the ship's load profiles are analyzed, and a representative power profile is generated.
- Step 2: The combined optimal system topology and operation problem is formulated and solved, using the representative profile from Step 1 as input. The total system lifetime cost is optimized, and the optimal design, including stability constraints, is obtained using Python interfaced with the specialized MIP solver SCIP.

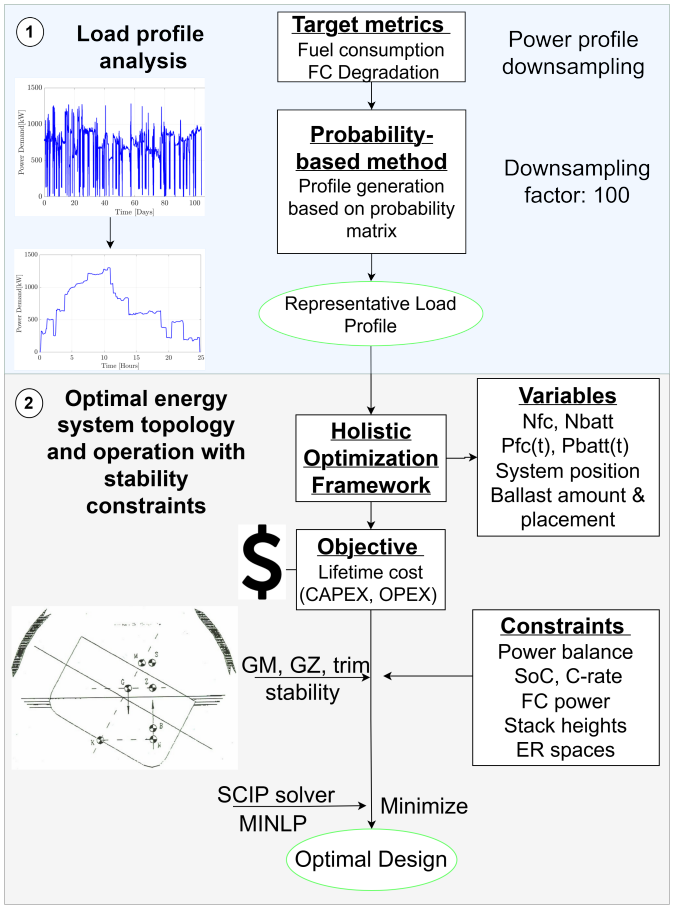

Figure 4.1: Methodology for power profile analysis and optimization

4.3.1 *Ship power profile analysis and synthesis*

Fig. 4.2 presents the propulsion power profile derived from the measured diesel-engine power output of the vessel in its original configuration. The data were collected by the vessel operator from onboard monitoring sensors over a one-year period (2022). The dataset includes multiple trips, routes and operating conditions, and represents the vessel's complete annual sailing activity excluding port stays. The annual profile (Fig. 4.2) spans approximately 100 sailing days and is assumed to be repeated twice every year over the vessel's lifetime.

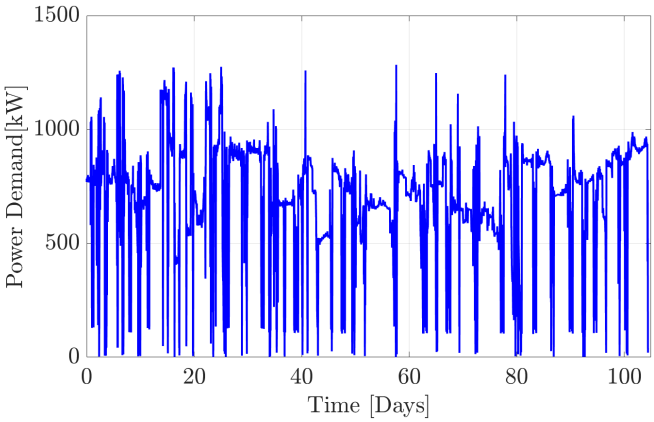

Figure 4.2: Diesel engine annual power data

Since the case ship operates across multiple routes and under varying operating conditions, directly optimizing over the full annual power profile (30,000 data at a 5-minute resolution) is computationally intensive. Therefore, a representative profile is generated from the full annual dataset to enable accurate and computationally-efficient design and operation analysis.

One-year of diesel engine power data, recorded at a 5-minute sampling interval, are analysed using a probability-based approach to generate a representative timeseries. A downsampling factor of 100 is applied, reducing the original 30,000 operational data (corresponding to 100 sailing days excluding port stays) to a reduced dataset of 300 data (1 sailing day) that can be efficiently handled by the available computational power. The representativeness of the reduced power profile is assessed by comparing fuel consumption and fuel cell degradation estimates obtained from the reduced dataset against those calculated using the full annual dataset. Deviations of up to ±5% in fuel consumption and fuel cell degradation between the reduced profile (300 data) and the full annual dataset (30,000 data) are considered acceptable, and the reduced representative profile can be used for the lifetime cost optimization. The ±5% tolerance reflects realistic operational variability (e.g., weather, trim changes, navigation decisions) and represents a small margin given the substantial reduction in dataset size.

Fuel consumption is calculated using Eq. (4.1):

$$F_{\mathrm{FC}}(t) = a\,P_{\mathrm{FC}}^2(t) + b\,P_{\mathrm{FC}}(t) + c \tag{4.1}$$

where $F_{\mathrm{FC}}(t)$ and $P_{\mathrm{FC}}(t)$ are the fuel consumption and the power output of the fuel cell as functions of time, respectively. The coefficients a, b, and c are 0.0066, 1.4025, and 1.8306, respectively, derived from the efficiency curve of a 100 kW stack as provided by the manufacturer [117]. It should be noted that auxiliary power consumption associated with balance-of-plant components is not included in this formulation and may lead to a slight underestimation of total fuel consumption.

The total fuel consumption of a single voyage, F_{total}, is computed in kilograms (kg) using Eq. (4.2):

$$F_{\text{total}} = N_{\text{FC}} \cdot \sum_{t=0}^{t_{\text{final}}} \left(F_{\text{FC}}(t) \cdot \Delta t \cdot k_{e\text{-}m} \right). \tag{4.2}$$

where:

- t represents discrete time steps over the power profile duration,
- $\Delta t = 0.0833$ h (5 minutes) is the sampling interval,
- $k_{e\text{-}m} = 0.03$ kg/kWh is the energy-to-mass conversion coefficient [118].

Based on [59], fuel cell degradation is dominated by transient loading effects. Therefore, a transient load-based degradation-proxy is computed as the cumulative absolute change in fuel cell power between successive time steps (Eq. (4.3)) and is used only for relative comparison of load ramping behaviour between the reduced and the full annual profile.

$$D_{\text{FC}} = \sum_{t=1}^{t_{\text{final}}} \left| P_{\text{FC}}(t) - P_{\text{FC}}(t-1) \right| \tag{4.3}$$

4.3.1.1 *Probability-based profile generation method*

The representative load profile is generated using a probability-based approach in which a probability matrix is constructed from the full annual dataset. The original dataset, consisting of 30,000 data, is structured into a matrix, where:

- Rows correspond to power changes between successive 5-minute intervals.
- Columns represent power value intervals (e.g., 0-100, 100-200…1200-1300 kW).

Each matrix entry represents the number of data that fall within a specific combination of power range and power-change category. To generate a reduced dataset, the matrix is normalized to represent the probability of occurrence of each power-level and power-change combination. For example, in the original annual dataset containing 1,000 data within the 600-700 kW power range and 0-1 kW power-change category, a reduced dataset of 300 points (corresponding to a downsampling factor of 100) should contain approximately 10 such data to preserve representativeness.

The reduced power profile is generated by random sampling from the joint probability distribution defined by the matrix. The resulting profile is then evaluated by comparing fuel consumption and fuel cell degradation estimates obtained from the reduced dataset against those calculated using the full annual profile. Deviations within predefined tolerance limits (±5%) are considered acceptable. Lower downsampling factors increase the likelihood of obtaining a representative profile within fewer iterations, but they also increase the number of data and, consequently, the computational time required for simulations.

An alternative algorithmic downsampling approach based on the Ramer Douglas Peucker (RDP) algorithm [119] was also evaluated. However, the probability-based approach is used for all analyses presented in this work. Details of the RDP-based approach are provided in Appendix A.

4.3.2 *Optimal system topology and operation*

In this section, the framework for the simultaneous design and operation optimization problem including system operation, placement and ship stability constraints is presented.

4.3.2.1 *System operation constraints*

The main energy systems required for the retrofitted hydrogen-based version include fuel cells, hydrogen tank, batteries, converters, DC switchboard, inverter, propulsion motor, and gearbox.

The operational constraints of the fuel cell system are shown in Eq. (4.4)–Eq. (4.6):

$$P_{\text{FC,min}} \leq P_{\text{FC}}(t) \leq P_{\text{FC,max}} \tag{4.4}$$

$$\left| P_{\text{FC}}(t) - P_{\text{FC}}(t+1) \right| \leq P_{\text{FC,max}} - P_{\text{FC,min}} \tag{4.5}$$

$$P_{\text{FC,initial}} = P_{\text{FC,final}} = P_{\text{FC,min}} \tag{4.6}$$

The fuel cell power is constrained within 10–100% of its rated capacity, as expressed in Eq. (4.4) [117]. Eq. (4.5) represents a ramping condition, assuming that the fuel cell can increase or decrease power across its entire operational range within successive 5-minute intervals [117]. Finally, Eq. (4.6) imposes a boundary condition, ensuring that the fuel cell power at both the initial and final time steps is maintained at the minimum level of 10 kW.

The state of charge expression for the battery (SoC_{batt}), derived from [45], is given in Eq. (4.7):

$$\text{SoC}_{\text{batt}}(t) = \text{SoC}_{\text{batt}}(t-1) - \frac{P_{\text{batt}}(t) \cdot \Delta t}{E_{\text{batt,rated}}} \tag{4.7}$$

where, $P_{\text{batt}}(t)$ is the battery power (positive indicates discharging) as a function of time, Δt is the time interval between successive measurements (5 minutes), and $E_{\text{batt,rated}}$ is the rated capacity of the battery, which is 60 kWh [84].

The constraints for the battery system are defined in Eq. (4.8)-Eq. (4.11):

$$C_{\text{rate,min}} \leq C_{\text{rate}}(t) \leq C_{\text{rate,max}} \tag{4.8}$$

$$P_{\text{batt}}(t) = C_{\text{rate}}(t) \cdot E_{\text{batt,rated}} \tag{4.9}$$

$$\text{SoC}_{\text{batt,min}} \leq \text{SoC}_{\text{batt}}(t) \leq \text{SoC}_{\text{batt,max}} \tag{4.10}$$

$$\text{SoC}_{\text{initial}} = \text{SoC}_{\text{final}} \tag{4.11}$$

The $C_{\text{rate}}(t)$ is constrained between -1 and 1, as specified in the system datasheet [84]. To minimize degradation, the battery SoC is maintained within the 20–80% range, as recommended by the manufacturer [84]. The initial and final SoC are set to 50%, ensuring energy balance without requiring shore charging. Consequently, the net battery contribution ratio accounting for the total charge and discharge power over the voyage should approach zero.

The power supplied by the system must match the demand at each time step, as shown in Eq. (4.12):

$$N_{\text{FC}} \cdot P_{\text{FC}}(t) + N_{\text{batt}} \cdot P_{\text{batt}}(t) = \frac{P_{\text{diesel}}(t)}{\eta_{\text{conv}} \cdot \eta_{\text{inv}} \cdot \eta_{m} \cdot \eta_{\text{gb}}} \tag{4.12}$$

where:

- N_{FC} and N_{batt} are the number of fuel cells and batteries, respectively (design variables).
- $P_{FC}(t)$ and $P_{batt}(t)$ are the control variables. The total fuel cell power is equally distributed to all fuel cells and the total battery power is equally shared across all batteries. Here, an optimization-based power split is used for cost evaluation, rather than the LPF-based EMS of Chapter 3 which is intended for real-time control.
- $P_{diesel}(t)$ is the original diesel engine power output as a function of time (for the direct-drive propulsion system).
- $\eta_{conv}, \eta_{inv}, \eta_m, \eta_{gb}$ are the efficiencies of converters, inverter, propulsion motor, and gearbox, respectively, required for the retrofitted hydrogen-based powertrain. The shaft efficiency and the controllable pitch propeller efficiency are assumed to be the same in the original and the new design.

The analysis includes the unidirectional fuel cell converters and the bidirectional battery converters. Each power-supply component is assigned a dedicated converter, as expressed in Eq. (4.13), Eq. (4.14):

$$N_{FC} = N_{FC,conv} \tag{4.13}$$

$$N_{batt} = N_{batt,conv} \tag{4.14}$$

4.3.2.2 *System placement*

The placement of systems within the existing engine room space must comply with guidelines and regulations set by the classification societies [120], [121]. Additionally, hydrogen-based general arrangements from other ships are referenced to guide the conceptual retrofitting of the case vessel [122].

The fuel cells are split symmetrically into two rooms (port and starboard), separated by a gastight bulkhead, in compliance with safety regulations [120], [121]. If one room is isolated after a fault, the other room can still supply power. The battery systems are placed in a dedicated space, adjacent to the fuel cell room. To enhance safety and system reliability, the converter room and the propulsion motor room (including inverter, motor and gearbox) are separated, ensuring that a failure in the main electrical distribution system does not result in complete propulsion loss.

The fuel cells, batteries and converters can be stacked in vertical groups. The lowest unit in any stack is positioned at a vertical distance of 1 meter above the keel, based on the general arrangement of the vessel, and each stack can contain up to five units. This allows sufficient vertical clearance with enough space to lift out the top unit for maintenance or replacement. All engine room compartments are designed with sufficient space for access, inspection, and maintenance, allowing for easy removal and replacement of degraded or malfunctioning components. A set of predefined feasible positions (slots) within the engine room, based on regulations and other general arrangements [120], [121], [122], is used as input to the optimization model. Each component has x (longitudinal distance from the aft

perpendicular), y (transverse distance from the centerline), and z (vertical distance from keel) coordinates. The optimization model searches over many feasible layouts and selects which slots to use for the required number of components to satisfy ship stability constraints. The engine room layout and system arrangement will be presented in the results, at Section 4.4.2.1.

To meet the vessel's energy requirements and space constraints, liquefied hydrogen (LH_2) is selected as the fuel storage method. Type-C, cylindrical LH_2 tanks are used due to their ease of construction and lower cost compared to other designs such as circular [123]. The tank volume, weight, and diameter are calculated as shown in Eq. (4.15) - Eq. (4.17):

$$v_{\mathrm{LH_2,tank}} = F_{\mathrm{total}} \cdot N_{\mathrm{trips,refuel}} \cdot v_{\mathrm{spec}} \cdot f_{\mathrm{margin,tank}} \tag{4.15}$$

$$w_{\mathrm{LH_2,tank}} = F_{\mathrm{total}} \cdot N_{\mathrm{trips,refuel}} \cdot w_{\mathrm{spec}} \cdot f_{\mathrm{margin,tank}} \tag{4.16}$$

$$D_{\mathrm{LH_2,tank}} = \sqrt{\frac{4 \cdot v_{\mathrm{LH_2,tank}}}{\pi \cdot L_{\mathrm{LH_2,tank}}}} \tag{4.17}$$

where:

- $v_{\mathrm{LH_2,tank}}$ is the volume of the LH_2 tank (m^3)
- $w_{\mathrm{LH_2,tank}}$ is the weight of the LH_2 tank (kg)
- $N_{\mathrm{trips,refuel}}$ is the number of trips before refuelling. This parameter affects the tank size and thus the ship stability
- $v_{\mathrm{spec}} = 0.0248$ m^3/kg is the volumetric specification of the LH_2 tank [88]
- $w_{\mathrm{spec}} = 8.7$ kg/kg is the gravimetric specification of the LH_2 tank [88]
- $f_{\mathrm{margin,tank}} = 1.4$ is the LH_2 tank margin factor used to account for reduced filling limits (60%) due to thermal expansion and lifetime increases in fuel consumption from system degradation, based on regulations [124]
- $D_{\mathrm{LH_2,tank}}$ is the diameter of the LH_2 tank (m)
- $L_{\mathrm{LH_2,tank}}$ is the length of the LH_2 tank (m)

The LH_2 tank is placed on the open deck between the superstructure and cargo hold to reduce the risks associated with leaks, allowing hydrogen to disperse in the atmosphere. According to regulations, the LH_2 tank should be placed at least 20% of the vessel's breadth away from the side shell plating to prevent damage from side collisions [120]. It is oriented transversally in symmetry with the centerline to minimize sloshing effects. The maximum tank length should not exceed 7.5 m. The maximum available volume for the tank placement at the upper deck is 212 m^3,without obstructing visibility from the bridge.

4.3.2.3 *Ship stability constraints*

The vessel originally used a direct-drive diesel propulsion system. For the hydrogen retrofit, the main diesel engine (11.6 tons) and 275 tons of diesel fuel, with a Vertical Center of Gravity (VCG) of 4.1 m, are removed. Furthermore, the original design required 28 tons of ballast to satisfy the stability requirements, which are recalculated for the new design. The diesel fuel tanks are structurally integrated at the bottom and sides of the vessel. Most of the original diesel fuel tanks remain unused in the hydrogen-based design. These spaces could potentially be repurposed for ballast or cargo storage. However, this would require significant structural modifications and detailed engineering assessments, which are beyond the scope of this study. For the VCG assessment, the masses and vertical moments of the removed items are subtracted and those of the new hydrogen components are added. The reduction in weight by removing 275 tons of diesel fuel significantly alters the weight distribution.

The main added components/parameters in the new design are summarized below:

- Fuel cells (primary energy source)
- Batteries (low-load support and peak-shaving)
- Converters, inverters, DC switchboard and propulsion motor
- Gearbox
- LH_2 tank and hydrogen fuel
- Ballast to satisfy stability requirements

To minimize additional investment costs and maintain efficiency under varying load conditions, the original controllable pitch propeller is retained in the hydrogen-powered design.

In the event of a major failure in the hydrogen-based system, the vessel has an emergency diesel generator located in a dedicated compartment at the aft end of the superstructure.

As stated in [122], a weight margin factor of 2% of original lightship (23.4 tons) is applied in the retrofitted design to account for increased weight due to:

- Structural reinforcements required for the integration of hydrogen storage tank and fuel cell systems.
- Additional auxiliary and safety systems (ventilation, fire suppression etc.) necessary for compliance with operational and regulatory standards.

The new total weight of the vessel after the removal and the addition of the necessary systems is computed as shown in Eq. (4.18):

$$W_{\text{new,total}} = W_{\text{original}} - W_{\text{removed}} + W_{\text{added}} \tag{4.18}$$

The total new weight ($W_{\text{new,total}}$) is constrained to remain within $\pm 5\%$ of the original total weight of the diesel-based version with the use of the required amount

of ballast. This ensures that the retrofitted and original designs maintain similar hydrodynamic resistance and propulsive power requirements.

The following equations and constraints are related to ship stability analysis. The Vertical Center of Gravity of each component (VCG_i) is the distance from its geometric center to the keel of the vessel and the total VCG is calculated based on the ratio of the sum of contributions of the vertical moments and weights (w) of the systems, as shown in Eq. (4.19):

$$VCG = \frac{\sum_i (w_i \cdot VCG_i)}{\sum_i w_i} \tag{4.19}$$

According to the stability booklet of the case ship, the total VCG of the vessel should not exceed 5.044 m. When a vessel's tank (fresh water, ballast, hydrogen etc.) is partially filled, the liquid's movement causes a virtual rise in the VCG, impacting stability. This free surface moment (FSM) effect is calculated using Eq. (4.20):

$$FSM_{\text{tank}} = I_{\text{tank}} \cdot \rho \tag{4.20}$$

where:

- I_{tank} is the transverse moment of inertia of a tank (m^4)
- ρ is the liquid density (ton/m^3)

For the retrofitted design FSM_{new} is computed as shown in Eq. (4.21):

$$FSM_{\text{new}} = FSM_{\text{original}} - FSM_{\text{diesel}} + FSM_{\text{LH}_2,\text{tank}} + FSM_{\text{ballast}} - FSM_{\text{ballast,removed}} \tag{4.21}$$

where:

- FSM_{original} is the total FSM of the diesel-based version.
- FSM_{diesel} is the FSM contribution from the removed diesel fuel.
- $FSM_{\text{LH}_2,\text{tank}}$ is the FSM effect from the added hydrogen fuel.
- FSM_{ballast} is the FSM contribution of the additional ballast required in the new design to ensure compliance with the stability regulations. To minimize FSM effects, ballast tanks are assumed to remain fully filled throughout the voyage.
- $FSM_{\text{ballast,removed}}$ is the FSM contribution of removed ballast from the original design.

The FSM for a half-filled cylindrical LH_2 tank is calculated using Eq. (4.22), Eq. (4.23):

$$FSM_{\text{LH}_2,\text{tank}} = I_{\text{LH}_2,\text{tank}} \cdot \rho_{\text{LH}_2} \tag{4.22}$$

$$I_{\text{LH}_2,\text{tank}} = \frac{1}{12} D^3_{\text{LH}_2,\text{tank}} \cdot L_{\text{LH}_2,\text{tank}} \tag{4.23}$$

The virtual rise in VCG (GG') captures the effect of FSM on the VCG. It is computed as shown in Eq. (4.24):

$$GG' = \frac{FSM_{\text{new}}}{W_{\text{new,total}}} \tag{4.24}$$

In the homogeneously loaded condition, additional ballast can be placed in the existing water ballast tanks of the vessel. To prevent excessive heeling moments, ballast is distributed symmetrically in the transverse direction, with one tank on the port side and another on the starboard side. To determine the optimal ballast configuration, various tank placement combinations along the vessel's length are evaluated. The inclusion of ballast configuration selection introduces a combinatorial aspect to the optimization problem, as it requires the evaluation of discrete combinations of ballast arrangements (amount and position of ballast required to satisfy stability constraints).

The longitudinal center of gravity (LCG) is a key parameter in assessing the trim of the retrofitted vessel. It is measured from the aft perpendicular, and can be computed as shown in Eq. (4.25):

$$LCG = \frac{\sum_i (w_i \cdot LCG_i)}{\sum_i (w_i)} \tag{4.25}$$

The trim (m) represents the difference between vessel's aft and forward drafts, and is calculated using Eq. (4.26):

$$Trim = \frac{(LCG - LCB) \cdot W_{\text{total}}}{MCT \cdot 100} \tag{4.26}$$

where:

- LCB is the longitudinal center of buoyancy (m),
- W_{total} is the total displacement of the vessel (tons),
- MCT is the moment to change trim (ton·m/cm).

The vessel is designed to operate at specific trim values to minimize hydrodynamic resistance and fuel consumption. Although IMO regulations do not specify mandatory trim constraints, maintaining a trim deviation within +/- 0.05 meters from the original design, as shown in Eq. (4.27), can be critical for optimal performance.

$$|Trim_{\text{new}} - Trim_{\text{original}}| \leq 0.05 \text{ (m)} \tag{4.27}$$

The original trim value in the homogeneous loaded condition is -0.42 meters, where the negative sign indicates a trim by stern. The LCB and MCT values are derived from the hydrostatic data in the vessel's stability booklet. For the retrofitted hydrogen-based design, they are obtained using linear interpolation, within the optimization framework, based on the new displacement $W_{\text{new,total}}$.

The following stability constraints in Eq. (4.28)–Eq. (4.33), based on IMO regulations, must be satisfied for the case vessel. These constraints apply to both the original and the retrofitted design:

$$GM = KM - VCG > 0.3 \text{ (m)} \tag{4.28}$$

$$GZ_{\max} > 0.2 \text{ (m)} \tag{4.29}$$

$$\varphi\left(GZ_{\max}\right) > 25^{\circ} \tag{4.30}$$

$$Area_{GZ:(0^{\circ}-30^{\circ})} > 0.055 \text{ (m·rad)} \tag{4.31}$$

$$Area_{GZ:(0^{\circ}-40^{\circ})} > 0.090 \text{ (m·rad)} \tag{4.32}$$

$$Area_{GZ:(30^{\circ}-40^{\circ})} > 0.030 \text{ (m·rad)} \tag{4.33}$$

where:

- GM is the distance between the vessel's center of gravity and its transverse metacenter (a virtual point where the vertical lines of upright and heeled centers of buoyancy intersect). GM represents the initial stability of the vessel and it should be at least 0.3 meters for sufficient transverse stability.
- KM is the distance between the keel of the vessel and its transverse metacenter. KM is determined from the hydrostatic tables similar to LCB and MCT, and it depends on the ship's hull shape and displacement.
- GZ righting arm is the horizontal distance between the vessel's center of gravity and the vertical line passing through the center of buoyancy when the ship is heeled at an angle φ.

The GZ at a certain heeling angle φ is determined using Eq. (4.34):

$$GZ(\varphi) = (KN - VCG) \cdot \sin(\varphi) \tag{4.34}$$

where:

- the $KN \cdot \sin(\varphi)$ values from the cross curves of stability represent the horizontal lever from the keel to point N, the intersection of the buoyant-force line with the ship's centerline plane.

The $KN \cdot \sin(\varphi)$ values are provided in the stability booklet of the case vessel for various displacements at the heeling angles of 0, 2, 5, 10, 12, 15, 20, 30, 40, 50, and 60 degrees. Linear interpolation can be performed similarly to KM, LCB, and MCT to obtain the KN values at the corresponding displacements.

The GZ–φ curve is a graphical representation of the ship's stability characteristics at different heeling angles. The IMO has imposed constraints for certain areas under the GZ curve (0°–30°, 0°–40°, and 30°–40°), as shown in Eq. (4.31)–Eq. (4.33). These areas can be estimated using the trapezoidal rule [125]. This method approximates the integral of the function $GZ(\varphi)$ over an interval $[\varphi_i, \varphi_{i+1}]$. The total area under the curve over a set of n intervals is obtained by summing the contributions over each interval, as shown in Eq. (4.35):

$$\text{Area}_{GZ:(\varphi_1-\varphi_2)} = \frac{1}{2} \cdot \sum_{i=1}^{n} \big(GZ(\varphi_i) + GZ(\varphi_{i+1}) \big) \cdot (\varphi_{i+1} - \varphi_i) \tag{4.35}$$

where φ_i and φ_{i+1} are consecutive heel values (in radians) within the range of φ_1 to φ_2.

The stability constraints (*VCG*, *trim* etc.) are active constraints within the optimization framework. The model searches over many feasible layouts and selects positions for the components and ballast in order to satisfy these constraints.

4.3.2.4 *Optimization objective function*

The objective function to be minimized is the total lifetime cost which consists of:

- Capital expenditure (CAPEX) – the initial investment cost.
- Net present value of operational expenditures (NPV_{OPEX}) – discounted to account for the time value of money over the vessel's lifetime.

The relationship is expressed mathematically as shown in Eq. (4.36):

$$\min_{(N_{\text{FC}}, N_{\text{batt}}, P_{\text{FC}}(t), P_{\text{batt}}(t))} \left(\text{CAPEX} + \text{NPV}_{\text{OPEX}}\right) \tag{4.36}$$

The CAPEX is calculated as shown in Equations Eq. (4.37)–Eq. (4.39):

$$\text{CAPEX} = \text{CAPEX}_{\text{systems}} + \text{CAPEX}_{\text{tank}} \tag{4.37}$$

$$\text{CAPEX}_{\text{systems}} = \sum_{\text{systems}} \left(N_{\text{system}} \cdot P_{\text{system,rated}} \cdot C_{\text{system}}\right) \tag{4.38}$$

$$\text{CAPEX}_{\text{tank}} = F_{\text{total}} \cdot N_{\text{trips,refuel}} \cdot f_{\text{margin,tank}} \cdot C_{\text{tank}} \tag{4.39}$$

where:

- *system* refers to engine room main components (fuel cells, batteries, converters, inverter, motor, gearbox).
- N_{system} is the number of units for each system.
- $P_{\text{system,rated}}$ is the rated power (kW).
- C_{system} is the investment cost per unit capacity (\$/kW).
- C_{tank} is the tank cost per unit mass of stored LH_2 (\$/kg).

Eq. (4.39) links the LH_2 tank CAPEX to the required mass of hydrogen stored onboard between refuelling events, $F_{\text{total}} \cdot N_{\text{trips,refuel}}$, adjusted by $f_{\text{margin,tank}}$ to account for reduced filling limits and lifetime increase in fuel consumption. The resulting required stored hydrogen mass is multiplied by C_{tank} (\$/kg LH_2 stored) to obtain the tank capital cost. This formulation ensures that the tank CAPEX scales directly with the hydrogen storage requirement.

The CAPEX values for the components are derived from the authors' previous study [59], which documents the full cost methodology, source breakdown, and applicable reference years for each cost input. Depending on the component, cost values are taken from peer-reviewed literature, industry/vendor data, or forward-looking projections from energy-transition reports. Therefore, reference years differ across cost items. Uncertainty in rapidly changing costs (e.g., hydrogen price) is handled through sensitivity analysis in this study.

The NPV_{OPEX} includes fuel expenses, maintenance and component replacement costs over the vessel's remaining lifetime after retrofitting. It is calculated using Eq. (4.40):

$$\begin{aligned} NPV_{\text{OPEX}} = & \sum_{t=1}^{T} \left(\frac{F_{\text{annual},t} \cdot C_{h2}}{(1+r)^t} \right) \\ & + \left(\frac{b_{\text{FC,replace},t} \cdot N_{\text{FC}} \cdot P_{\text{FC,rated}} \cdot C_{\text{FC,replace}}}{(1+r)^t} \right) \\ & + \left(\frac{b_{\text{batt,replace},t} \cdot N_{\text{batt}} \cdot E_{\text{batt,rated}} \cdot C_{\text{batt,replace}}}{(1+r)^t} \right) \\ & + \left(\frac{\sum C_{\text{system,maint},t}}{(1+r)^t} \right) \end{aligned} \tag{4.40}$$

where:

- F_{annual} is the annual fuel consumption (kg/year)
- C_{h2} is the hydrogen price with a baseline value of 6$/kg [59].
- $r = 5\%$ is the discount rate [59]
- t is the time index (in years)
- $T = 20$ years is the remaining lifetime of the vessel after retrofitting
- $b_{\text{FC,replace},t}$ is the binary variable for fuel cell replacement in year t. According to the manufacturer, the fuel cells are replaced after 20,000 operating hours [89], [117]
- $b_{\text{batt,replace},t}$ is the binary variable for battery replacement in year t. The batteries are assumed to be replaced every 7 years based on the authors' previous study [59]
- $C_{\text{FC,replace}}$ and $C_{\text{batt,replace}}$ ($/kW) are the replacement costs for fuel cells and batteries respectively, assumed to be 50% of their initial CAPEX, based on projected cost reductions due to technological advancements and increased market adoption [59]
- $C_{\text{system,maint},t}$ ($/kW/year) is the annual maintenance cost of each system, obtained from [59]

The annual fuel consumption is initially determined based on the total fuel consumption per trip and the number of trips per year, as shown in Eq. (4.41):

$$F_{\text{annual}} = F_{\text{total}} \cdot N_{\text{trips,annual}} \tag{4.41}$$

The number of annual trips $(N_{\text{trips,annual}})$ is 200, with the power demand data of 100 sailing days, from Fig. 4.2, repeated twice every year.

To capture the effects of fuel cell degradation and hydrogen boil-off losses, the fuel consumption is calculated annually using a boil-off loss factor (b_{h2}) and a degradation factor (d). A 0.2% daily loss of stored hydrogen due to boil-off is assumed, based on [126]. For the boil-off factor (b_{h2}), the cumulative hydrogen loss

per refuelling cycle is calculated. To simplify the model, a constant boil-off factor is assumed over time, under the assumption that periodic tank inspections and regular insulation upgrades mitigate long-term changes in boil-off rates.

The degradation factor (d) is derived from the relationship between voltage drop and fuel consumption increase. The nominal cell voltage is 0.7 V, and fuel cell replacement occurs when the voltage drops by 10% from its nominal value [29]. Fuel cell degradation is represented using a simplified lifetime-based approach rather than a detailed physics-based model. This avoids relying on degradation coefficients reported in the literature that are primarily derived from automotive operating conditions (e.g., Ref. [82]) and may lead to unreliable results for maritime operation. The fuel cell is assumed to experience a total voltage drop of 10% over its operational lifetime [29], at which point replacement occurs according to the manufacturer provided lifetime limits (20,000 operating hours), corresponding to approximately 4 years under the considered operational profile. The total voltage drop is therefore distributed uniformly over the replacement interval, and the annual voltage drop, (dV_{annual}), is calculated as the total allowable voltage drop divided by the number of years until replacement (Eq. (4.42)). This constant annual voltage drop is then used to approximate the annual increase in fuel consumption due to degradation, which is a critical contributor to total lifetime cost.

$$dV_{\text{annual}} = \frac{dV_{\text{total}}}{Y_{\text{replace}}} \tag{4.42}$$

where:

- $dV_{\text{total}} = 10\% \cdot 0.7 = 0.07$ V is the total voltage drop
- Y_{replace} is the number of years until replacement

This lifetime-based degradation formulation is used only in the lifetime cost model and is distinct from the transient load-based degradation proxy used in Section 4.3.1 to assess the representativeness of the reduced power profiles.

Fuel cell efficiency, η_{FC}, is directly proportional to its operating voltage [127] and shown in Eq. (4.43):

$$\eta_{\text{FC}} = \frac{V_{\text{cell}}}{V_{\text{reversible}}} \tag{4.43}$$

where:

- $V_{\text{cell}} = 0.6$–0.8 V is the actual cell operating voltage [117]
- $V_{\text{reversible}} = 1.23$ V is the theoretical reversible voltage under ideal conditions

Since hydrogen consumption is inversely proportional to efficiency for a given power output, the annual increase in fuel consumption due to degradation can be approximated by Eq. (4.44):

$$\frac{dF}{F_{\text{annual,initial}}} \cong \frac{dV_{\text{annual}}}{V_{\text{cell,nominal}}} \tag{4.44}$$

where:

- dF is the annual increase in fuel consumption

- $F_{\text{annual,initial}}$ is the initial annual fuel consumption
- $V_{\text{cell,nominal}} = 0.7$ V is the nominal cell voltage

Thus, the degradation factor (d) is obtained from Eq. (4.45):

$$d = 1 + \frac{dF}{F_{\text{annual,initial}}} \tag{4.45}$$

The annual fuel consumption over the vessel's operational lifetime (T) is computed iteratively, incorporating both boil-off losses and degradation effects, as shown in Eq. (4.46):

$$F_{\text{annual},t} = F_{\text{annual},t-1} \cdot (1 + b_{h2}) \cdot d \tag{4.46}$$

After fuel cell replacements, the annual fuel consumption is reset to its original value. This approach ensures that the model dynamically captures the combined effects of fuel cell degradation and boil-off losses while maintaining realistic operational assumptions regarding fuel cell lifespan and system replacements.

The key model variables and parameters for the cost optimization and stability analysis are summarized in Table 4.1.

Table 4.1: Main optimization parameters

Design/control variables and cost parameters	
N_{FC}	Number of fuel cells – design variable
N_{batt}	Number of batteries – design variable
P_{FC}	Fuel cell power – control variable (kW)
P_{batt}	Battery power – control variable (kW)
SoC_{batt}	Battery state of charge (%)
F_{total}	Voyage fuel consumption (kg)
$N_{\text{trips,annual}}$	Number of annual trips
CAPEX	Capital expenses ($)
NPV_{OPEX}	NPV of Operational Expenses ($)
C_{system}	System cost per unit ($/kW)
$C_{\text{FC,replace}}$	Fuel cell replacement cost ($/kW)
$C_{\text{batt,replace}}$	Battery replacement cost ($/kW)
$C_{\text{system,maint}}$	System maintenance cost ($/kW/year)
C_{h2}	Green hydrogen price ($/kg)
b_{h2}	Boil-off factor
d	Degradation factor
System placement and stability parameters	
x, y, z	Component / ballast coordinates (m)
$N_{\text{trips,refuel}}$	Number of trips before refuelling
$D_{\text{LH2,tank}}$	Diameter of hydrogen tank (m)
w	Weight of each system (kg)
VCG	Vertical center of gravity (m)
FSM	Free surface moment (ton·m)
GG'	Virtual rise in VCG (m)
GM	Metacentric height (m)
KM	Keel-to-metacenter distance (m)
GZ	Righting lever (m)
φ	Heeling angle (°)
LCG	Longitudinal center of gravity (m)
LCB	Longitudinal center of buoyancy (m)
MCT	Moment to change trim (ton·m/cm)
Trim	Trim of the vessel (m)

4.3.2.5 *Optimization solver*

The framework is a MINLP optimization with combinatorial aspects that is solved using the SCIP solver.

- Mixed-integer: binary, integer, and continuous variables for decision making.
- Nonlinear: Bilinear terms with the product of design and control variables introducing non-convexity (Eq. (4.12),Eq. (4.2)).
- Combinatorial: Discreet selection of configurations from a set of predefined feasible positions (slots) (system placement in the engine room, and selection of ballast amount and position to satisfy stability constraints).

SCIP is an open-source solver developed for MILP and MINLP problems. It is used in this study to manage the complexity of the optimization problem and provide high-quality solutions. SCIP solves MINLPs to global optimality using a spatial branch-and-bound algorithm, which combines branch-and-infer and branch-and-cut methods [128]. The key techniques utilized by SCIP include:

- Pre-solving: Simplifies the problem (to improve computational efficiency) by removing redundant variables and constraints, and tightening bounds.
- Branch-and-bound exploration: Divides the problem into smaller subproblems by branching on variables. Each subproblem is solved using linear or nonlinear relaxations to compute dual bounds, guiding the search toward the optimal solution.
- Cutting planes: Adds linear or nonlinear cuts to eliminate infeasible or suboptimal regions, tightening the relaxation and reducing the search space.
- Heuristics: Uses primal heuristics to quickly identify good feasible solutions, reducing the optimality gap and accelerating convergence.

During the solution process, SCIP continuously updates the primal bound (best feasible solution found up to a certain point) and the dual bound (best possible solution from relaxations). Convergence is achieved when the difference between the two (optimality gap) is zero, which indicates that the optimal solution has been found. In this study, SCIP was run with a 0% optimality-gap termination criterion.

Heuristic and metaheuristic solvers such as genetic algorithms are widely used for the optimal design of ship energy systems [45]. These methods rely on stochastic processes and can provide good solutions but without any guarantee of global optimality. They often require extensive computational resources and fine-tuning to achieve satisfactory results. Unlike heuristic methods, SCIP uses a branch-and-bound algorithm that enables effective exploration of the solution space without excessive computational demands, making it a reliable choice for this application [128].

4.4 RESULTS AND DISCUSSION

4.4.1 *Power profile analysis results*

The representative load profile, shown in Fig. 4.3, was synthesized using the probability-based profile generation method.

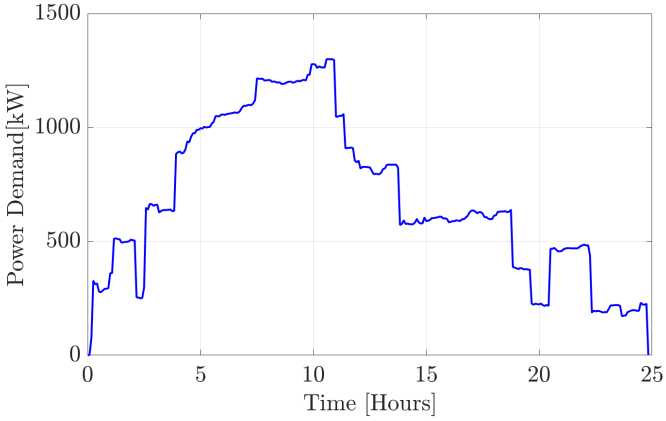

Figure 4.3: Representative profile generated using the probability-based profile generation method

To enable direct comparison with the full annual dataset, the reduced profile was scaled up using the downsampling factor to ensure both profiles cover the same duration. The resulting deviations are 0.33% in fuel consumption and 4% in fuel cell degradation relative to the annual profile, both within the ±5% acceptance threshold.

Due to the stochastic nature of the sampling procedure, the profile generation was repeated ten times, and the reduced one-day profile shown in Fig. 4.3 was selected based on minimal deviations from the full annual dataset. This representative profile is subsequently used in the lifetime cost optimization.

The statistics of the power levels and load ramps for the full annual profile and the representative profile generated using the probability-based method are presented in Appendix B.

4.4.2 *Energy system topology and lifetime cost optimization results*

Section 4.4.2.1 focuses on the system selection and arrangement , and Section 4.4.2.2 presents the optimization (cost and stability) results. Finally, in Section 4.4.2.3, alternative design arrangements are discussed.

4.4.2.1 *System selection and placement*

The selected 100-kW proton exchange membrane fuel cell stack operates within an efficiency range of 48-62% and exhibits high specific power and power density compared to other fuel cells [117], [89]. At the beginning of life, the peak power output of the stack is 120 kW. Over its operational lifespan, degradation leads to a 17% reduction in peak power, resulting in a rated power of 100 kW at the end of life [117], [89].

The variable fuel cell output voltage requires regulation via DC-DC converters to ensure stable integration with the ship's power system [129]. For compatibility between fuel cells and converters, the output voltage and current ranges of the fuel cell must align with the input specifications of the unidirectional converter. The converters must regulate the output voltage to the DC bus level of 700 V. The same fuel cell and converter systems were utilized in the conceptual design of a hydrogen fuelled ferry [89], [130]. According to Bye et al. [130], the lowest recorded converter efficiency at end-of-life conditions was 98.2%. Therefore, a DC-DC converter efficiency of 98.5% is assumed in this study.

A 60-kWh lithium-iron phosphate battery pack, with a nominal output voltage of 576 V, is selected for low-load support and peak-shaving [84]. The same DC-DC converter hardware can be used in unidirectional mode for the fuel cells and in bidirectional mode for the batteries, allowing onboard charging from excess fuel cell power [129].

The 700-V DC switchboard distributes current from power sources to consumers via converters and inverters [131]. It consists of: the main busbars, bus-tie breaker, connection points for power supply and consumer modules, circuit breaker, fuses, and additional control/monitoring equipment.

The DC-AC converter (inverter), also referred to as variable frequency drive, converts DC power from the switchboard into AC power for the electric propulsion motor. A 1400-kW AC induction motor (AMI 500L8W) is selected to cover the peak propulsive power demand (Fig. 4.3), and an additional margin for increased power demand [132]. Based on the representative load profile (Fig. 4.3) and the equipment specifications, the motor is expected to operate with an average efficiency of 96% [132].

A 1400 kW inverter (ACS880-104LC) is selected for motor control, with an average efficiency of 98.5% [133]. The inverter and motor nominal voltages are matched at 690 V. The inverter's nominal output current exceeds the motor's current, ensuring its capability to operate under full-load conditions. The inverter also supports frequency control of 50 Hz, with potential variations depending on the inverter settings.

A gearbox is required to match the propeller's rotational speed with the motor's output speed. At the most frequent operating speed range of 9-11 knots, the controllable pitch propeller operates at 110-150 revolutions per minute (rpm). To achieve compatibility, the gearbox must reduce the motor speed from 750 rpm to approximately 130 rpm, requiring a reduction ratio of 5.76. A continuous- duty gearbox (MGN 2026V) rated at 1489 kW, with a 6:1 reduction ratio is selected to align the motor and propeller speeds [134]. A gearbox efficiency of 98% is assumed based on [135].

The optimization model was solved with the SCIP solver, achieving a 0% optimality gap. The optimal propulsion system design consists of 14x100 kW fuel cells and 3x60 kWh batteries. The final retrofitted configuration, including all the main systems and their locations within the engine room compartments, is shown in Fig. 4.4.

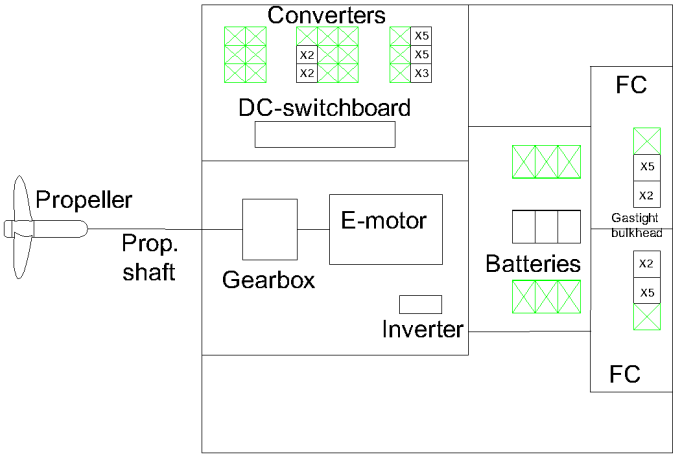

Figure 4.4: Engine room layout for the optimal propulsion system design

The portable water tanks are positioned at the sides of the vessel, outside the illustrated machinery compartments, as per the original design.

Green boxes with 'X' represent positions available for placement that were not chosen by the optimization model. All other boxes contain the number of units that are placed in the specific positions for each system category (fuel cells, batteries, converters etc.).

Each fuel cell room contains seven modules, separated by a gastight bulkhead. The fuel cells are arranged symmetrically about the centerline and stacked vertically in groups of up to five units. The three battery modules are located in a dedicated compartment adjacent to the fuel cell rooms and positioned along the centerline ($y = 0$) to minimize transverse moment effects. The fuel cell converters and battery converters are located in the electrical machinery room. The inverter, motor, and gearbox are installed in the propulsion room. Some of the fuel cells and fuel cell converters are arranged in five-module vertical stacks, highlighting their limited influence on the vessel's vertical stability. Auxiliary and safety-related equipment can be accommodated within separate compartments or in the remaining available spaces of the engine room. It should be noted that the specific placement of components represents one feasible configuration identified by the optimization model, and alternative arrangements may also satisfy the imposed placement and stability constraints.

Several propulsion system arrangements were evaluated before selecting the final configuration:

- Single motor–gearbox in-line with the propeller shaft and propeller – This is the simplest configuration incorporating the fewest number of components.
- Offset configuration with dual motor–dual gearbox perpendicular to a single propeller shaft – This configuration provides increased component redundancy but introduces shaft alignment challenges, motor synchronization issues, and limited engine room space.
- Dual-shaft, twin-screw, dual-motor–gearbox – This configuration offers maximum propulsion redundancy, but requires significant design modifications and detailed hydrodynamic analysis to retrofit the original single-shaft diesel-based design.
- Single shaft, dual-motor, single/dual gearbox configuration – This configuration limits the available horizontal engine room space and introduces complexities in motor synchronization.

The inline configuration with a single motor, gearbox, shaft and propeller was chosen due to its: simplicity, lower cost, reduced weight, ease of access and maintainability. This arrangement also provides sufficient space for auxiliary and safety equipment without introducing challenges related to motor synchronization and shaft alignment. Furthermore, propulsion system redundancy is not a primary design criterion, as the original diesel-based design utilized a similar configuration. Consequently, in the event of a motor or drive failure, propulsion would be unavailable, consistent with the original single-engine, single-shaft propulsion architecture, requiring standard emergency procedures.

4.4.2.2 *Optimal cost and stability results*

The total lifetime energy system cost of the optimal design (14x100 kW fuel cells, and 3x60 kWh batteries) is estimated at 22.9$ million. The contributions of individual cost categories to the total cost are illustrated in Fig. 4.5.

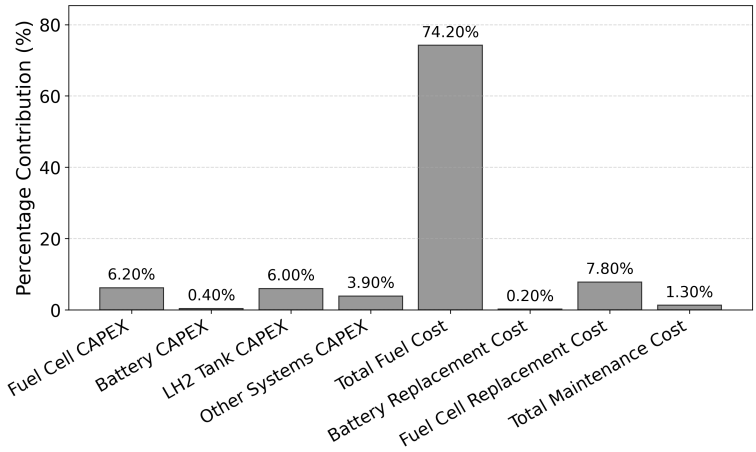

Figure 4.5: Cost contributions to total lifetime cost

Fuel cost is the dominant contributor to total lifetime cost accounting for 74.2%. Since hydrogen consumption is price-inelastic for the selected configuration, total lifetime cost scales proportionally with hydrogen price. Consequently a ±x% change in hydrogen price leads to a ±0.742x% change in total lifetime cost (e.g., a 50% increase in hydrogen price results in a 37.1% increase in total lifetime cost). Total CAPEX (including replacement costs) accounts for 24.5% of the total lifetime cost. The 'Other Systems CAPEX' category (Fig. 4.5) includes investment costs for converters, inverter, motor and gearbox. The battery system and the total maintenance costs of all systems contribute minimally to the total lifetime cost.

The optimal power distribution between the fuel cells and the batteries is shown in Fig. 4.6.

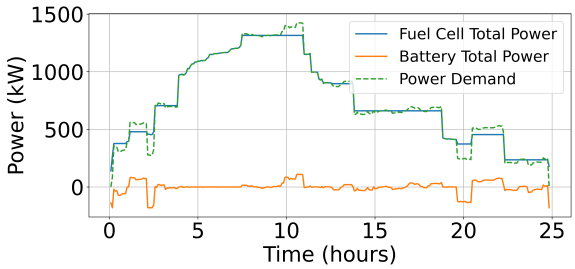

Figure 4.6: Optimal power distribution between fuel cells and batteries

At the beginning and end of the voyage, the batteries are charged using excess fuel cell power, since the fuel cells cannot operate below 10% of their rated power. Throughout the voyage, the fuel cells provide the majority of the power demand, while the batteries are mainly used for low-load support and peak shaving. At the end of the voyage, the battery is charged back to 50%, as shown in Fig. 4.7, to avoid shore charging due to limited available infrastructure.

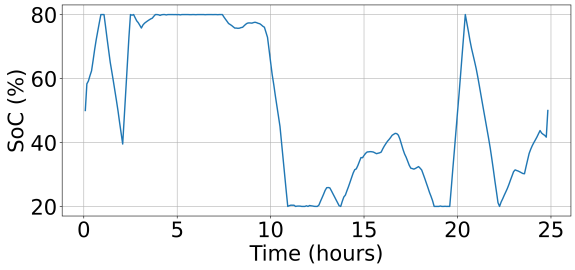

Figure 4.7: Battery SoC

The total fuel consumption, F_{total}, after retrofitting, is 1049.3 kg per trip. The annual fuel consumption variations, including fuel cell degradation and boil-off effects are depicted in Fig. 4.8. There is a 2.5% annual increase in fuel consumption due to fuel cell degradation, and a 0.8% increase in the required hydrogen consumption due to cumulative boil-off per refueling cycle. The annual hydrogen consumption

increases up to years 4, 8, 12, 16, and 20. At the fuel cell replacement intervals, the consumption is reset to its initial value and the same increasing trend is repeated in the subsequent cycle.

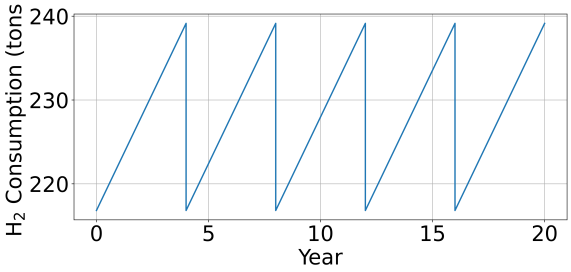

Figure 4.8: Annual fuel consumption changes

The LH_2 tank is placed at the open deck with a VCG of 10.5 meters. It weighs 51.1 tons, and its volume is 146 m^3, with a diameter of 4.97 meters. With this tank size, the vessel requires refueling every 4 sailing days (voyages). Furthermore, there is sufficient space at the upper deck for equipment inspection and maintenance. To satisfy the trim and vertical stability constraints, the vessel requires 171.5 tons of ballast with a VCG at 0.53 meters and an LCG of 26.67 meters. The total weight of the main engine room components in the retrofitted design (fuel cells, motor etc.) is 15.3 tons which is only 3.7 tons higher than the original diesel engine. After retrofitting, the vessel's total weight decreases by 1%, from 4835.8 tons to 4786.8 tons.

The LH_2 tank and the ballast placement significantly impact the vessel's stability, while the engine room components have minor effects due to their low weight compared to the total ship displacement. However, in ship designs with similar installed power but significantly smaller displacement (e.g., ferries), the positioning of engine room components is expected to have a more pronounced impact on stability.

The stability results for the homogeneous loaded departure condition (for the retrofitted design) are summarized in Table 4.2 and the GZ curve is shown in Fig. 4.9.

Table 4.2: Stability results for the retrofitted vessel

Parameter	Value	Criterion
VCG	5.01 (m)	< 5.044
GM	0.36 (m)	> 0.3
$GZ_{\max}$	0.55 (m)	> 0.2
$\varphi(GZ_{\max})$	50°	$> 25°$
$\text{Area}_{GZ:(0°-30°)}$	0.068 (m·rad)	> 0.055
$\text{Area}_{GZ:(0°-40°)}$	0.136 (m·rad)	> 0.090
$\text{Area}_{GZ:(30°-40°)}$	0.068 (m·rad)	> 0.030
$Trim_{\text{new}}$	-0.39 (m)	± 5 cm

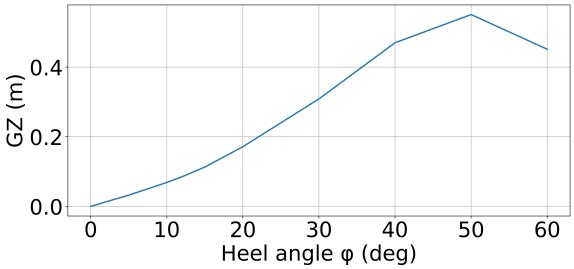

Figure 4.9: GZ curve

Table 4.2 presents the stability results for the homogeneous loaded departure condition, confirming compliance with the IMO intact stability criteria. The GZ curve and underlying area were validated against the original diesel-powered vessel to ensure minimal errors from the trapezoidal rule. Stability checks were also conducted for homogeneous loaded arrival and ballast conditions to verify regulatory compliance. In the ballast departure condition the GM of the vessel is 1.74 meters, which is much higher than the minimum of value of 0.3 meters required by the regulations. The trim of the vessel can be adjusted in laden arrival, ballast departure and arrival conditions by rearranging the ballast.

4.4.2.3 *Alternative design arrangements*

The impacts of various design choices on the optimization results are analyzed below, to offer insights into alternative design considerations and arrangements.

Removing one fuel cell or one battery from the optimal design does not satisfy the optimization constraints (infeasible problem) due to insufficient energy supply at peak loads, and insufficient low-load support respectively. Adding one additional 100-kW fuel cell in the optimal design reduces fuel cost by 1.4% through more efficient operation at lower power levels, but increases CAPEX by 2.8%, resulting in a 0.06% rise in total lifetime cost. Incorporating an additional 60-kWh battery reduces fuel cost by 0.1%, but raises CAPEX by 1.1%, leading to a total cost increase

of 0.19%. Further increases of system capacity result in higher total lifetime costs since the CAPEX increase outweighs the reductions in fuel consumption cost from more fuel-efficient operation at lower fuel cell power levels. From the above, further assurance can be obtained that the configuration of 14x100 kW fuel cells and 3x60 kWh batteries is the global optimum.

Placing a single LH_2 tank below the main deck could further improve stability by lowering the VCG. However, this would reduce available cargo space by approximately 10% and require additional auxiliary systems, safety equipment, and structural reinforcements, thereby increasing total cost. Alternatively, dividing the hydrogen storage into two tanks could improve redundancy and reliability in case of failure. However, due to space constraints on the upper deck, one tank would need to be placed on the open deck and the other in the cargo space. This arrangement complicates equipment routing and auxiliary system integration, increases boil-off rates (due to smaller tank diameters), and raises total system CAPEX [123],[124]. Placing an LH_2 tank below the open deck is a viable option for vessels with limited deck space and high VCG, such as containerships. For such designs, exploring different tank shapes and layouts could optimize fuel storage utilization [136].

Compared to Chapter 3, where a real-time LPF control-based approach was used for system and cost evaluation, the present analysis in this chapter introduces a probability-based profile synthesis and a MINLP optimization framework for combined system sizing, operation and spatial arrangement. Despite differences in system operation, particularly in the fuel cell dispatch, which shifts from load-following in Chapter 3 to a more optimized operating pattern that reduces transient loading (in this chapter), as well as the role of the battery, which shifts from load smoothing and ramp support to peak shaving, the resulting cost trends remain generally consistent, supporting the validity of both approaches. However, the inclusion of stability and placement constraints leads to different design outcomes. In particular, the optimized LH_2 tank size is reduced to approximately 145 m^3 as larger capacities required to cover the most demanding voyage (e.g., 193 m^3 in Chapter 3) are not compatible with the imposed design and stability constraints. This highlights a key trade-off between operational range and feasible design integration. Overall, the present analysis in this chapter provides additional design-level insights by linking system sizing, operation, and spatial feasibility.

4.5 CONCLUSION

This chapter presents a holistic framework for optimal ship system design and operation. The novelty of this chapter is that it incorporates a power profile analysis and synthesis method, energy system topology, ship stability, and lifetime cost minimization in a unified optimization framework. The original diesel mechanical propulsion system of a general cargo vessel is retrofitted with hydrogen fuel cells and batteries to lower its environmental footprint. Given the urgent need to decarbonize existing fleets to meet IMO emission targets, this study offers valuable insights into the retrofitting of conventional vessels with novel energy systems. Additionally, the versatility of the optimization model allows it to be adapted for the design of newbuild vessels with minimal modifications.

The following key results can be summarized:

- The probability-based profile generation approach produced a downsampled load profile with deviations of less than 5% in fuel consumption and fuel cell degradation compared to the original annual propulsive power data, enabling computationally efficient lifetime cost optimization with minimal loss of accuracy.
- The optimal configuration includes 14×100 kW fuel cells and 3×60 kWh batteries. The batteries support low-load operations and peak shaving, and they are charged from excess fuel cell power, without requiring shore charging. Oversizing either fuel cells or batteries was found to increase total lifetime cost, as the additional CAPEX outweighs fuel cost savings achieved through more fuel-efficient operation.
- The retrofitted design includes a single LH_2 tank (146 m^3, 4.97 m diameter) placed on the main deck with a VCG of 10.5 m, providing a range of 4 days without refuelling.
- The total ship weight of the retrofitted design is 1% lower than the original diesel-based version with the use of the necessary amount of ballast.
- The optimal retrofitted design satisfies all vertical stability and trim constraints using 171 tons of ballast at a VCG of 0.53 m and an LCG of 26.67 m in the homogeneous loaded condition. For this vessel, retrofit feasibility primarily depends on LH_2 storage sizing/placement, which directly determines ballast requirements. Engine-room components have a comparatively minor effect on vessel stability due to their low weight relative to ship displacement; several fuel cells and converters are arranged in five-module vertical stacks, highlighting their limited influence on vertical stability.
- The total lifetime cost of the optimal design is estimated at $22.9 million, with a baseline fuel price of 6 $/kg. Fuel costs have the largest contribution (74.2%) to total cost, while CAPEX (including replacements) accounts for 24.5%. Battery CAPEX and total maintenance costs together contribute less than 2% of the lifetime cost.
- Neglecting key real-world effects such as powertrain efficiency changes after retrofitting, degradation- driven increases in fuel consumption, and operating profile variability across routes can lead to non-robust designs and misleading lifetime cost outcomes.

Overall, these results demonstrate that cost-optimal and technically feasible solutions require the coupled consideration of system sizing, topology, operation, and stability constraints within a unified lifetime cost optimization framework. From a broader design and decision-making perspective, the results provide clarity on the feasibility of hydrogen-based ship retrofits under realistic technical and economic constraints. The viability of hydrogen-fuelled systems primarily depends on storage integration constraints and fuel price assumptions rather than power and propulsion system sizing alone. As such, the proposed framework supports informed assessment of when and under which conditions hydrogen-based ship

energy systems become viable options for decarbonization, thereby supporting decision-making for maritime decarbonization strategies.

In Chapter 5, the impact of weather variability on the power profiles and lifetime cost is investigated.

5

DESIGN AND OPERATION INCLUDING WEATHER-DRIVEN SPEED VARIABILITY

This chapter is reproduced from: Mylonopoulos et al. [137]

ABSTRACT

This study presents a framework for designing and optimizing ship energy systems including weather-driven speed variability and navigation safety constraints. Navigation risks including resonance, surf-riding, and successive high-wave impacts, are calculated using five years of hourly weather data. Random speed variations (up to ±5%) are applied to a baseline speed profile to capture operational uncertainty, and safety-based speed reductions (up to 40%) are applied when required. Course changes are excluded. Treating navigation risks as constraints, operating profiles are generated for different weather conditions. For a conceptually retrofitted cargo ship, hydrogen fuel cell and battery capacities, and their power distribution, are optimized for each operating profile to minimize lifetime energy system cost and assess the effects of weather-induced power variation. Results show that speed and weather variability can significantly change power demand, requiring fuel cell capacities between 700 and 1500 kW. The most common configuration is a 1200 kW fuel cell system with 180 kWh of battery capacity, covering 39% of laden profiles, while full power coverage requires 1500 kW. Lifetime cost outcomes exhibit a 5th–95th percentile spread of -10.3% to +11.1% relative to mean cost. The results demonstrate the significant influence of weather variability on system sizing and cost.

5.1 INTRODUCTION

Shipping facilitates approximately 90% of global trade [1]. Despite its vital economic role, the sector is responsible for about 10% of the global NO_x emissions and 3% of CO_2 emissions [2]. Without effective mitigation measures, this percentage may increase substantially [3]. To meet the stringent regulations imposed by regulatory bodies, there is an urgent need for more energy-efficient and environmentally sustainable ships. Enhancing hydrodynamic performance, particularly through sailing speed optimization, remains a key strategy for reducing fuel consumption in both newbuilt and retrofit ships. Moreover, there is growing interest for alternative 'green' fuels such as hydrogen, as substitute for diesel, to lower the lifecycle emissions and ensure regulatory compliance [138].

Ship fuel efficiency and operational performance are highly sensitive to external disturbances which introduce uncertainty into the vessel's speed and power profiles [139]. If neglected, these variations in operating conditions can lead to suboptimal designs and under or over-estimation of lifetime costs, ultimately affecting economic feasibility.

Several studies have explored the impact of operational uncertainty on ship performance. Esmailian et al. [139] addressed both weather-related and epistemic uncertainty, during the design stage, optimizing hull and propeller parameters for realistic sea conditions. Lang and Mao [140] presented a semi-empirical model to predict ship's speed loss at arbitrary wave headings, improving accuracy for voyage optimization. The model estimates added resistance in irregular seas by extending validated formulae originally developed for head regular wave conditions [141]. Seo and Oh [142] analyzed short-term variability in speed–power performance using sea trial data and Monte Carlo simulations, identifying shaft power measurement uncertainty as the dominant factor. Coraddu et al. [143] modelled speed and displacement as stochastic variables over long-term operational data to evaluate energy efficiency operational indicators via Monte Carlo analysis. Similarly, Fan et al. [144] developed a Monte Carlo-based energy efficiency model that incorporates environmental parameters (wind, waves, current, water depth), cargo loading, and speed. While the above studies focus on performance prediction or operational assessment under uncertainty, the present work extends this line of research by incorporating weather-driven speed variability into the energy system design optimization of a hydrogen-fuelled ship.

In recent years, various operational strategies have been adopted to reduce fuel consumption and emissions in the maritime sector. Among these, slow steaming, the intentional reduction of sailing speed, has received considerable attention for its potential to significantly improve fuel efficiency, albeit at the cost of reduced voyage frequency and potential revenue loss [145]. Numerous studies have highlighted the potential economic and environmental benefits of this approach, which are highly dependent on vessel type, size, trade routes, charter rates, and fuel prices [145], [146], [147], [148]. Additionally, weather routing has become a widely adopted operational strategy for optimizing both fuel efficiency and voyage safety by adjusting the ship's route and speed based on forecasted environmental conditions [149]. Zis et al. [149] presented a survey of ship weather-routing, categorizing existing methods and their application areas. Kytariolou and Themelis [150] developed a

routing optimization tool that incorporates forecasted weather data and seakeeping constraints, enabling both fuel-efficient and safe passage planning. Fabbri and Vicen-Bueno [151] highlighted the importance of navigational risk assessment, while de Gracia et al. [152] demonstrated how weather-informed routing can reduce fatigue damage and protect hull integrity under varying sea states. Pennino et al. [153] used a Dijkstra-based routing model to enhance seakeeping performance with minimal impact on voyage duration. While these studies clearly demonstrate the advantages of slow steaming for fuel efficiency and weather routing for enhancing safety under environmental uncertainty, there is limited literature exploring speed adjustments as a proactive safety measure, rather than solely to reduce fuel consumption or emissions.

The previously referenced studies have extensively explored strategies for reducing fuel consumption and emissions through operational adjustments and hydrodynamic performance improvements. In recent years, there has been increasing interest toward alternative fuelled ships, to achieve substantial emission reductions. Hydrogen fuel cells have emerged as a promising zero-emission alternative to conventional diesel propulsion systems, with their adoption seen as vital for regulatory compliance [59]. Several studies have focused on energy system sizing and operation for hydrogen-fuelled ships. Pivetta et al. [47] and Dall'Armi et al. [29] conducted multi-objective optimizations accounting for fuel cell and battery degradation, while Dall'Armi et al. [46] extended this work by incorporating uncertainty in fuel and component costs using Montecarlo simulations. Bassam et al. [66] evaluated multiple system configurations to identify the optimal topology in terms of total energy system cost. Other studies focused on developing energy management strategies for control of fuel cell-battery hybrid ship systems to optimize the power distribution for fixed design parameters [26], [30], [31], [63]. However, the previous optimization studies assume static or simplified power profiles without accounting for variability in power demand due to operational uncertainty. This may limit the accuracy of lifetime cost assessments and energy system design and operation. Only a few energy system design and operation optimization studies have introduced some degree of operational variability. Vieira et al. [11] evaluated two uniform-demand scenarios by scaling the baseline power profile by $\pm 10\%$ across all timesteps: one profile fixed at +10% and another fixed at -10%, and Wang et al. [45] used four pre-defined power profiles based on historical vessel data for a nested design and control optimization. Both studies [11], [45] perform multi-objective optimizations, for diesel-fuel cell-battery hybrid systems, in terms of costs and emissions, and consider only a few fixed power profiles to represent how the vessel operates, which means they may not capture the full variability that occurs under real weather and sea conditions. The present work extends this line of research by introducing weather-driven speed variability based on 5 years of weather data, and by incorporating navigation risk-based speed constraints into a lifetime cost minimization framework.

To the best of the authors' knowledge, no study to date addresses lifetime cost optimization for vessel propulsion systems under operational uncertainty and weather-induced speed profile variability. This research addresses this gap by focusing on the design and lifetime operation of hydrogen-based ship energy systems.

The key contributions of this chapter are highlighted below:

- Development of a holistic framework that jointly optimizes energy system sizing and operation by integrating weather-driven speed profile variability into a lifetime cost minimization problem.
- Incorporation of safety-driven speed adjustments as a proactive operational strategy for reducing navigation risks under adverse weather conditions.

The remainder of this chapter is organized as follows: Section 5.2 outlines the specifications and operational characteristics of the case vessel. Section 5.3 describes the proposed methodology for the lifetime cost optimization, including speed profile variability. Section 5.4 discusses the key results from the optimization analysis. Finally, Section 5.5 draws conclusions and offers recommendations for future research.

5.2 CASE STUDY

The case vessel in this study is a 90-meter-long, 12.5-meter-wide general cargo ship with an approximate deadweight of 3700 tons [59]. It is assumed to operate along a fixed route in the Baltic Sea between Sweden and Lithuania, completing 80 laden and 80 ballast voyages annually, each lasting around 29 hours (depending on the speed). This repeated voyage enables an investigation into how variability in speed and power demand, due to different weather conditions, affects the lifetime cost. A baseline speed profile (Fig. 5.1), and the course over ground of the vessel as a function of time, derived from historical onboard measurement data, are used as input to the analysis. To reduce the ship's environmental footprint, its original diesel engine propulsion system is conceptually replaced by a proton exchange hydrogen fuel cell system, supported by lithium-ion batteries [59]. The vessel is assumed to have a remaining operational lifetime of 20 years after retrofitting.

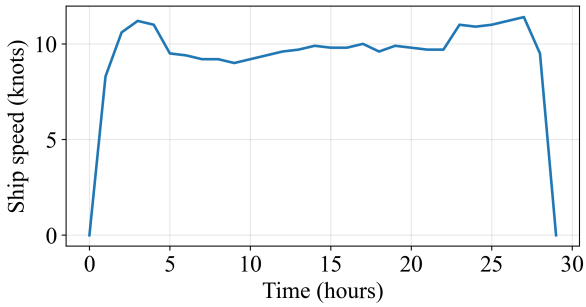

Figure 5.1: Baseline speed profile of the case ship (17-18 March 2022)

5.3 METHODOLOGY

The proposed methodology, illustrated in Fig. 5.2 consists of two main steps:

- Step 1: Data collection and analysis.

Historical weather and ship operational data are gathered. ERA5 hourly wind and wave data [154], along with onboard measurements of ship speed and heading, are used as input to calculate relative wind and wave directions.

- Step 2: Lifetime cost optimization.

  Operating profiles are created by starting from the original ship speed profile, then applying a $\pm 5\%$ random speed variation (at each time step) to reflect operational uncertainty, and then applying the necessary adjustments to ship speed driven by weather conditions to mitigate navigation risks (surf-riding, resonance and successive high-wave impacts). Ship resistance and power demand are then calculated based on the resulting speed profiles.

  An optimization framework is developed to quantify the impact of speed and power-profile variability on lifetime cost of the ship energy system. The framework optimizes total fuel-cell and battery capacities, and their time-varying power outputs, to minimize the Net Present Value (NPV) of total lifetime cost for each operating profile. The selected design configuration must cover all the power profiles (including extreme power demand scenarios). Model outputs include the optimal design parameters and the lifetime cost distribution.

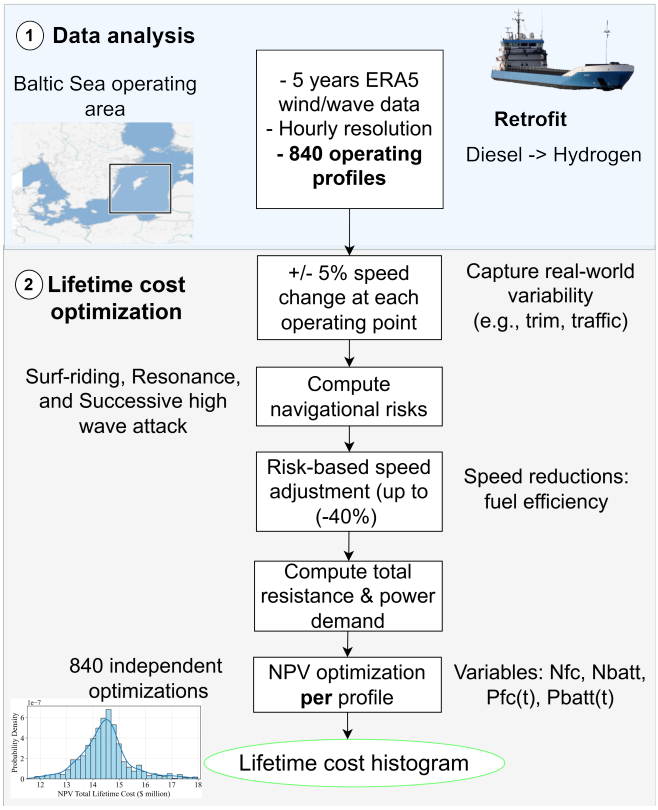

Figure 5.2: Methodology diagram

5.3.1 *Data collection and analysis*

To capture seasonal and interannual weather variability, while maintaining computational efficiency, operating periods from all days of each month over the last five years are selected, resulting in a broad representation of realistic operating conditions across multiple seasons and years. The objective of the study is energy system sizing and lifetime cost assessment under realistic operating conditions, rather than maneuvering performance or vessel response to short-duration transient power spikes. Given the largely steady operating profile of the case vessel [59], the adopted hourly temporal resolution is considered appropriate for the present techno-economic scope. High temporal resolution environmental data are typically available only from in-situ measurements, which usually cover limited spatial areas and short time periods, and therefore do not provide the multi-year spatial coverage required for the present analysis. Sub-hourly environmental fluctuations are not expected to change optimal system capacities within the lifetime cost-driven system sizing framework developed in this study.

The wind speed, wind direction, significant height of combined wind waves and swell, mean wave direction, and wave period are extracted from the ERA5 dataset to

generate load profiles for different weather conditions along the vessel's operational route [141], [154].

A total of 840 operating profiles are generated (14 profiles per month over 5 years, each lasting approximately 29 hours depending on ship speed), each corresponding to a distinct set of historical hourly wind and wave conditions extracted from ERA5 [154]. Each profile represents one deterministic weather-based operating case. For a given case (profile), the vessel is assumed to perform 80 round trips per year (80 laden voyages and 80 ballast return voyages) over its 20-year remaining lifetime under the same environmental conditions represented by that profile. The ballast leg is included by reversing the vessel heading while maintaining the same hourly environmental conditions and baseline speed profile. This ensures that the lifetime cost calculation reflects complete round trips (laden and ballast) for each weather case. Considering both laden and ballast loading conditions reflects realistic commercial vessel operation and avoids bias in lifetime cost estimation that would arise from modelling only a single loading condition or a single sailing direction.

The 840 profiles are not assumed to occur within the same operational year. Instead, each profile is analyzed independently to evaluate how different realistic weather conditions affect optimal system sizing and lifetime cost. The optimization is performed independently for each of the 840 weather-based power profiles. This allows the assessment of how different realistic environmental and operating conditions influence optimal system sizing and lifetime cost. In contrast to approaches that assume a single power profile repeated over the lifetime [66], [29], the present study quantifies the variability of optimal designs and cost outcomes across a wide range of historical operating conditions. The final selected configuration is chosen to ensure full power coverage across all profiles, incorporating a practical capacity margin for robustness. Here, robustness of the design refers to the ability of the selected configuration to satisfy power demand and operational constraints across the full range of considered operating profiles and environmental conditions, without requiring redesign or capacity adjustments.

The wave period, wave height, ship's speed, and relative wave direction are critical parameters for assessing navigational risks [155].

5.3.2 *Optimization framework*

5.3.2.1 *Generation of speed and power demand profiles*

Weather variability is represented through five years of historical ERA5 wind and wave data, from which 840 distinct hourly weather-based operating profiles are constructed. These profiles capture realistic environmental variability across a wide range of operating conditions from multiple seasons and years. Within each profile, the environmental conditions are treated as deterministic, as each profile represents one specific historical weather-based operating case. The objective of this modelling approach is to capture realistic weather-driven operational variability rather than to perform full probabilistic metocean uncertainty propagation. In addition to weather effects, a random speed variation of up to ±5% is applied at each time step to represent operational variability unrelated to environmental conditions, such as trim changes, machinery control deviations, pilotage decisions, and traffic effects,

based on discussions with the vessel operators. The selected bound is intended to represent modest operational variability while keeping the resulting profiles close to the baseline speed profile.

For each speed profile, after applying the random speed changes, the associated navigation risks, including surf-riding, resonance, and successive high wave attacks, are calculated and assessed to ensure safe and realistic operating conditions.

Surf-riding typically occurs when a vessel sails in following or stern quartering seas (waves approaching from astern) and is situated on the forefront of a steep wave. This can lead to rapid accelerations and potentially trigger the broaching-to phenomenon, where the ship experiences an uncontrollable yawing motion and large heeling angles, increasing the risk of capsizing. According to the guidelines provided by the International Maritime Organization (IMO) [155], surf-riding risks are particularly high within the following conditions shown in Eq. (5.1), Eq. (5.2):

$$1.8 \leq \frac{V_s}{\sqrt{L}} \leq 3 \tag{5.1}$$

and

$$135^\circ \leq \alpha \leq 225^\circ \tag{5.2}$$

where:

- V_s is the ship speed (knots),
- $L = 90\,\text{m}$ is the ship's length,
- α is the relative wave direction (degrees).

Resonance refers to the amplification of ship motions when the wave encounter period (T_E) is almost equal to the ship's natural roll period (T_N) or half of it. The two periods are defined as shown in Eq. (5.3) and Eq. (5.4) based on [155], [156].

$$T_E(t) = \frac{3 \cdot T_w^2(t)}{3 \cdot T_w(t) + V_s(t) \cdot \cos(\alpha)} \ \text{(s)} \tag{5.3}$$

$$T_N = \frac{2 \cdot \pi \cdot 0.38 \cdot B}{\sqrt{g \cdot GM}} \ \text{(s)} \tag{5.4}$$

where:

- t is the time (seconds),
- T_w is the wave period (seconds),
- $B = 12.5\,\text{m}$ is the ship's breadth,
- $g = 9.81\,\text{m/s}^2$ is the gravitational acceleration,
- GM is the transverse metacentric height: 0.36 m. in laden condition and 1.74 m. in ballast condition [116].

To mitigate resonance-related risks, such as synchronous rolling (Eq. (5.5)) and parametric rolling (Eq. (5.6)), the following criteria are applied [157]:

$$\left| T_E(t) - T_N \right| > 1 \text{ s} \tag{5.5}$$

$$\left| T_E(t) - 0.5 \cdot T_N \right| > 1 \text{ s} \tag{5.6}$$

These constraints ensure that the wave encounter period does not closely match the ship's natural period or half of it, thus reducing the likelihood of resonance.

According to the IMO [155], successive wave attack risks can be present, at following or stern quartering seas, for the operating conditions shown in Eq. (5.7) and Eq. (5.8):

$$1.6 \leq \frac{V_s}{T_w} \leq 2.4 \tag{5.7}$$

and

$$140^\circ \leq \alpha \leq 220^\circ \tag{5.8}$$

The successive wave attack risks are particularly high for significant wave heights $h_s > 0.04 \cdot L$ [155].

To mitigate the risks of surf-riding, resonance, and successive high-wave attacks, the ship's speed is adjusted while assuming a fixed course throughout the voyages. Course changes are out of scope for this study, as the focus is on evaluating speed-based risk mitigation and its impact on energy system and lifetime cost. Discussions with vessel operators indicated that engine power reduction, and thus speed adjustment, is their primary risk-mitigation strategy. Based on these discussions, the minimum required speed adjustment is applied when necessary, within operational bounds, limited to a maximum reduction of 40%, which was identified by the vessel operators as the practical limit in real operation. Such speed reductions can enhance safety, improve fuel efficiency, and limit peak power demand and energy system size. Speed increases were not considered as a mitigation strategy, as increasing engine power to avoid resonance condition would lead to higher fuel consumption and is not commonly applied in practice according to vessel operators. The resulting safety-adjusted speeds are then used to determine the voyage duration for the fixed sailing distance, which in turn affects the fuel consumption per trip.

For each scenario, the updated speed profiles are used to estimate the total ship resistance (R_t), as shown in Eq. (5.9):

$$R_t = R_{\text{calm}} + R_{\text{wave}} + R_{\text{wind}} \tag{5.9}$$

where:

- R_{calm} is the calm water resistance (N), derived from the resistance–speed curves of the case ship for both laden and ballast conditions. The resistance-speed curves (provided by the vessel operators) are shown in Fig. 5.3. Within the available speed range, resistance values are obtained by linear interpolation of the provided data. Outside this range, linear extrapolation is applied to ensure continuity of the power demand curve. The extrapolated low-speed values have a negligible impact on optimal system sizing and lifetime cost.

- R_{wave} is the added wave resistance (N).
- R_{wind} is the added wind resistance (N).

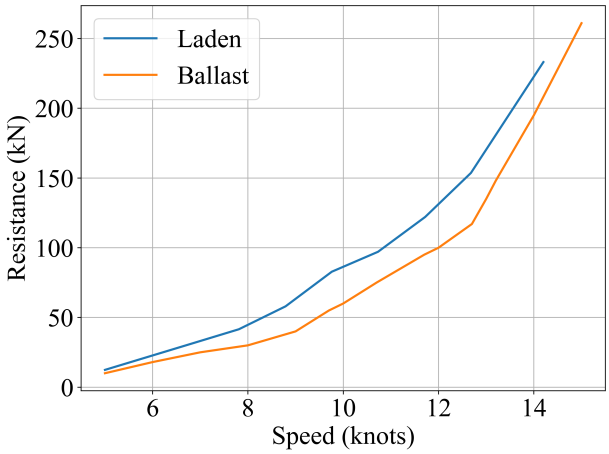

Figure 5.3: Resistance-speed curves for laden and ballast conditions

The added wind resistance is calculated using Eq. (5.10), based on [158]:

$$R_{\text{wind}} = 0.5 \cdot \rho_A \cdot A_{XV} \cdot C_{AA}(\psi_{WR}) \cdot V_{WR}^2 \tag{5.10}$$

where:

- $\rho_A = 1.225$ kg/m^3 is the air density.
- A_{XV} (m^2) is the vessel's transverse projected area to the wind: 117.2 m^2 in the laden condition and 143.1 m^2 in ballast. The higher value in the ballast condition reflects the reduced draft, which increases the above-water area exposed to wind.
- $C_{AA}(\psi_{WR})$ is the wind resistance coefficient as a function of the relative wind direction, derived from [141].
- V_{WR} (m/s) is the relative wind velocity, computed using Eq. (5.11), based on [159].

$$V_{WR} = \sqrt{V_{s,\text{ms}}^2 + V_{TW}^2 + 2\, V_{s,\text{ms}} \cdot V_{TW} \cdot \cos(\alpha)} \tag{5.11}$$

where:

- $V_{s,\text{ms}} = 0.5144 \cdot V_s$ is the ship speed converted from knots to m/s.
- V_{TW} (m/s) is the true wind speed from ERA5.

The maximum added wave resistance (X_d), over relative wave directions from head to 30° off-bow, can be calculated using Eq. (5.12), based on [160]:

$$X_d = 1336 \cdot (5.3 + V_{s,\text{ms}}) \cdot \left(\frac{B \cdot d_r}{L}\right)^{0.75} \cdot h_s^2 \tag{5.12}$$

where:

- d_r is the ship's mean draft: 5.3 m in laden condition and 3.23 m in ballast condition.

The added wave resistance for any relative wave direction can be approximated using Eq. (5.13), based on [140], [160]:

$$R_{\text{wave}} = \begin{cases} X_d \cdot \cos^2(\alpha), & \alpha \in [0, 90] \cup [270, 360], \\ 0, & \text{otherwise.} \end{cases} \tag{5.13}$$

This approach aligns with other studies that have assumed zero added wave resistance in following and stern quartering seas [141], [161] noting that the degree of uncertainty in estimating this component often exceeds its actual magnitude. The widely adopted STA-1 and STA-2 methods assign zero added resistance for relative wave directions between 90° and 270° [139], [158]. Hence, in following and stern-quartering seas (90° - 270°), the added wave resistance is approximated as zero. In these conditions, the added resistance is generally small and may even become negative due to wave-assisted propulsion effects. Therefore, using a zero approximation provides a reasonable first-order representation for the purpose of this study, which focuses on energy system sizing and lifetime cost assessment rather than detailed hydrodynamic modelling, which would increase modelling and computational complexity. In addition, peak power demand in the dataset is mainly driven by head and bow-quartering sea states, which can be calculated using the IMO-provided formulation from Eq. (5.12). While recent research has introduced more advanced semi-empirical models for added wave resistance [161], [162], [163], [164], incorporating such detailed models lies beyond the scope of this study.

The required propulsive power demand (P_{demand}) in kW, is then calculated using Eq. (5.14), based on [139]:

$$P_{\text{demand}} = \frac{R_t \cdot V_{s\_ms}}{1000 \cdot \eta_t} \tag{5.14}$$

where:

- η_t is the total propulsive efficiency. The values are provided, by the vessel operators, as a function of ship speed for both laden and ballast conditions, and are summarized in Table 5.1. Within the available speed range, propulsive efficiency values are obtained by linear interpolation of the provided data. Outside this range, linear extrapolation is applied to ensure continuity of the power demand curve. The extrapolated low-speed values have a negligible impact on optimal system sizing and lifetime cost.

Table 5.1: Propulsive efficiency as a function of speed for laden and ballast

Ship speed (knots)	η_t-laden	η_t-ballast
5	0.631	0.736
6	0.629	0.735
7	0.624	0.733
8	0.618	0.729
9	0.609	0.723
10	0.598	0.714
11	0.601	0.704
12	0.595	0.698
13	0.585	0.689
14	0.565	0.668

The resistance-based propulsion power estimation (Eq. (5.14)) captures the dominant hydrodynamic contributions (calm-water resistance, added wind and wave resistance) relevant for system-level techno-economic analysis. However, it does not aim to reproduce exact historical shaft power measurements, which are influenced by additional in-service factors such as hull fouling, machinery condition, operational scheduling decisions, and traffic constraints. Therefore, the present framework is intended for energy system sizing and lifetime cost assessment under various weather-driven scenarios rather than time-series replication of specific historical voyages.

5.3.2.2 *Total cost optimization*

The goal of the optimization is to determine the optimal system capacities and power distribution between fuel cells and batteries, for each power profile, that minimize the NPV, under operational uncertainty and weather-driven speed profile variability.

The fuel consumption as a function of time is calculated using the quadratic expression shown in Eq. (5.15):

$$F_{\mathrm{FC}}(t) = a \cdot P_{\mathrm{FC}}^2(t) + b \cdot P_{\mathrm{FC}}(t) + c \tag{5.15}$$

where:

- t represents the discrete time steps.
- $P_{\mathrm{FC}}(t)$ is the fuel cell power output in kW, at time step t (control variable).
- $a = 0.0066$, $b = 1.4025$, $c = 1.8306$ are the coefficients derived from the fuel cell efficiency curve, provided by the manufacturer [117]. The fuel cell stack is rated at 100 kW. Fig. 5.4 shows the characteristic curve of the fuel cell; fuel consumption (expressed in kW) on the y axis, and output power (kW) on

the x axis [47]. The F_{FC} (kW) is derived from the ratio of output power over efficiency.

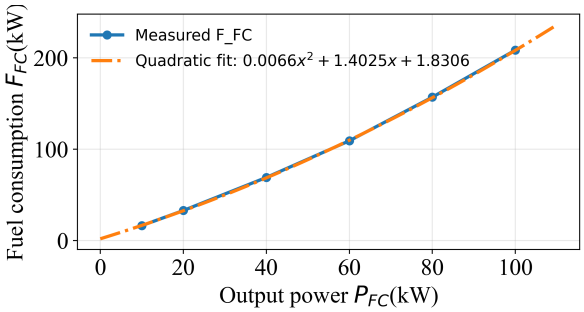

Figure 5.4: Fuel consumption curve

The total fuel consumption for a single voyage, accounting for all fuel cells, is computed in kilograms using Eq. (5.16):

$$F_{\text{total}} = N_{\text{FC}} \cdot \sum_{t=0}^{t_{\text{final}}} \left(F_{\text{FC}}(t) \cdot \Delta t \cdot k_{e\text{-}m} \right). \tag{5.16}$$

where:

- N_{FC} is the number of 100-kW fuel cells (design variable).
- Δt is the time step duration. Its value is 1 hr, aligned with the temporal resolution of the ERA5 environmental data used in this study. This 1-hr time step is consistent with practices commonly adopted in the literature for weather-driven ship performance assessment studies [151], [140], but also for energy system design-operation analysis [165], [166], [167].
- $k_{e\text{–}m} = 0.03$ kg/kWh is the energy-to-mass conversion coefficient [118].

The battery SoC as a function of time is expressed based on [45], as shown in Eq. (5.17):

$$\text{SoC}_{\text{batt}}(t) = \text{SoC}_{\text{batt}}(t-1) - \frac{P_{\text{batt}}(t) \cdot \Delta t}{E_{\text{batt,rated}}} \tag{5.17}$$

where:

- $P_{\text{batt}}(t)$ is battery power output in kW, at time step t (control variable). Positive power values indicate discharging.
- $E_{\text{batt,rated}} = 60$ kWh is the rated energy capacity of the battery, based on the manufacturer data [84].

To limit degradation, the battery C-rate is constrained between -1 and 1, and the SoC is bound between 20–80% [84]. The initial and final SoC are set to 50% for energy balance without requiring shore charging.

The constraint for the power balance at each time step is shown in Eq. (5.18), ensuring that the combined output from fuel cells and batteries matches the power demand.

$$N_{\text{FC}} \cdot P_{\text{FC}}(t) + N_{\text{batt}} \cdot P_{\text{batt}}(t) = \frac{P_{\text{demand}}(t)}{\eta_{\text{conv}} \cdot \eta_{\text{inv}} \cdot \eta_{\text{motor}} \cdot \eta_{\text{gb}}} \tag{5.18}$$

where:

- N_{batt} is the number of 60-kWh batteries (design variable). The installed battery capacity should be at least 180 kWh for emergency conditions [59].
- $P_{\text{demand}}(t)$ is the required power demand at time step t.
- η_{conv}, η_{inv}, η_{motor}, and η_{gb} are the efficiencies of the converters, inverter, propulsion motor, gearbox for the new powertrain, taken as: 0.985, 0.985, 0.96, and 0.98 respectively, based on literature and manufacturer-based values as documented in the authors' previous study [116]

This power balance equation is a mixed integer nonlinear constraint due to the product of integer design variables and continuous control variables.

The objective of the optimization problem is to minimize the total lifetime cost, which includes the initial capital expenditure (CAPEX) and the NPV of operational expenditure (OPEX), as expressed in Eq. (5.19):

$$\underset{(N_{\text{FC},i},\, N_{\text{batt},i},\, P_{\text{FC}}(t),\, P_{\text{batt}}(t))}{\text{minimize}} \left(\text{CAPEX}_i + \text{NPV}_{\text{OPEX},i}\right) \tag{5.19}$$

where:

- i denotes each operating profile.

This objective function is a mixed-integer nonlinear equation due to the product of integer design variables and continuous control variables.

The initial investment (CAPEX) includes the purchase costs for the fuel cell and battery systems, as shown in Eq. (5.20):

$$\text{CAPEX}_i = N_{\text{FC},i} \cdot P_{\text{FC,rated}} \cdot C_{\text{FC}} + N_{\text{batt},i} \cdot E_{\text{batt,rated}} \cdot C_{\text{batt}} \tag{5.20}$$

where:

- $P_{\text{FC,rated}} = 100$ kW is the rated fuel cell power.
- $C_{\text{FC}} = 1014$ \$/kW is the cost per kW for the fuel cell stack [59].
- $C_{\text{batt}} = 492$ \$/kWh is the cost per kWh for the battery [59].

The NPV of OPEX includes both the discounted fuel costs and component replacement costs and is calculated as shown in Eq. (5.21):

$$\text{NPV}_{\text{OPEX},i} = \text{NPV}_{\text{replace},i} + \text{NPV}_{\text{fuel},i} \tag{5.21}$$

The NPV of the replacement costs is calculated as shown in Eq. (5.22):

$$\mathrm{NPV}_{\mathrm{replace},i} = \sum_{t=1}^{T} \left(\frac{b_{\mathrm{FC,replace},t} \cdot N_{\mathrm{FC},i} \cdot P_{\mathrm{FC,rated}} \cdot C_{\mathrm{FC,replace}}}{(1+r)^t} + \frac{b_{\mathrm{batt,replace},t} \cdot N_{\mathrm{batt},i} \cdot E_{\mathrm{batt,rated}} \cdot C_{\mathrm{batt,replace}}}{(1+r)^t} \right) \tag{5.22}$$

where:

- t is the time index in years, and $T = 20$ years is the vessel's remaining lifetime.
- $b_{\mathrm{FC,replace},t}$ is the binary variable for fuel cell replacement in year t (approximately every 4 years, based on 20,000 operating hours [59], [117]).
- $b_{\mathrm{batt,replace},t}$ is the binary variable for battery replacement in year t (assumed every 7 years [59]).
- $C_{\mathrm{FC,replace}}$ and $C_{\mathrm{batt,replace}}$ are the replacement fuel cell and battery costs in \$/kW, assumed to be 50% of their initial CAPEX, based on projected price reductions with increased market adoption [59].
- $r = 0.05$ is the discount rate [68], [86], [87].

Fuel cell lifetime is represented using a simplified approach based on manufacturer-provided limits [116], while battery replacement timing is based on the degradation analysis presented in [59]. In the present study, degradation is therefore represented through time-based replacement rather than detailed dynamic aging modelling. This avoids relying on degradation parameters mainly derived from automotive applications, which may not accurately reflect maritime operating conditions and could yield unreliable results [116]. This approach remains consistent with the techno-economic scope of the present framework.

The NPV of the lifetime fuel cost for each profile is calculated as shown in Eq. (5.23):

$$\mathrm{NPV}_{\mathrm{fuel},i} = \sum_{t=1}^{T} \frac{F_{\mathrm{total},i} \cdot N_{\mathrm{trips,annual}} \cdot C_{\mathrm{h2}}}{(1+r)^t} \tag{5.23}$$

where:

- $N_{\mathrm{trips,annual}}$ is the number of annual trips.
- $C_{\mathrm{h2}} = 6\$/\mathrm{kg}$ is the baseline price of hydrogen fuel, based on [59]. Due to fuel price uncertainty, the impact of different green hydrogen prices (3\$/kg and 9\$/kg) on the total lifetime cost will be discussed.

The resulting optimization is a Mixed Integer Nonlinear Programming (MINLP) problem solved with the open-source solver SCIP. SCIP uses various techniques including presolving, branch-and-bound search, cutting planes, and heuristics to efficiently explore the design space without excessive computational demands [128].

The optimization framework produces a distribution of optimal solutions, with required system capacities and power distribution between fuel cells and batteries for each power profile. The selected design should cover the power profiles of the ship with the minimum NPV.

5.4 RESULTS AND DISCUSSION

5.4.1 *Data collection and analysis results*

The minimum, maximum, and mean values of the wind and wave parameters, obtained from ERA5 data, are summarized in Table 5.2. Over the past five years, conditions across the vessel's operating area are generally moderate. The mean significant wave height is 1.03 m. and the mean wind speed is 6.77 m/s. Higher wind speeds are consistently associated with higher significant wave heights in the dataset, reflecting the physical dependency between the two parameters. Similarly, relative wind and wave directions are generally aligned, with only small deviations across operating points, as expected when local wind drives wave development. About 9% of the operating points show angular differences greater than 50°, likely reflecting swell contributions.

Table 5.2: ERA5 weather data

Weather parameter	Min.	Mean	Max.
Wave height (m)	0.13	1.03	4.65
Wave period (s)	2.36	4.95	9.15
Wind speed (m/s)	1.10	6.77	16.7

For data validation purposes, wind direction measurements from onboard log data and ERA5 are compared, as shown in Fig. 5.5. These wind profiles span from 12:00 on 17 March 2022 until 17:00 on the following day. The two datasets exhibit similar overall trends, with minor differences in wind direction observed throughout the baseline voyage. These deviations are primarily attributed to the spatial and temporal resolution differences: ERA5 provides hourly, spatially averaged data over the vessel's operating area, which may not fully capture localized gusts or small-scale phenomena. In contrast, the onboard measurements are recorded at a higher frequency (every 5 minutes) enabling finer resolution of local conditions. Larger discrepancies are observed at the beginning and end of the voyage, likely due to vessel manoeuvring or stationary periods at port. However, these effects are limited and do not significantly influence the overall trend. Therefore, for the purpose of this study, the accuracy of ERA5 data is deemed sufficient.

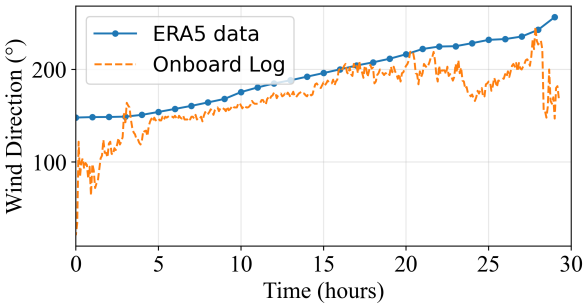

Figure 5.5: Wind direction comparison: Onboard log vs ERA5 (baseline profile)

5.4.2 *Optimization results*

5.4.2.1 *Navigation risk reduction*

By applying risk-based speed adjustments, the total risk in the dataset decreases substantially from 25.25% to 6.38% (of total operating points of all profiles), with an average speed reduction of 17.6%. Specifically, the resonance risk is reduced from 13.04% to 4.51% and the successive wave attack risk from 12.21% to 1.88%. Surf-riding and broaching risks are absent throughout, since the velocity-to-length ratios $(V_s/\sqrt{L})$ remain below the critical threshold of 1.8. This finding is consistent with feedback from the vessel operators, who confirmed that surf riding is not a concern for the case vessel.

A further reduction in risk from 6.38% to 4.28% could, theoretically, be achieved through modest speed increases (up to 10%), by shifting the encounter frequency away from the natural ship frequency at certain relative wave directions where speed reductions (up to 40%) are not effective. However, this option was not recommended by vessel operators, primarily due to its negative impact on fuel efficiency.

Additional sensitivity tests also showed that unrealistically large speed reductions up to 90% would reduce the remaining risk to approximately 1.6%, confirming that most residual cases arise from the imposed practical speed-reduction limit rather than modelling limitations.

The remaining risks (6.38% of operating points) correspond mainly to resonance conditions in near-beam seas ($\alpha \approx 90^\circ$ or 270°), where speed adjustments have limited influence on the wave encounter period (Eq. (5.3)). Based on discussions with the vessel operators, such residual risks may occur in real ship operations but are considered operationally manageable for this vessel, provided they occur under rare conditions and do not coincide with exposure to critical sea states. For the case vessel, these critical conditions correspond to short wave periods of approximately 4-8 seconds combined with significant wave heights exceeding 4 meters. The residual risk cases in the dataset do not coincide with these conditions, so they are considered operationally manageable. Course changes or weather routing could further reduce the remaining risks, but investigating coupled speed-routing strategies lies outside the scope of the present study.

5.4.2.2 *Weather impact on power profiles and energy system sizing*

The sizing analysis focuses on the laden part of the voyage, which represents the scenario with maximum resistance and power demand. The ballast condition involves lower energy demands and does not drive energy system sizing. Once the design configuration is selected based on the most energy-intensive (laden) power profiles, the total lifetime cost is estimated by also including the ballast voyages to account for the total lifetime fuel consumption over full round trips. For the ballast condition, the same baseline speed profile as the laden leg is applied, with a 180° heading change (reverse track), and power demand is recalculated, for each power profile, using ballast-condition parameters.

The vessel's power demand is estimated using the safety-adjusted speeds. The resulting probability distribution of power demand during sailing in laden condition is shown in Fig. 5.6. The mean power demand is 778 kW. The 90^{th} and 95^{th} percentiles occur at 1181 kW and 1286 kW, respectively. The low-power region corresponds to cases where large speed reductions (30–40%) are applied at already low operating speeds (e.g., 8 knots) to mitigate navigation risks.

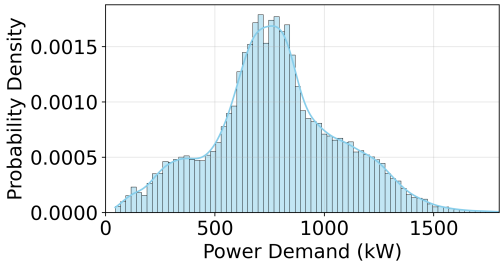

Figure 5.6: Histogram of power demand during sailing periods in laden condition

The distributions of required fuel cell and battery capacities, for all the different operating profiles in laden condition, are shown in Fig. 5.7. The mean fuel cell capacity is approximately 1200 kW, with 58% of all simulations falling within the 1200-1300 kW range (Fig. 5.7a). These values result from the optimization-based design process applied to each operating profile. Low fuel cell capacities of 700-900 kW are required in 2.86% of the profiles, primarily due to frequent and substantial speed reductions applied for safe operation. High capacities of 1400-1500 kW are required in 12.5% of the profiles, primarily driven by high added resistance in combination with relatively high speeds (e.g., >10.5 knots) at the specific operating points. These cases usually involve near-head seas, where the safety logic does not trigger speed reductions (no surf-riding, resonance, or successive wave attack risks), so the vessel keeps its speed while facing high resistance. The battery capacity histogram shows a much more skewed distribution, with a mean of 258 kWh and 83.5% of the cases concentrated in the 180–300 kWh range (Fig. 5.7b), where the battery is used primarily for peak shaving. Battery capacities exceeding 480 kWh occur only in 5.3% of the profiles, corresponding to rare scenarios with short periods of high peak power or cases with highly fluctuating power demand induced by random speed changes and safety-based speed adjustments. In such scenarios, a

larger battery capacity is selected to buffer peaks, maintain fuel cell efficiency, and satisfy SoC constraints. Overall, because the battery is primarily used for peak shaving and its optimal capacity remains limited across most profiles, the adopted hourly temporal resolution is expected to be sufficient for determining optimal system capacities within the present lifetime cost-driven sizing framework.

The most frequent configuration across all simulations in laden condition, consists of a 12x100 kW fuel cell system and a 3x60 kWh battery system, covering 39% of the laden power profiles. The remaining load profiles either require more battery capacity (Fig. 5.7b) or exhibit sustained peak loads above 1.2 MW which require higher installed fuel cell capacity (Fig. 5.7a). For full power coverage of all profiles with 1200 kW fuel cell capacity, the ship's speed would need to be reduced. However, this would result in fewer voyages and lower revenue, and for that reason it is not chosen. Thus, although the fuel cell and battery capacities are shown as separate distributions for clarity in Fig. 5.7a and Fig. 5.7b, each simulation corresponds to a coupled optimal fuel cell-battery configuration. The separate histograms are used to highlight the sizing sensitivity of each component, while the suitability of the design is assessed through their combined operation.

Torque and thrust variations due to wave-induced propeller inflow fluctuations are not modeled in this study. Instead, their main effect is represented indirectly through the weather-driven speed variations and the resulting changes in resistance and propulsive power demand. Given the hourly resolution of the analysis, this level of representation is considered sufficient for system sizing and lifetime cost evaluation, while a more detailed hydrodynamic model could further refine transient load and degradation estimates.

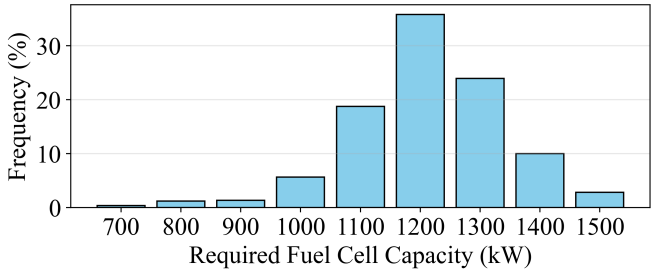

(a)

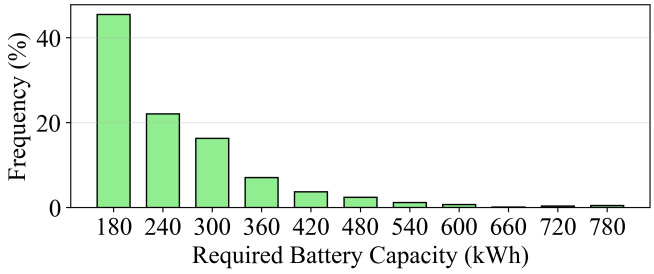

(b)

Figure 5.7: Histograms of required system capacities: (a) Fuel cells, (b) Batteries. Frequencies are expressed as percentages of all laden power profiles.

Some of the vessel's power profiles, for different weather conditions, are plotted in Fig. 5.8:

- An average-power operating profile (Fig. 5.8a), without any navigation risks and speed reductions applied. The optimizer selects 12x100 kW fuel cells and 3x60 kWh batteries for this power profile.
- A low-power operating profile (Fig. 5.8b) that takes longer to complete (33.9 hours) due to frequent and high-speed reductions applied for safe operation. An average speed reduction of 19.9% is applied across 53.3% of this profile's operating points to eliminate resonance and successive wave-attack risks. The optimizer selects low system capacities of 7x100 kW fuel cells and 3x60 kWh batteries.
- A high-power operating profile (Fig. 5.8c) during winter conditions, with high operating speed (>10.5 knots) at near-head seas (high added resistance without triggering speed reductions) for over 2 hours near the end of the voyage. The optimizer selects 15x100 kW fuel cells and 3x60 kWh batteries.
- A power profile experiencing strong fluctuations (Fig. 5.8d). High-speed reductions are applied to eliminate risks at two operating points (around 28 h and 30 h), with high speed between these points at 29 h (without risk-based reductions), resulting in a peak demand of 1275 kW. The optimizer selects

10x100 kW fuel cells and 9x60 kWh batteries to buffer this short-duration high-power peak.

Based on the above, for full power coverage, the installed fuel cell capacity needs to be 1500 kW. Such design choices align with common maritime practice, where a 20–25% capacity margin is often included for the main power source to enhance reliability under extreme conditions. Hence, the selected configuration consists of 15x100 kW fuel cells and 3x60 kWh batteries.

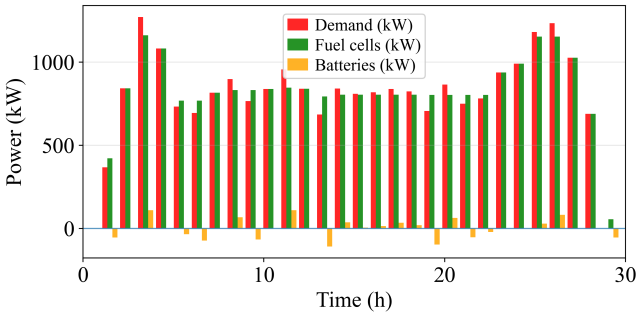

(a)

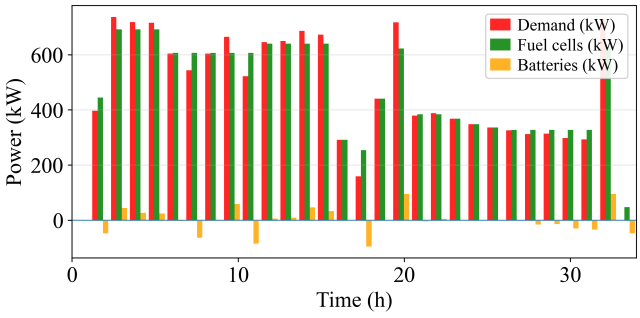

(b)

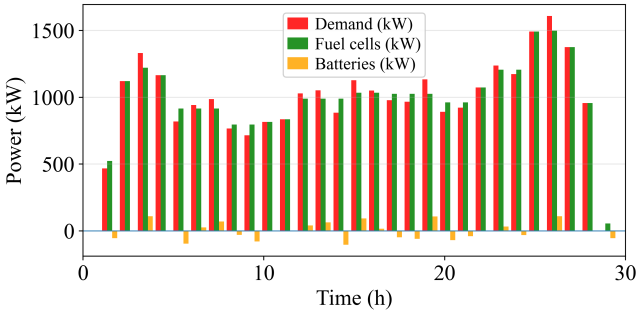

(c)

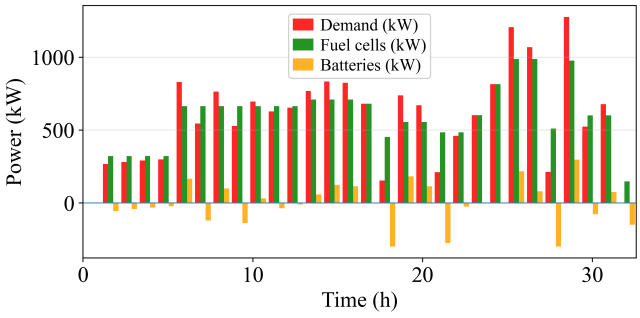

(d)

Figure 5.8: Vessel power profiles for different weather conditions: (a) Average-power, (b) Low-power, (c) High-power, (d) Fluctuating (short-period high peak).

The vessel's power demand depends on the combined influence of ship speed and weather conditions (significant wave height, wind speed, relative wind and wave directions). Table 5.3 presents selected cases under different speeds and weather conditions. To examine the contribution of each factor three pairs of operating points are compared:

1. ship speed varies under similar seas (between operating points A/B),
2. relative wave directions vary for the same ship speed (between operating points C/D),
3. significant wave height and wind speed vary for similar relative wave directions and ship speeds (between operating points E/F).

The columns Δ in Table 5.3 present the changes between the operating points.

In case 1 (operating points A and B), where wind and wave conditions remain unchanged, the power demand depends on ship speed. Case 2, covering operating points C and D, highlights the critical role of relative wave direction: At identical ship speeds, when relative wind and wave directions shift from near-head seas (point C: 352°) to near-following seas (point D: 175°), the resulting change affects added resistance and thus power demand. This effect is particularly pronounced in higher sea states, where added resistance becomes dominant. Case 3, for operating points E and F, illustrates the influence of environmental severity: even at identical ship speeds and similar relative directions, power demand differs substantially due to higher significant wave height and stronger winds at point E.

The operating points in Table 5.3 are illustrative examples used to examine the impact of ship speed, relative wave direction, and sea severity on power demand. The magnitude of power changes depends on the specific speeds and sea states.

Table 5.3: Illustrative cases of speed–weather interaction on power demand (columns show paired comparison of operating points)

Variable	Operating points								
	A	B	Δ	C	D	Δ	E	F	Δ
Ship speed (knots)	11.6	9.3	−20%	9.7	9.7	*	9.1	9.1	*
Wave height (m)	1.3	1.3	*	0.42	0.35	*	1.71	0.24	−86%
Wind speed (m/s)	9.2	9.1	*	4.34	4.63	*	9.56	4.46	−53%
Rel. wave dir. (°)	235	247	*	352	175	177°	13.3	2.9	*
Rel. wind dir. (°)	250	254	*	340	191	149°	15.9	7.4	*
Results									
Added Resist. (kN)	0	0	0%	7.9	0	−100%	42.7	5.3	−87%
Calm Resist. (kN)	119	71	−41%	81.3	81.3	0%	65	65	0%
Power (kW)	1303	608	−53%	810	740	−8.7%	895	590	−34%

* the specific values do not affect the power changes between the pairs of operating points

5.4.2.3 *Lifetime cost optimization for the selected design*

The probability distribution of the NPV of total lifetime costs, for the selected configuration (15x100 kW fuel cells and 3x60 kWh batteries), across all voyage profiles is shown in Fig. 5.9. The distribution has a mean NPV of $14.9 million (with a baseline fuel price of 6$/kg), and the 5th - 95th percentile range spans from $13.4 - $16.6 million ($3.2 million spread), corresponding to approximately -10.3% and +11.1% deviations relative to the mean, respectively. This highlights the significant influence of weather variability on the total lifetime cost. Fuel costs account for 76% of total lifetime cost while fuel cell and battery CAPEX (including replacement costs) account for 24%. Within this capital-related share, fuel cell replacement contributes approximately 12.8% of total lifetime cost, while battery-related costs (initial investment and replacement) represent approximately 1% under the baseline scenario. This indicates that degradation-related costs have a limited influence on total lifetime cost compared to fuel expenditure.

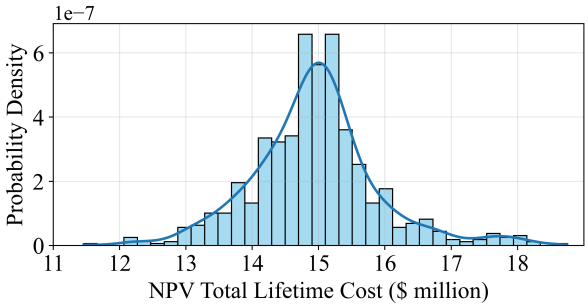

Figure 5.9: Histogram of total lifetime cost (baseline fuel price: 6$/kg)

If the installed fuel-cell capacity is increased from 1500 to 1600 kW (1 additional fuel cell module), the mean lifetime cost rises by 1.2%, due to the 6.4% total CAPEX increase (including replacements), which outweighs the 0.4% fuel cost reduction that results from a more fuel-efficient part-load operation. Similarly, if the installed battery capacity is increased from 180 to 240 kWh (1 additional battery pack), the mean lifetime cost rises by 0.4%, with a 1.3% total CAPEX increase. Hence, further capacity increases do not provide an economic advantage.

Given the fuel price dominance (76% of total cost), future changes in green hydrogen prices will have a major influence on total lifetime cost. Hydrogen prices and usage remain uncertain due to several external factors, such as electricity prices and renewable energy availability. The hydrogen price variations examined below are evaluated for the selected configuration, without re-optimizing system capacities for each price scenario.

A reduction in fuel price from 6$/kg to 3$/kg, in case of large large-scale green-hydrogen deployment, would lower the mean NPV and narrow the lifetime cost distribution spread since fuel expenses are the largest share of total lifetime cost. A lifetime cost distribution for a green hydrogen price of 3$/kg (50% reduction), based on PwC predictions [103], is shown in Fig. 5.10. The mean NPV is $9.26 million and the 5th - 95th percentile range spans from $8.5 to $10.1 million ($1.6 million

spread), which correspond to -8.21% and +9.07% deviations relative to the mean NPV respectively.

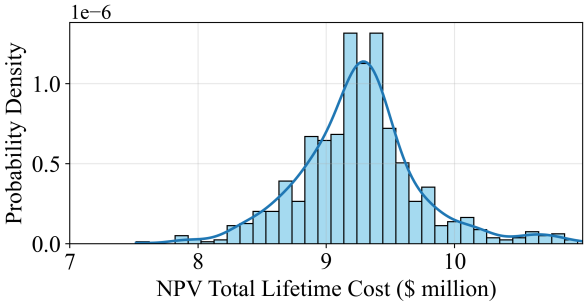

Figure 5.10: Lifetime cost distribution for a fuel price of 3$/kg

Conversely, a fuel price increase from 6$/kg to 9$/kg, in case of limited hydrogen availability, would widen the distribution spread as shown in Fig. 5.11, with a mean NPV of $20.6 million and a 5th - 95th percentile range spanning from $18.3 to $23.1 million ($4.8 million spread), corresponding to –11.1% and 12.1% deviations relative to the mean NPV.

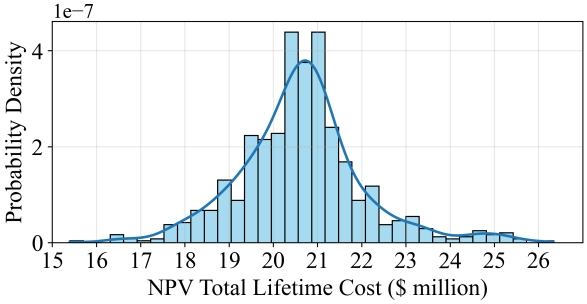

Figure 5.11: Lifetime cost distribution for a fuel price of 9$/kg

Another uncertain parameter is the number of lifetime voyages. If the vessel completes 5 fewer round trips per year, due to the speed reductions or potential port delays, the total lifetime cost is reduced by 4.8%, but the total income may also be reduced due to the lower voyage frequency. Due to the high unpredictability and the lack of reliable income data, the estimation of revenues is out of scope in this study.

The SCIP solver reported an optimality gap of 0% for all simulations, confirming that the optimization model consistently achieved globally optimal solutions [128].

5.5 CONCLUSIONS

This chapter presents a holistic MINLP framework for ship energy system design and NPV-based lifetime cost optimization, incorporating weather-driven speed

profile variability and navigation safety constraints. The analysis demonstrates how weather variability affects power profiles, required energy system capacities, and total lifetime cost. While the framework is applicable to various ship types and propulsion systems, it is particularly valuable for hydrogen-powered vessels, due to the high fuel price, system costs and sensitivity to load variability.

The following key results can be summarized:

- The total risk in the dataset decreases substantially from 25.25% to 6.38% (of total operating points) after applying safety-based speed reductions to mitigate resonance and successive high-wave impacts. Residual risks remain for rare scenarios (e.g., resonance at near-beam sea conditions), but these are considered operationally manageable for the case vessel, since they do not coincide with the critical sea states identified for this vessel (short wave periods of 4-8 seconds combined with significant wave heights exceeding 4 meters).

- The combined influence of varying ship speed and weather conditions can significantly alter the vessel's power demand, requiring fuel cell capacities between 700 and 1500 kW, depending on the power profile.

- The most frequent configuration across operating profiles is a 1200 kW fuel cell system with a 180 kWh battery system (for peak shaving), covering 39% of laden profiles. Some profiles require higher fuel cell capacity for sustained peaks and/or higher battery capacity to buffer fluctuations. The selected design configuration consists of 1500 kW installed fuel cell capacity and 180 kWh battery capacity. Further system capacity increases are not cost-effective.

- The optimization across operating profiles for the selected design configuration and a baseline fuel price of 6$/kg results to a lifetime cost distribution with a 5^{th}–95^{th} percentile range of -10.3% to +11.1% around the mean NPV ($14.9 million), highlighting the impact of operational and environmental variability. Fuel price reductions, in case of large-scale green hydrogen deployment and increased market adoption, would narrow this cost spread since fuel expenses are the largest share (76%) of the total lifetime cost.

Future extensions of this framework can include coupled speed-routing optimization, and enhanced hydrodynamic modelling through more advanced added wave resistance formulations. From a techno-economic perspective, the framework could be extended to include price-dependent re-optimization of system capacities under alternative hydrogen cost scenarios, and higher resolution transient operating profiles to assess short-duration power spikes, battery dispatch dynamics, degradation-aware replacement strategies, and validation against in-service power measurements.

6

CONCLUSIONS AND RECOMMENDATIONS

The key contribution of this thesis is the development of a holistic framework that jointly optimizes energy system design and operation from a lifetime economic perspective, accounting for system placement and ship stability constraints, as well as operating profile variability driven by weather effects and route-dependent operational data.

This chapter is organized as follows: In Section 6.1, each RQ is addressed, and the overall findings are summarized and reflected upon. In Section 6.2 the limitations of this thesis are summarized and in Section 6.3 recommendations for future research directions are proposed.

6.1 ANSWERS TO RESEARCH QUESTIONS

- **RQ1**: What methods, solvers, and objective functions are used for modeling and optimization of hydrogen-based and hybrid ship energy systems?

To answer RQ1, a detailed literature review was presented in Chapter 2. It was demonstrated that optimization of ship energy systems has been widely studied using physics-based modeling combined with mathematical programming and metaheuristic techniques. The most frequently applied methods include GA, PSO, and Dynamic Programming, with fuel cost and emissions being the dominant objectives particularly for diesel-hybrid ships. For hydrogen fuel cell-battery systems, the literature focuses on operational optimization and EMS, while integrated design-operation optimization and lifetime cost assessment remain limited. Chapter 3 - Chapter 5 address this gap.

- **RQ2**: How can the design and lifetime cost implications of retrofitting a diesel fuelled ship to a hydrogen fuel cell-battery configuration be quantified under varying economic scenarios?

To answer RQ2, Chapter 3 presented a lifetime techno-economic analysis of the case-study retrofit using a real-time EMS. The results show that lifetime economic performance is strongly driven by fuel price assumptions and carbon taxation. For the considered scenarios, the NPV of the hydrogen retrofit ranges from $2.2 million

lower to $18.8 million higher than the diesel baseline. Fuel cell degradation was found to be a critical factor, leading to a 24.5% increase in hydrogen consumption over the fuel cell lifetime and resulting in replacement after approximately 26,300 operating hours ($\sim$ 5 years), which is close to the manufacturer-provided lifetime limits (25,000 hours). From a design perspective, the main engine room components of the hydrogen-based version are comparable to the diesel configuration, with an increase of only 1.5 tons in weight and approximately 1.6 m^3 in volume. However, hydrogen storage introduces significant integration challenges. An LH_2 tank volume of 193 m^3, including a 40% capacity margin factor validated with industry input, is required to cover the most fuel-demanding voyage, raising significant space and safety constraints. Overall, retrofit feasibility is driven mainly by lifetime fuel economics and hydrogen storage integration. Engine-room machinery size is not the limiting factor for the studied vessel.

- **RQ3**: How can a single representative operating profile be synthesized from multiple routes and operating conditions, enabling accurate and computationally efficient lifetime cost optimization?

To answer RQ3, Chapter 4 developed a probability-based profile synthesis methods to downsample the annual propulsive power data into a single representative operating profile, preserving fuel consumption and fuel cell degradation that are critical for accurate lifetime cost optimization. The annual dataset was reduced by a predefined downsampling factor of 100. Compared to the original annual power data, the profile generated by the probability-based method achieved deviations of 0.33% in fuel consumption and 4% in degradation, satisfying the predefined $\pm 5\,\%$ acceptance thresholds for both criteria. Overall, these results demonstrate that the probability-based representative profile can replace the full annual dataset for computationally efficient lifetime cost optimization with minimal loss of accuracy. This confirms that statistically representative profile synthesis is sufficient for lifetime design and operation optimization of ship energy systems, and is particularly useful for vessels operating across multiple routes and under diverse operating and environmental conditions.

- **RQ4**: How can the energy system of a hydrogen fuelled vessel be optimally designed, from a system sizing and topology perspective, considering ship stability and safety constraints?

To answer RQ4, Chapter 4 developed a coupled system design and operation optimization framework in which component sizing, system topology, and power distribution are optimized simultaneously within an NPV-based lifetime cost minimization problem, subject to ship stability and safety constraints. The results show that lifetime cost is dominated by fuel expenditure, which accounts for approximately 74% of total cost, while total CAPEX, including component replacements, contributes 24.5%. Battery CAPEX and total maintenance expenditure together contribute less than 2% of the total lifetime cost. Fuel cells are optimally sized as the primary power source, while batteries are sized for low-load support and peak shaving. Oversizing either component increases total lifetime cost, as additional CAPEX outweighs fuel savings from small efficiency gains. Ignoring powertrain

efficiency changes after retrofitting can lead to underestimation of the optimal energy system sizes. From a ship stability perspective, hydrogen storage is the dominant design driver for the retrofit. Removal of 275 tons of diesel fuel from the original design, combined with placement of a 51 ton LH_2 tank on the upper deck, corresponding to refuelling every 4 sailing days in the case study, significantly alters the weight distribution and requires 171.5 tons of ballast (VCG 0.53 m, LCG 26.6 m) to satisfy the trim and vertical stability constraints. Engine-room components have a comparatively minor effect on vessel stability due to their low weight relative to ship displacement; several fuel cells and converters are arranged in five-module vertical stacks, highlighting their limited influence on vertical stability. Total vessel weight after retrofitting is approximately 1% lower than the original diesel configuration. Overall, these results demonstrate that cost-optimal and technically feasible solutions require the coupled consideration of system sizing, topology, operation, and stability constraints within a unified lifetime cost optimization framework.

- **RQ5**: How can the impacts of weather variability and navigation risks on the ship power profiles, required system capacities, and lifetime cost be assessed?

To answer RQ5, Chapter 5 incorporated weather-driven speed variability and navigation safety constraints into the lifetime design-operation optimization framework. The results show that weather variability significantly alters ship speed and power profiles. Depending on the operating conditions, power profiles ranged from prolonged low-power operation with frequent speed reductions required to mitigate resonance and successive high-wave impacts, to high-power winter scenarios driven by increased added resistance in head seas, as well as profiles with short-duration power peaks, all of which significantly influence optimal fuel cell and battery sizing. Relative to the capacity required under average operating conditions, a fuel cell capacity margin of approximately 25% was required to ensure full power coverage across all scenarios. Across the considered power profiles, there was a lifetime cost spread of approximately -10% to +11% around the mean NPV for a baseline hydrogen price of 6 $/kg. Higher fuel prices widen the cost distribution, while lower fuel prices narrow it, since the fuel cost is the largest share of the total lifetime cost. Overall, the findings demonstrate that neglecting weather variability and navigation safety constraints can lead to non-robust system designs and inaccurate lifetime cost outcomes, highlighting their importance for realistic and economically sound ship energy system optimization.

To summarize, this thesis addressed the following problem statement:

How can the energy systems of hydrogen-fuelled ships be designed and operated from a lifetime cost perspective, under realistic operational and regulatory constraints?

Overall, this thesis demonstrates that hydrogen-fuelled ship energy systems should be designed and operated to minimize lifetime cost while satisfying practical integration, stability, and operational constraints. Fuel expenditure dominates total lifetime cost, and economic viability is therefore highly sensitive to green hydrogen price assumptions. For the studied cargo vessel, fuel cells act as the main power source covering the majority of propulsion demand, while batteries support low-load operation and peak shaving. Oversizing either component increases lifetime cost,

as additional CAPEX outweigh fuel savings from small efficiency gains. Hydrogen storage is the main constraint shaping technical feasibility. Tank sizing, driven by refuelling requirements, directly affects system integration and determines the ballast needed to satisfy the trim and stability criteria, while engine-room machinery has a comparatively minor influence for the studied vessel. Neglecting key real-world effects such as powertrain efficiency changes after retrofitting, degradation-driven increases in fuel consumption, and operating profile variability across routes and environmental conditions can lead to non-robust designs and misleading lifetime cost outcomes.

6.2 LIMITATIONS

While this thesis develops a comprehensive framework for design and operation of hydrogen ship energy systems, the following limitations are acknowledged:

- **Propulsion-focused power demand**: Auxiliary loads (hotel loads, cooling, safety systems, and balance-of-plant) are not considered. For the original diesel-based vessel, shaft generator data indicate that conventional auxiliary electrical demand is on the order of 3-4% of propulsion power across the operating dataset. This should be interpreted as an indicative and partial estimate of auxiliary demand, as it may not capture all onboard consumers and does not represent additional loads associated with the hydrogen-based system, such as thermal management and balance-of-plant components. This suggests that inclusion of auxiliary loads would increase total power demand and lifetime cost, while propulsion remains the dominant contributor to overall demand for the reference vessel. The extent to which this affects system sizing and cost depends on the actual magnitude of total auxiliary demand, which is not captured in this study.
- **Simplified economic uncertainty**: Economic uncertainty is addressed through scenario-based variation of fuel prices and CAPEX, without explicit modeling of dynamic market evolution or hydrogen supply constraints.
- **Single case-study vessel**: Results are based on a retrofitted general cargo ship. Optimal designs, power profiles, cost distributions, and stability impacts are vessel- and mission-dependent.
- **No weather routing optimization**: Navigation risk mitigation is limited to speed adjustments, without route optimization.
- **Simplified added resistance modeling**: Added wave resistance is modeled using simplified assumptions, including zero resistance in following and stern-quartering seas.

6.3 RECOMMENDATIONS

Building on these limitations, several directions for future research are proposed:

- **Integration of auxiliary systems**: Extend the framework to include auxiliary loads and thermal management.
- **Advanced uncertainty modeling**: Incorporate stochastic or robust optimization to capture dynamic fuel markets and hydrogen availability.
- **Application to diverse vessel types**: Apply the framework to different ship types such as ferries and offshore vessels, to assess scalability.
- **Coupled weather routing and energy system optimization**: Integrate weather routing with speed control and energy system sizing
- **Enhanced hydrodynamic modeling**: Improve added resistance and seakeeping models for complex ship-wave interactions.

Appendices

A

EVALUATION OF AN ALTERNATIVE (RDP-BASED) PROFILE DOWNSAMPLING METHOD

This Appendix is part of Chapter 4. It documents the evaluation of an algorithmic-based donwsampling approach that was investigated as a potential alternative to the probability-based method, but not adopted in the main analysis.

A.1 OVERVIEW OF THE RDP-BASED APPROACH

As alternative to the probability-based profile generation method, a geometry-based downsampling approach using the Ramer Douglas Peucker (RDP) algorithm [119] was evaluated. The RDP algorithm simplifies a polyline (here, the power-time curve) by connecting the first and last points of a segment with a straight line and computing the maximum perpendicular distance of the intermediate points to that line. If this maximum distance is below a prescribed tolerance ε, the intermediate points in that segment are discarded; otherwise, the farthest point is retained and the procedure is applied recursively to the two resulting subsegments. This recursive process continues until the maximum perpendicular deviation between the original polyline and each line segment is no greater than ε, resulting in a simplified polyline with fewer points that preserves the overall geometric shape of the original curve. Increasing ε reduces the number of retained points (and computational cost) but decreases fidelity to the original profile, so ε represents a trade-off between computational efficiency and approximation accuracy.

When applied to power profiles, the method produces a reduced representation with variable time steps while preserving the overall geometric shape. In this study, the original annual load profile was reduced from 30,000 data to 300 data (corresponding to a reduction factor of 100) using an ε value of 0.9. The resulting profile spans the same total operating duration but includes variable time steps ranging from 5 minutes to 51 hours.

A.2 PERFORMANCE WITH RESPECT TO FUEL CONSUMPTION AND FUEL CELL DEGRADATION

The reduced profile obtained using the RDP algorithm was evaluated by comparing fuel consumption and fuel cell degradation estimates against those obtained from the full annual profile. The RDP-based reduction resulted in a deviation of -6.18% in fuel consumption, indicating that fuel consumption can be reasonably approximated despite the substantial reduction in dataset size.

In contrast the deviation in fuel cell degradation was -69%, demonstrating that the RDP algorithm fails to preserve transient load variations that are critical for degradation assessment. As illustrated in Fig. A.1, the RDP-based reduced profile introduces significant power deviations at specific time intervals compared to the original profile.

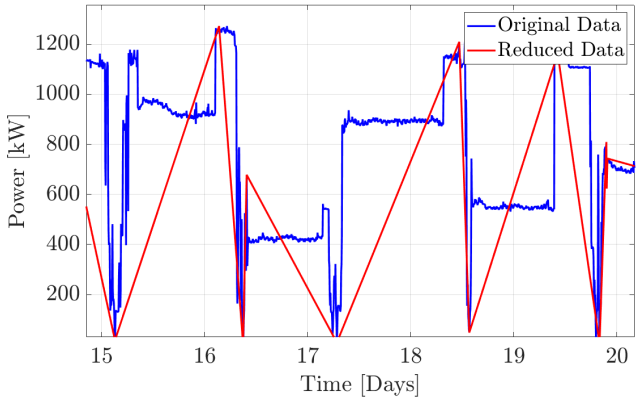

Figure A.1: RDP: Zoomed-in comparison of the profiles in the 15-20 days period

A.3 RATIONALE FOR EXCLUSION FROM THE MAIN ANALYSIS

Due to its inability to accurately represent degradation-relevant dynamics, the RDP-based approach was not adopted for the generation of representative load profiles in this work. Achieving acceptable degradation estimates with RDP would require a substantially larger number of retained data (in the range of thousands), which would significantly increase computational cost. Additionally, the variable time steps produced by RDP complicate integration with the subsequent optimization framework.

For these reasons, the probability-based method described in the main text was selected for all analyses presented in this study.

B

POWER AND RAMP STATISTICS FOR THE PROBABILITY-BASED PROFILE SYNTHESIS METHOD

The power-level and load ramps statistics presented in this Appendix are part of Chapter 4 and are provided for diagnostic purposes only. The representativeness of the reduced, probability-based profile is assessed in the main text using deviations in fuel consumption and fuel cell degradation metrics (±5% acceptance threshold), rather than through direct matching of individual statistical descriptors.

Table B.1 and Table B.2 report selected descriptive statistics of the power levels and load ramps for the full annual profile and the representative profile generated using the probability-based method.

Table B.1: Power level statistics
(P10 and P90 denote the 10^{th} and 90^{th} percentiles of the power-level distribution)

Statistic (kW)	Annual profile	Representative profile
Mean power	696	685
P10–P90 power	349–917	220–1202
Max power	1284	1300

Table B.1 summarizes the mean power, P10–P90 power range, and the maximum power level. The mean power of the representative profile differs by only 1.6% from that of the annual profile, which is consistent with the very small deviation observed in total fuel consumption (0.33%). The P10–P90 range indicates that the representative profile operates within a comparable power envelope. Differences in percentile bounds are expected due to the stochastic nature of the sampling procedure and the substantial reduction in dataset size.

Table B.2: Load ramp statistics
(P10 and P90 denote the 10^{th} and 90^{th} percentiles of the load-ramp distribution)

Statistic (kW)	Annual profile	Representative profile
Mean $\lvert\Delta P\rvert$	15.9	16.5
Median $\lvert\Delta P\rvert$	3	2.5
P10–P90 $\lvert\Delta P\rvert$	0–30	0.5–25

Table B.2 summarizes statistics of absolute power changes between successive time steps ($\lvert\Delta P\rvert$), including the mean, median and the P10–P90 ramp range. The close agreement in mean and median ramp magnitudes indicates that typical load-ramping behaviour is well presented in the reduced profile. The P10–P90 ramp range further confirms that the magnitude of common transient events is preserved, which is consistent with the small deviation observed in the degradation-related proxy (4%) used during profile selection.

BIBLIOGRAPHY

[1] L. Khan, J. J. R. Macklin, B. C. D. Peck, O. Morton and J.-B. R. G. Souppez, "A review of wind-assisted ship propulsion for sustainable commercial shipping: Latest developments and future stakes", *in Proceedings of the Wind Propulsion Conference*, 2021. DOI: 10.3940/rina.win.2021.05.

[2] D. Gritsenko, "Regulating GHG emissions from shipping: Local, global, or polycentric approach?", *Marine Policy*, vol. 84, pp. 130–133, 2017. DOI: 10.1016/j.marpol.2017.07.010.

[3] International Maritime Organization. "2023 IMO strategy on reduction of GHG emissions from ships", Accessed: 27 Sep. 2025. [Online]. Available: https://www.imo.org/en/ourwork/environment/pages/2023-imo-strategy-on-reduction-of-ghg-emissions-from-ships.aspx.

[4] "EEXI and CII — ship carbon intensity and rating system: Frequently asked questions", International Maritime Organization, Accessed: 27 Sep. 2025. [Online]. Available: https://www.imo.org/en/MediaCentre/HotTopics/Pages/EEXI-CII-FAQ.aspx.

[5] O. B. Inal, J. F. Charpentier and C. Deniz, "Hybrid power and propulsion systems for ships: Current status and future challenges", *Renewable and Sustainable Energy Reviews*, vol. 156, 2022, Art. no. 111965. DOI: 10.1016/j.rser.2021.111965.

[6] H. K. Fathy, J. A. Reyer, P. Y. Papalambros and A. Ulsov, "On the coupling between the plant and controller optimization problems", *Proceedings of the 2001 American Control Conference*, IEEE, vol. 3, 2001, pp. 1864–1869.

[7] A. Rasheed, O. San and T. Kvamsdal, "Digital twin: Values, challenges and enablers from a modeling perspective", *IEEE Access*, vol. 8, pp. 21 980–22 012, 2020. DOI: 10.1109/ACCESS.2020.2970143.

[8] F. Mylonopoulos, H. Polinder and A. Coraddu, "A comprehensive review of modeling and optimization methods for ship energy systems", *IEEE Access*, vol. 11, pp. 32697 –32 707, 2023. DOI: 10.1109/ACCESS.2023.3263719.

[9] P. Wu and R. Bucknall, "Hybrid fuel cell and battery propulsion system modelling and multi-objective optimisation for a coastal ferry", *International Journal of Hydrogen Energy*, vol. 45, no. 4, pp. 3193–3208, 2020. DOI: 10.1016/j.ijhydene.2019.11.152.

[10] M. Ganjian, H. B. Farahabadi, M. A. Alirezapouri and M. R. Firuzjaei, "Optimal design strategy for fuel cell-based hybrid power system of all-electric ships", *International Journal of Hydrogen Energy*, vol. 50, pp. 1558–1571, 2024. DOI: 10.1016/j.ijhydene.2023.07.258.

[11] G. T. Vieira, D. F. Pereira, S. I. Taheri, K. S. Khan, M. B. Salles, J. M. Guerrero and B. S. Carmo, "Optimized configuration of diesel engine-fuel cell-battery hybrid power systems in a platform supply vessel to reduce CO_2 emissions", *Energies*, vol. 15, no. 6, 2022, Art. no. 2184. DOI: 10.3390/en15062184.

[12] N. Vasilikis, R. Geertsma and A. Coraddu, "A multi-objective optimisation framework for the design of ship energy systems under operational and environmental uncertainty", *Applied Energy*, vol. 402, 2025, Art. no. 126829. DOI: 10.1016/j.apenergy.2025.126829.

[13] J. Zhu, L. Chen, B. Wang and L. Xia, "Optimal design of a hybrid electric propulsive system for an anchor handling tug supply vessel", *Applied Energy*, vol. 226, pp. 423–436, 2018. DOI: 10.1016/j.apenergy.2018.05.131.

[14] Z. Jianyun, C. Li, X. Lijuan and W. Bin, "Bi-objective optimal design of plug-in hybrid electric propulsion system for ships", *Energy*, vol. 177, pp. 247–261, 2019. DOI: 10.1016/j.energy.2019.04.079.

[15] H. Lan, S. Wen, Y. Y. Hong, D. C. Yu and L. Zhang, "Optimal sizing of hybrid pv/diesel/battery in ship power system", *Applied Energy*, vol. 158, pp. 26–34, 2015. DOI: 10.1016/j.apenergy.2015.08.031.

[16] W. Wang, L. Chen and X. Liang, "Optimal sizing of sail-assisted pv/shore power hybrid propulsion systems", *Proceedings of the International Offshore and Polar Engineering Conference*, Oct. 2020.

[17] K. Zhan, H. Gao, H. Chen and Z. Lin, "Optimal retrofitting of a hybrid propulsion system using nsga-ii algorithm for trailing suction hopper dredger", *2015 IEEE Electric Ship Technologies Symposium, ESTS 2015*, Institute of Electrical and Electronics Engineers Inc., Jul. 2015, pp. 201–206. DOI: 10.1109/ESTS.2015.7157888.

[18] J. Zhu and C. Li, "Multi-objective optimal design of a plug-in hybrid electric propulsion system for a catamaran", *Proceedings of the 29th International Offshore and Polar Engineering Conference (ISOPE)*, Jun. 2019.

[19] Z. Wang, L. Chen, F. Guo and W. Bin, "Optimal design of hybrid electric propulsive system for a mini polar cruise", *Proceedings of the 31st International Offshore and Polar Engineering Conference (ISOPE)*, Rhodes, Greece, Jun. 2021.

[20] E. Nivolianiti, Y. L. Karnavas and G. Chatziaslanoglou, "Techno-economic and life cycle cost analysis for hybrid short-sea passenger vessels based on optimization of different energy storage configurations and management", *Energy Conversion and Management*, vol. 343, 2025, Art. no. 120148. DOI: 10.1016/j.enconman.2025.120148.

[21] J. J. Valera-Garcia and I. Atutxa-Lekue, "On the optimal design of hybrid-electric power systems for offshore vessels", *IEEE Transactions on Transportation Electrification*, vol. 5, no. 1, pp. 324–334, 2019. DOI: 10.1109/TTE.2018.2883870.

[22] A. Dolatabadi and B. Mohammadi-Ivatloo, "Stochastic risk-constrained optimal sizing for hybrid power system of merchant marine vessels", *IEEE Transactions on Industrial Informatics*, vol. 14, no. 12, pp. 5509–5517, 2018. DOI: 10.1109/TII.2018.2824811.

[23] L. Kistner, A. Bensmann and R. Hanke-Rauschenbach, "Optimal design of a distributed ship power system with solid oxide fuel cells under the consideration of component malfunctions", *Applied Energy*, vol. 316, 2022, Art. no. 119052. DOI: 10.1016/j.apenergy.2022.119052.

[24] R. B. Cardenas, O. Mo and G. Guidi, "Optimal sizing of battery energy storage systems for hybrid marine power system", *Proceedings of the IEEE Electric Ship Technologies Symposium (ESTS): Emerging Technologies for the Future Electric Ship*, IEEE, Arlington, TX, USA, Aug. 2019, pp. 293–302.

[25] Y. Sun, Q. Xu, Y. Yuan and B. Yang, "Optimal energy management of fuel cell hybrid electric ships considering fuel cell aging cost", *in Proceedings of the IEEE IAS Industrial and Commercial Power Systems Conference (ICPS)*, Weihai, China, Jul. 2020, pp. 240–245. DOI: 10.1109/ICPSAsia48933.2020.9208534.

[26] J. Han, J. F. Charpentier and T. Tang, "An energy management system of a fuel cell/battery hybrid boat", *Energies*, vol. 7, no. 5, pp. 2799–2820, 2014. DOI: 10.3390/en7052799.

[27] D. Mitropoulou, M. Kalikatzarakis, T. van Der Klauw, A. J. Blokland, R. D. Geertsma, A. M. Bucurenciu and D. Dembinskas, "Multi-objective optimisation and energy management: Adapt your ship to every mission", *Proceedings of the International Ship Control Systems Symposium*, vol. 1, Institute of Marine Engineering Science & Technology, 2020. DOI: 10.24868/issn.2631-8741.2020.015.

[28] Y. Xiang and X. Yang, "An ECMS for multi-objective energy management strategy of parallel diesel electric hybrid ship based on ant colony optimization algorithm", *Energies*, vol. 14, no. 4, 2021, Art. no. 810. DOI: 10.3390/en14040810.

[29] C. Dall'armi, D. Pivetta and R. Taccani, "Health-conscious optimization of long-term operation for hybrid PEMFC ship propulsion systems", *Energies*, vol. 14, no. 13, 2021, Art. no. 3813. DOI: 10.3390/en14133813.

[30] Z. Zhang, C. Guan and Z. Liu, "Real-time optimization energy management strategy for fuel cell hybrid ships considering power sources degradation", *IEEE Access*, vol. 8, pp. 87 046–87 059, 2020. DOI: 10.1109/ACCESS.2020.2991519.

[31] A. M. Bassam, A. B. Phillips, S. R. Turnock and P. A. Wilson, "Development of a multi-scheme energy management strategy for a hybrid fuel cell driven passenger ship", *International Journal of Hydrogen Energy*, vol. 42, no. 1, pp. 623–635, 2017. DOI: 10.1016/j.ijhydene.2016.08.209.

[32] K. Hein, Y. Xu, G. Wilson and A. K. Gupta, "Coordinated optimal voyage planning and energy management of all-electric ship with hybrid energy storage system", *IEEE Transactions on Power Systems*, vol. 36, no. 3, pp. 2355–2365, 2021. DOI: 10.1109/TPWRS.2020.3029331.

[33] C. Shang, D. Srinivasan and T. Reindl, "Economic and environmental generation and voyage scheduling of all-electric ships", *IEEE Transactions on Power Systems*, vol. 31, no. 5, pp. 4087–4096, 2016. DOI: 10.1109/TPWRS.2015.2498972.

[34] P. Wu, J. Partridge, E. Anderlini, Y. Liu and R. Bucknall, "Near-optimal energy management for plug-in hybrid fuel cell and battery propulsion using deep reinforcement learning", *International Journal of Hydrogen Energy*, vol. 46, no. 80, pp. 40 022–40 040, 2021. DOI: 10.1016/j.ijhydene.2021.09.196.

[35] P. Wu, J. Partridge and R. Bucknall, "Cost-effective reinforcement learning energy management for plug-in hybrid fuel cell and battery ships", *Applied Energy*, vol. 275, 2020, Art. no. 115258. DOI: 10.1016/j.apenergy.2020.115258.

[36] S. Kim and J. Kim, "Optimal energy control of battery hybrid system for marine vessels by applying neural network based on equivalent consumption minimization strategy", *Journal of Marine Science and Engineering*, vol. 9, no. 11, 2021, Art. no. 1228. DOI: 10.3390/jmse9111228.

[37] F. D. Kanellos, "Optimal power management with GHG emissions limitation in all-electric ship power systems comprising energy storage systems", *IEEE Transactions on Power Systems*, vol. 29, no. 1, pp. 330–339, 2014. DOI: 10.1109/TPWRS.2013.2280064.

[38] F. D. Kanellos, A. Anvari-Moghaddam and J. M. Guerrero, "A cost-effective and emission-aware power management system for ships with integrated full electric propulsion", *Electric Power Systems Research*, vol. 150, pp. 63–75, 2017. DOI: 10.1016/j.epsr.2017.05.003.

[39] Z. H. Zhao, "Improved fuzzy logic control-based energy management strategy for hybrid power system of FC/PV/battery/SC on tourist ship", *International Journal of Hydrogen Energy*, vol. 47, no. 16, pp. 9719–9734, 2022. DOI: 10.1016/j.ijhydene.2022.01.040.

[40] L. Zhu, J. Han, D. Peng, T. Wang, T. Tang and J. F. Charpentier, "Fuzzy logic based energy management strategy for a fuel cell/battery/ultra-capacitor hybrid ship", *in 2014 1st International Conference on Green Energy (ICGE)*, Sfax, Tunisia, Mar. 2014, pp. 107–112. DOI: 10.1109/ICGE.2014.6835406.

[41] T. Kopka, A. Coraddu and H. Polinder, "Optimal energy management of fc-battery shipboard power system using dynamic programming", *IEEE International Conference on Electrical Systems for Aircraft, Railway, Ship Propulsion and Road Vehicles & International Transportation Electrification Conference (ESARS-ITEC)*, IEEE, 2024, pp. 1–6. DOI: 10.1109/ESARS-ITEC60450.2024.10819881.

[42] T. Kopka, A. Coraddu and H. Polinder, "Distributed mpc for cost-optimal control of fc-battery shipboard microgrids", *IEEE Seventh International Conference on DC Microgrids (ICDCM)*, IEEE, 2025, pp. 1–6. DOI: 10.1109/ICDCM63994.2025.11144727.

[43] C. Löffler, R. Geertsma, H. Polinder and A. Coraddu, "Optimizing fuel consumption of a dual-fuel full-electric vessel using model predictive control", *IEEE International Conference on Electrical Systems for Aircraft, Railway, Ship Propulsion and Road Vehicles & International Transportation Electrification Conference (ESARS-ITEC)*, IEEE, 2024, pp. 1–6.

[44] C. Löffler, T. Kopka, R. Geertsma, H. Polinder and A. Coraddu, "Optimizing energy management for full-electric vessels: A health-aware approach with hydrogen and diesel employing equivalent consumption minimization strategy", *IEEE Transportation Electrification Conference and Expo, Asia-Pacific (ITEC Asia-Pacific)*, 2023. DOI: 10.1109/ITECAsia-Pacific59272.2023.10372270.

[45] X. Wang, U. Shipurkar, A. Haseltalab, H. Polinder, F. Claeys and R. R. Negenborn, "Sizing and control of a hybrid ship propulsion system using multi-objective double-layer optimization", *IEEE Access*, vol. 9, pp. 72 587–72 601, 2021. DOI: 10.1109/ACCESS.2021.3080195.

[46] C. Dall'Armi, D. Pivetta and R. Taccani, "Uncertainty analysis of the optimal health-conscious operation of a hybrid PEMFC coastal ferry", *International Journal of Hydrogen Energy*, vol. 47, no. 21, pp. 11 428–11 440, 2022. DOI: 10.1016/j.ijhydene.2021.10.271.

[47] D. Pivetta, C. Dall'Armi and R. Taccani, "Multi-objective optimization of hybrid PEMFC/Li-ion battery propulsion systems for small and medium size ferries", *International Journal of Hydrogen Energy*, vol. 46, no. 72, pp. 35 949–35 960, 2021. DOI: 10.1016/j.ijhydene.2021.02.124.

[48] M. Soleymani, A. Yoosofi and M. Kandi-D, "Sizing and energy management of a medium hybrid electric boat", *Journal of Marine Science and Technology (Japan)*, vol. 20, no. 4, pp. 739–751, 2015. DOI: 10.1007/s00773-015-0327-0.

[49] P. Wu and P. Bucknall, "On the design of plug-in hybrid fuel cell and lithium battery propulsion systems for coastal ships", *Proceedings of the 13th International Marine Design Conference (IMDC)*, Helsinki, Finland, Jun. 2018, pp. 1–10.

[50] J. Zhu, L. Chen, X. Wang and L. Yu, "Bi-level optimal sizing and energy management of hybrid electric propulsion systems", *Applied Energy*, vol. 260, 2020, Art. no. 114134. DOI: 10.1016/j.apenergy.2019.114134.

[51] F. Balsamo, C. Capasso, D. Lauria and O. Veneri, "Optimal design and energy management of hybrid storage systems for marine propulsion applications", *Applied Energy*, vol. 278, 2020, Art. no. 115629. DOI: 10.1016/j.apenergy.2020.115629.

[52] A. Letafat, M. Rafiei, M. Sheikh, M. Afshari-Igder, M. Banaei, J. Boudjadar and M. H. Khooban, "Simultaneous energy management and optimal components sizing of a zero-emission ferry boat", *Journal of Energy Storage*, vol. 28, 2020, Art. no. 101215. DOI: 10.1016/j.est.2020.101215.

[53] L. Chen, Y. Tong and Z. Dong, "Li-ion battery performance degradation modeling for the optimal design and energy management of electrified propulsion systems", *Energies*, vol. 13, no. 7, 2020, Art. no. 1629. DOI: 10.3390/en13071629.

[54] T. Hofman, M. Naaborg and E. Sciberras, "System-level design optimization of a hybrid tug", *Proceedings of the IEEE Vehicle Power and Propulsion Conference (VPPC)*, IEEE, Belfort, France, Dec. 2017, pp. 1–6.

[55] S. Durgaprasad, A. Coraddu, E. Heyneman, C. Lamproye and H. Polinder, "A scenario-based integrated battery sizing and power plant scheduling under variable fuel prices and maritime operational profiles", *Energy Conversion and Management: X*, vol. 28, 2025, Art. no. 101240. DOI: https://doi.org/10.1016/j.ecmx.2025.101240.

[56] S. Durgaprasad, A. Coraddu and H. Polinder, "An analysis of maritime battery requirements and a decision tree for optimal chemistry selection", *Energy Reports*, vol. 14, pp. 4851–4871, 2025. DOI: https://doi.org/10.1016/j.egyr.2025.11.086.

[57] H. Chen, Z. Zhang, C. Guan and H. Gao, "Optimization of sizing and frequency control in battery/supercapacitor hybrid energy storage system for fuel cell ship", *Energy*, vol. 197, 2020, Art. no. 117285. DOI: 10.1016/j.energy.2020.117285.

[58] Y. Si, R. Wang, S. Zhang, W. Zhou, A. Lin and G. Zeng, "Configuration optimization and energy management of hybrid energy system for marine using quantum computing", *Energy*, vol. 253, 2022, Art. no. 124131. DOI: 10.1016/j.energy.2022.124131.

[59] F. Mylonopoulos, S. Durgaprasad, A. Coraddu and H. Polinder, "Lifetime design, operation, and cost analysis for the energy system of a retrofitted cargo vessel with fuel cells and batteries", *International Journal of Hydrogen Energy*, vol. 91, pp. 1262–1273, 2024. DOI: 10.1016/J.IJHYDENE.2024.10.235.

[60] United Nations Conference on Trade and Development (UNCTAD), "Review of maritime transport 2022", United Nations Conference on Trade and Development, Geneva, Switzerland, UNCTAD/RMT/2022, 2022. [Online]. Available: https://unctad.org/publication/review-maritime-transport-2022.

[61] S. Fang, Y. Wang, B. Gou and Y. Xu, "Toward future green maritime transportation: An overview of seaport microgrids and all-electric ships", *IEEE Transactions on Vehicular Technology*, vol. 69, no. 1, pp. 207–219, 2020. DOI: 10.1109/TVT.2019.2950538.

[62] F. Mylonopoulos, E. Boulougouris, N. L. Trivyza, A. Priftis, M. Cheliotis, H. Wang and G. Shi, "Hydrogen vs. batteries: Comparative safety assessments for a high-speed passenger ferry", *Applied Sciences (Switzerland)*, vol. 12, no. 6, 2022, Art. no. 2919. DOI: 10.3390/app12062919.

[63] A. M. Bassam, A. B. Phillips, S. R. Turnock and P. A. Wilson, "An improved energy management strategy for a hybrid fuel cell/battery passenger vessel", *International Journal of Hydrogen Energy*, vol. 41, no. 47, pp. 22 453–22 464, 2016. DOI: 10.1016/j.ijhydene.2016.08.049.

[64] F. Fan, V. Aditya, Y. Xu, B. Cheong and A. K. Gupta, "Robustly coordinated operation of a ship microgird with hybrid propulsion systems and hydrogen fuel cells", *Applied Energy*, vol. 312, 2022, Art. no. 118738. DOI: 10.1016/j.apenergy.2022.118738.

[65] Z. Wang and X. Li, "Research on multi-objective optimization of capacity allocation for marine hybrid energy storage system", *IOP Conference Series: Earth and Environmental Science*, vol. 692, IOP Publishing Ltd, Mar. 2021. DOI: 10.1088/1755-1315/692/2/022106.

[66] A. M. Bassam, A. B. Phillips, S. R. Turnock and P. A. Wilson, "Sizing optimization of a fuel cell/battery hybrid system for a domestic ferry using a whole ship system simulator", *2016 International Conference on Electrical Systems for Aircraft, Railway, Ship Propulsion and Road Vehicles and International Transportation Electrification Conference (ESARS-ITEC)*, 2016. DOI: 10.1109/ESARS-ITEC.2016.7841333.

[67] B. Lagemann, E. Lindstad, K. Fagerholt, A. Rialland and S. O. Erikstad, "Optimal ship lifetime fuel and power system selection", *Transportation Research Part D: Transport and Environment*, vol. 102, 2022, Art. no. 103145. DOI: 10.1016/j.trd.2021.103145.

[68] B. Lagemann, S. Lagouvardou, E. Lindstad, K. Fagerholt, H. N. Psaraftis and S. O. Erikstad, "Optimal ship lifetime fuel and power system selection under uncertainty", *Transportation Research Part D: Transport and Environment*, vol. 119, 2023, Art. no. 103748. DOI: 10.1016/j.trd.2023.103748.

[69] M. D. Al-Falahi, J. Coleiro, S. D. Jayasinghe, H. Enshaei, V. Garaniya, C. Baguley and U. Madawala, "Techno-economic feasibility study of battery-powered ferries", *IEEE 4th Southern Power Electronics Conference (SPEC)*, 2018. DOI: 10.1109/SPEC.2018.8636010.

[70] H. Wang, M. Z. Aung, X. Xu and E. Boulougouris, "Life cycle analysis of hydrogen powered marine vessels—case ship comparison study with conventional power system", *Sustainability (Switzerland)*, vol. 15, no. 17, 2023, Art. no. 12946. DOI: 10.3390/su151712946.

[71] O. B. Inal, B. Zincir, C. Dere and J.-F. Charpentier, "Hydrogen fuel cell as an electric generator: A case study for a general cargo ship", *Journal of Marine Science and Engineering*, vol. 12, no. 3, 2024, Art. no. 432. DOI: 10.3390/jmse12030432.

[72] P. Karvounis, G. Theotokatos and E. Boulougouris, "Environmental-economic sustainability of hydrogen and ammonia fuels for short sea shipping operations", *International Journal of Hydrogen Energy*, vol. 57, pp. 1070–1080, 2024. DOI: 10.1016/j.ijhydene.2024.01.058.

[73] J. C. Gomez Trillos, D. Wilken, U. Brand and T. Vogt, "Life cycle assessment of a hydrogen and fuel cell ropax ferry prototype", *Progress in Life Cycle Assessment 2019*, ser. Sustainable Production, Life Cycle Engineering and Management, S. Albrecht, M. Fischer, P. Leistner and L. Schebek, Eds., Cham: Springer, 2021.

[74] F. Mylonopoulos, T. Kopka, A. Coraddu and H. Polinder, "Model-based parametric study for comparison of system configurations and control of a hydrogen hybrid cargo vessel", *in Proceedings of the Modelling and Optimisation of Ship Energy Systems (MOSES)*, 2023. DOI: 10.59490/moses.2023.671.

[75] N. Ma, W. Zhao, W. Wang, X. Li and H. Zhou, "Large scale of green hydrogen storage: Opportunities and challenges", *International Journal of Hydrogen Energy*, vol. 50, pp. 379–396, 2024. DOI: 10.1016/j.ijhydene.2023.09.021.

[76] U. Hasturk, A. H. Schrotenboer, E. Ursavas and K. J. Roodbergen, "Stochastic cyclic inventory routing with supply uncertainty: A case in green-hydrogen logistics", *Transportation Science*, vol. 58, no. 2, pp. 315–339, 2024. DOI: 10.1287/trsc.2022.0435.

[77] D. A. Allan, C. N. Bates, M. J. Risbeck and J. B. Rawlings, "On the inherent robustness of optimal and suboptimal nonlinear mpc", *Systems and Control Letters*, vol. 106, pp. 68–78, 2017. DOI: 10.1016/j.sysconle.2017.03.005.

[78] zepp.Solutions. "Maritime hydrogen fuel cell systems", Accessed: 01 Feb. 2024. [Online]. Available: https://zepp.solutions/en/maritime-fuel-cell-systems/.

[79] C. Lorenzo, D. Bouquain, S. Hibon and D. Hissel, "Synthesis of degradation mechanisms and of their impacts on degradation rates on proton-exchange membrane fuel cells and lithium-ion nickel–manganese–cobalt batteries in hybrid transport applications", *Reliability Engineering and System Safety*, vol. 212, 2021, Art. no. 107369. DOI: 10.1016/j.ress.2020.107369.

[80] N. P. Reddy, R. Skjetne, O. S. Os and D. Papageorgiou, "A comparison of the state-of-the-art reinforcement learning algorithms for health-aware energy & emissions management in zero-emission ships", *IEEE Journal of Emerging and Selected Topics in Industrial Electronics*, vol. 5, no. 1, 2024. DOI: 10.1109/JESTIE.2023.3331230.

[81] Y. Feng and Z. Dong, "Integrated design and control optimization of fuel cell hybrid mining truck with minimized lifecycle cost", *Applied Energy*, vol. 270, 2020, Art. no. 115164. DOI: 10.1016/j.apenergy.2020.115164.

[82] T. Fletcher, R. Thring and M. Watkinson, "An energy management strategy to concurrently optimise fuel consumption & PEM fuel cell lifetime in a hybrid vehicle", *International Journal of Hydrogen Energy*, vol. 41, no. 46, pp. 21 503–21 515, 2016. DOI: 10.1016/j.ijhydene.2016.08.157.

[83] E. Schaltz, A. Khaligh and P. O. Rasmussen, "Influence of battery/ultracapacitor energy-storage sizing on battery lifetime in a fuel cell hybrid electric vehicle", *IEEE Transactions on Vehicular Technology*, vol. 58, no. 8, pp. 3882–3891, 2009. DOI: 10.1109/TVT.2009.2027909.

[84] Praxis Automation Technology B.V. "Greenbattery — electric energy storage", Accessed: 01 Feb. 2024. [Online]. Available: https://www.praxis-automation.eu/products/electric-energy-storage/.

[85] H. Ali, H. Beltran, N. J. Lindsey and M. Pecht, "Assessment of the calendar aging of lithium-ion batteries for a long-term—space missions", *Frontiers in Energy Research*, vol. 11, 2023. DOI: 10.3389/fenrg.2023.1108269.

[86] G. Soni, R. C. Neto and L. Moreira, "Hydrodynamic simulation of green hydrogen catamaran operating in lisbon, portugal", *Journal of Marine Science and Engineering*, vol. 11, no. 12, 2023, Art. no. 2273. DOI: 10.3390/jmse11122273.

[87] M. Perčić, N. Vladimir, I. Jovanović and M. Koričan, "Application of fuel cells with zero-carbon fuels in short-sea shipping", *Applied Energy*, vol. 309, 2022, Art. no. 118463. DOI: 10.1016/j.apenergy.2021.118463.

[88] J. W. Pratt and L. E. Klebanoff, "Feasibility of SF-BREEZE: A zero emission hydrogen fuel cell high speed passenger ferry", Sandia National Laboratories, Livermore, CA, USA, Sandia Report SAND2016-9719, 2016. [Online]. Available: https://energy.sandia.gov/wp-content/uploads/2016/10/SAND2016-9719.pdf.

[89] F. G. Aarskog, J. Danebergs, T. Strømgren and Øystein Ulleberg, "Energy and cost analysis of a hydrogen driven high speed passenger ferry", *International Shipbuilding Progress*, vol. 67, no. 1, 2020. DOI: 10.3233/ISP-190273.

[90] J. Cichowicz, G. Theotokatos and D. Vassalos, "Dynamic energy modelling for ship life-cycle performance assessment", *Ocean Engineering*, vol. 110, pp. 49–61, 2015. DOI: 10.1016/j.oceaneng.2015.05.041.

[91] TNO, "Power-2-fuel cost analysis, Smartport", TNO; SmartPort, Report, 2020. Accessed: 25 Sep. 2025. [Online]. Available: https://smartport.nl/wp-content/uploads/2020/09/CostAnalysis-Power-2-Fuel_def_2020.pdf.

[92] Deloitte China and Ballard Power Systems, "Fueling the future of mobility: Hydrogen and fuel cell solutions for transportation", Deloitte China, White paper, Jan. 2020.

[93] K. Kim, G. Roh, W. Kim and K. Chun, "A preliminary study on an alternative ship propulsion system fueled by ammonia: Environmental and economic assessments", *Journal of Marine Science and Engineering*, vol. 8, no. 3, 2020, Art. no. 183. DOI: 10.3390/jmse8030183.

[94] D. Thomas, "Cost reduction potential for electrolyser technology", Hydrogenics, Mississauga, ON, Canada, White paper/Technical report, 2018.

[95] X. Chen, S. Long, L. He, C. Wang, F. Chai, X. Kong, Z. Wan, X. Song and Z. Tu, "Performance evaluation on thermodynamics-economy-environment of pemfc vehicle power system under dynamic condition", *Energy Conversion and Management*, vol. 269, 2022, Art. no. 116082. DOI: 10.1016/j.enconman.2022.116082.

[96] V. Cigolotti, M. Genovese and P. Fragiacomo, "Comprehensive review on fuel cell technology for stationary applications as sustainable and efficient poly-generation energy systems", *Energies*, vol. 14, no. 16, 2021, Art. no. 4963. DOI: 10.3390/en14164963.

[97] L. Kistner, A. Bensmann and R. Hanke-Rauschenbach, "Potentials and limitations of battery-electric container ship propulsion systems", *Energy Conversion and Management: X*, vol. 21, 2024, Art. no. 100507. DOI: 10.1016/j.ecmx.2023.100507.

[98] H. K. Shin and S. K. Ha, "A review on the cost analysis of hydrogen gas storage tanks for fuel cell vehicles", *Energies*, vol. 16, no. 13, 2023, Art. no. 5233. DOI: 10.3390/en16135233.

[99] H. Derking, L. van der Togt and M. Keezer, "Liquid hydrogen storage: Status and future perspectives", Presentation, 2019.

[100] International Renewable Energy Agency (IRENA), "Electricity storage and renewables: Costs and markets to 2030", International Renewable Energy Agency (IRENA), Abu Dhabi, 2017. Accessed: 01 Mar. 2024. [Online]. Available: https://www.irena.org/publications/2017/Oct/Electricity-storage-and-renewables-costs-and-markets.

[101] O. Y. Edelenbosch, A. F. Hof, B. Nykvist, B. Girod and D. P. van Vuuren, "Transport electrification: The effect of recent battery cost reduction on future emission scenarios", *Climatic Change*, vol. 151, no. 2, pp. 95–108, 2018. DOI: 10.1007/s10584-018-2250-y.

[102] H. Chen, P. Pei and M. Song, "Lifetime prediction and the economic lifetime of proton exchange membrane fuel cells", *Applied Energy*, vol. 142, pp. 154–163, 2015. DOI: 10.1016/j.apenergy.2014.12.062.

[103] PwC. "The green hydrogen economy – predicting the decarbonisation agenda of tomorrow", Accessed: 23 Aug. 2025. [Online]. Available: https://www.pwc.com/gx/en/industries/energy-utilities-resources/green-hydrogen-cost.html.

[104] Ship & Bunker. "Rotterdam bunker prices — ship & bunker", Accessed: 01 Mar. 2024. [Online]. Available: https://shipandbunker.com/prices/emea/nwe/nl-rtm-rotterdam.

[105] Sustainable Ships. "EU ETS — sustainable ships", Accessed: 01 Mar. 2024. [Online]. Available: https://www.sustainable-ships.org/rules-regulations/eu-ets.

[106] European Commission. "FAQ — maritime transport in EU emissions trading system (ETS)", Accessed: 01 Mar. 2024. [Online]. Available: https://climate.ec.europa.eu/eu-action/transport/reducing-emissions-shipping-sector/faq-maritime-transport-eu-emissions-trading-system-ets_en.

[107] PwC Netherlands. "Energy transition: CO_2 levy & NL CO_2 tax (in dutch) — state of tax", Accessed: 01 Mar. 2024. [Online]. Available: https://www.pwc.nl/en/services/tax/webcast-series-state-of-tax/energy-transition.html.

[108] Getting to Zero Coalition. "Policy options for closing the competitiveness gap between fossil and zero-emission fuels in shipping", Global Maritime Forum, Accessed: 01 Mar. 2024. [Online]. Available: https://www.globalmaritimeforum.org/content/2021/11/INSIGH1.pdf.

[109] S. Karagiorgis, S. Nasiri and H. Polinder, "Implementation of ship hybridisation: Sizing a hybrid crew transfer vessel considering uncertainties", *Proceedings of the International Naval Engineering Conference (INEC)*, 2022.

[110] S. Z. A. Ghafri et al., "Hydrogen liquefaction: A review of the fundamental physics, engineering practice and future opportunities", *Energy and Environmental Science*, vol. 15, no. 7, pp. 2690–2731, 2022. DOI: 10.1039/d2ee00099g.

[111] L. Balestra and I. Schjølberg, "Modelling and simulation of a zero-emission hybrid power plant for a domestic ferry", *International Journal of Hydrogen Energy*, vol. 46, no. 18, pp. 10 924–10 938, 2021. DOI: 10.1016/j.ijhydene.2020.12.187.

[112] "ACS880 drive modules — optimized for cabinet assembly | industrial drives | ABB". Product page, ABB, Accessed: 01 Mar. 2024. [Online]. Available: https://new.abb.com/drives/low-voltage-ac/industrial-drives/acs880-drive-modules.

[113] "AXR 400ML6 680 kW 4160 V ABB high voltage induction motors 1193 rpm 60 hz". Product page, Bonnew Motors, Accessed: 25 Feb. 2024. [Online]. Available: https://motors.bonnew.com/axr-400ml6-680kw-4160v-60hz.html.

[114] "Wärtsilä 20 — diesel engine". Product page, Wärtsilä, Accessed: 01 Mar. 2024. [Online]. Available: https://www.wartsila.com/marine/products/engines-and-generating-sets/diesel-engines/wartsila-20.

[115] H. Wang, N. L. Trivyza, F. Mylonopoulos and E. Boulougouris, "Comparison of decarbonisation solutions for shipping: Hydrogen, ammonia and batteries", *Proceedings of the 14th International Marine Design Conference (IMDC)*, 2022.

[116] F. Mylonopoulos, A. Coraddu and H. Polinder, "A holistic framework for optimal ship energy system design, including operational requirements, lifetime cost, and vessel stability", *Energy Conversion and Management: X*, vol. 30, 2026, Art. no. 101685. DOI: 10.1016/j.ecmx.2026.101685.

[117] PowerCell Group. "Marine hydrogen fuel cell solutions", Accessed: 21 Jun. 2023. [Online]. Available: https://powercellgroup.com/segments/marine/.

[118] M. Banaei, F. Ghanami, M. H. Khooban and J. Boudjadar, "Cost-effective control of Roll-on/Roll-off emission-free ships", *in Proceedings of the 25th International Conference on Methods and Models in Automation and Robotics (MMAR)*, Międzyzdroje, Poland, Aug. 2021. DOI: 10.1109/MMAR49549.2021.9528473.

[119] U. Ehret and M. Neuper, "Applying the ramer-douglas-peucker algorithm to compress and characterize time-series and spatial fields of precipitation", *Geophysical Research Abstracts*, vol. 16, 2014.

[120] Bureau Veritas. "Bureau veritas unveils rules for hydrogen-fuelled ships", Marine & Offshore, Accessed: 10 Feb. 2025. [Online]. Available: https://marine-offshore.bureauveritas.com/newsroom/bureau-veritas-unveils-rules-hydrogen-fuelled-ships.

[121] DNV, *Handbook for Hydrogen Fueled Vessels, MarHySafe JDP Phase 1*, 1 ed. Høvik, Norway: DNV, 2021.

[122] J. W. Pratt and L. E. Klebanoff, "Optimization of zero emission hydrogen fuel cell ferry design, with comparisons to the sf–breeze", Sandia National Laboratories, Tech. Rep., Jan. 2018.

[123] T. K. Drube, J. M. Gerlach, T. S. Leach, B. Vogel and L. E. Klebanoff, "Exploring variations in the weight, size and shape of liquid hydrogen tanks for zero-emission fuel-cell vessels", *International Journal of Hydrogen Energy*, vol. 80, pp. 1441–1465, 2024. DOI: 10.1016/J.IJHYDENE.2024.06.420.

[124] L. E. Klebanoff, T. K. Drube, J. M. Gerlach and T. S. Leach, "Exploring liquid hydrogen tank technology for zero-emission fuel cell vessels", Sandia National Laboratories, Livermore, CA, Tech. Rep. SAND2024-01678, Feb. 2024, 100 p. [Online]. Available: https://www.maritime.dot.gov/innovation/meta/exploring-liquid-hydrogen-tank-technology-zero-emission-fuel-cell-vessels.

[125] S.-T. Yeh, "Using trapezoidal rule for the area under a curve calculation", *in Proceedings of the 27th Annual SAS Users Group International Conference (SUGI 27)*, Paper 229-27, SAS Institute, Orlando, FL, 14 Apr. 2002, pp. 1–5. [Online]. Available: https://support.sas.com/resources/papers/proceedings/proceedings/sugi27/p229-27.pdf.

[126] Kawasaki Heavy Industries Ltd. "Kawasaki proves excellent thermal-insulation performance for liquefied hydrogen storage tanks", Accessed: 13 Feb. 2025. [Online]. Available: https://global.kawasaki.com/en/corp/newsroom/news/detail/?f=20231211_8742.

[127] Metrohm. "Fuel cells part 1 – what is a fuel cell?", Accessed: 13 Feb. 2025. [Online]. Available: https://www.metrohm.com/en_nl/applications/application-notes/autolab-applikationen-anautolab/an-fc-001.html.

[128] K. Bestuzheva, A. Chmiela, B. Müller, F. Serrano, S. Vigerske and F. Wegscheider, "Global optimization of mixed-integer nonlinear programs with scip 8", *Journal of Global Optimization*, vol. 91, pp. 287–310, 2023. DOI: 10.1007/s10898-023-01345-1.

[129] ABB. "Traction inverters", Accessed: 13 Feb. 2025. [Online]. Available: https://new.abb.com/electric-drivetrains/traction-inverters.

[130] H. M. Bye, "Investigation of a 200 kw SiC-based IBC for high-speed hydrogen ferries", M.S. thesis, Norwegian University of Science and Technology (NTNU), Trondheim, Norway, 2019. [Online]. Available: https://ntnuopen.ntnu.no/ntnu-xmlui/handle/11250/2625864?locale-attribute=no.

[131] ABB. "Onboard dc grid™ marine and ports – electric solutions", Accessed: 13 Feb. 2025. [Online]. Available: https://new.abb.com/marine/systems-and-solutions/power-generation-and-distribution/onboard-dc-grid.

[132] ABB. "Technical catalog: High voltage induction motors", Accessed: 13 Feb. 2025. [Online]. Available: https://search.abb.com/library/Download.aspx?DocumentID=9AKK103508&LanguageCode=en&DocumentPartId=&Action=Launch.

[133] ABB. "ACS880 drive modules", Accessed: 13 Feb. 2025. [Online]. Available: https://www.abb.com/global/en/product/drives/low-voltage-ac-drives/industrial-drives/acs880-drive-modules.

[134] Hitachi Nico Transmission Co. "Marine gear capacity tables", Accessed: 13 Feb. 2025. [Online]. Available: https://www.hitachi-nico.jp/nico_image/catalog/pdf/h_02.pdf.

[135] W. Shi, D. Stapersma and H. T. Grimmelius, "Analysis of energy conversion in ship propulsion system in off-design operation conditions", *WIT Transactions on Ecology and the Environment*, vol. 121, pp. 1–12, 2009. [Online]. Available: https://www.witpress.com/Secure/elibrary/papers/ESUS09/ESUS09041FU1.pdf.

[136] S. Brouzas, M. Zadeh and B. Lagemann, "Essentials of hydrogen storage and power systems for green shipping", *International Journal of Hydrogen Energy*, vol. 100, pp. 1543–1560, 2025. DOI: 10.1016/j.ijhydene.2024.12.253.

[137] F. Mylonopoulos, A. Coraddu, H. Polinder and A. Orlandi, "Design and lifetime cost optimization of ship energy systems including weather-driven speed profile variability", *Ocean Engineering*, vol. 356, 2026, Art. no. 125220. DOI: 10.1016/j.oceaneng.2026.125220.

[138] P. Balcombe, J. Brierley, C. Lewis, L. Skatvedt, J. Speirs, A. Hawkes and I. Staffell, "How to decarbonise international shipping: Options for fuels, technologies and policies", *Energy Conversion and Management*, vol. 182, pp. 72–88, 2019. DOI: 10.1016/j.enconman.2018.12.080.

[139] E. Esmailian, S. Steen and K. Koushan, "Ship design for real sea states under uncertainty", *Ocean Engineering*, vol. 266, 2022, Art. no. 113127. DOI: 10.1016/j.oceaneng.2022.113127.

[140] X. Lang and W. Mao, "A practical speed loss prediction model at arbitrary wave heading for ship voyage optimization", *Journal of Marine Science and Application*, vol. 20, pp. 410–425, 2021. DOI: 10.1007/s11804-021-00224-z.

[141] International Organization for Standardization, *ISO 15016:2015 — ships and marine technology: Guidelines for the assessment of speed and power performance by analysis of speed trial data*, Geneva, Switzerland, 2015.

[142] D. W. Seo and J. Oh, "Uncertainty analysis of speed–power performance based on measured raw data in sea trials", *International Journal of Naval Architecture and Ocean Engineering*, vol. 13, pp. 396–404, 2021. DOI: 10.1016/j.ijnaoe.2021.04.001.

[143] A. Coraddu, M. Figari and S. Savio, "Numerical investigation on ship energy efficiency by monte carlo simulation", *Proceedings of the Institution of Mechanical Engineers Part M: Journal of Engineering for the Maritime Environment*, vol. 228, no. 3, pp. 220–234, 2014. DOI: 10.1177/1475090214524184.

[144] A. Fan, X. Yan, R. Bucknall, Q. Yin, S. Ji, Y. Liu, R. Song and X. Chen, "A novel ship energy efficiency model considering random environmental parameters", *Journal of Marine Engineering and Technology*, vol. 19, no. 4, pp. 215–228, 2020. DOI: 10.1080/20464177.2018.1546644.

[145] A. Farkas, N. Degiuli, I. Martić and C. G. Grlj, "Is slow steaming a viable option to meet the novel energy efficiency requirements for containerships?", *Journal of Cleaner Production*, vol. 374, 2022, Art. no. 133915. DOI: 10.1016/j.jclepro.2022.133915.

[146] N. Degiuli, I. Martić, A. Farkas and I. Gospić, "The impact of slow steaming on reducing CO_2 emissions in the mediterranean sea", *Energy Reports*, vol. 7, pp. 8131–8141, 2021. DOI: 10.1016/j.egyr.2021.02.046.

[147] N. Degiuli, I. Martić and C. G. Grlj, "Slow steaming as a sustainable measure for low-carbon maritime transport", *Sustainability*, vol. 16, no. 24, 2024, Art. no. 11169. DOI: 10.3390/su162411169.

[148] V. Pelić, O. Bukovac, R. Radonja and N. Degiuli, "The impact of slow steaming on fuel consumption and CO_2 emissions of a container ship", *Journal of Marine Science and Engineering*, vol. 11, no. 3, 2023, Art. no. 675. DOI: 10.3390/jmse11030675.

[149] T. P. Zis, H. N. Psaraftis and L. Ding, "Ship weather routing: A taxonomy and survey", *Ocean Engineering*, vol. 213, 2020, Art. no. 107697. DOI: 10.1016/j.oceaneng.2020.107697.

[150] A. Kytariolou and N. Themelis, "Ship routing optimisation based on forecasted weather data and considering safety criteria", *Journal of Navigation*, vol. 75, no. 6, pp. 1310–1331, 2022. DOI: 10.1017/S0373463322000613.

[151] T. Fabbri and R. Vicen-Bueno, "Weather-routing system based on metoc navigation risk assessment", *Journal of Marine Science and Engineering*, vol. 7, no. 5, 2019, Art. no. 127. DOI: 10.3390/jmse7050127.

[152] L. D. Gracia, N. Osawa, H. Tamaru and T. Fukasawa, "A comparative study on fatigue damage using a wave load sequence model", *KnE Engineering*, vol. 3, no. 1, pp. 160–170, 2018. DOI: 10.18502/keg.v3i1.1422.

[153] S. Pennino, S. Gaglione, A. Innac, V. Piscopo and A. Scamardella, "Development of a new ship adaptive weather routing model based on seakeeping analysis and optimization", *Journal of Marine Science and Engineering*, vol. 8, no. 4, 2020, Art. no. 270. DOI: 10.3390/JMSE8040270.

[154] Copernicus Climate Change Service. "ERA5 hourly data on single levels from 1940 to present", Accessed: 15 May 2025. [Online]. Available: https://doi.org/10.24381/cds.adbb2d47.

[155] International Maritime Organization (IMO), "Revised guidance to the master for avoiding dangerous situations in adverse weather and sea conditions", International Maritime Organization, London, Tech. Rep., 2007. Accessed: 15 May 2025. [Online]. Available: https://wwwcdn.imo.org/localresources/en/OurWork/Safety/Documents/Stability/MSC.1-CIRC.1228.pdf.

[156] A. Papanikolaou, *Ship Design: Methodologies of Preliminary Design*. Dordrecht: Springer, 2014. DOI: 10.1007/978-94-017-8751-2.

[157] P. Krata and W. Wawrzyński, "Prediction of the natural frequency of ship's roll with regard to various models of roll damping", *Journal of KONES*, vol. 23, no. 3, pp. 289–296, 2016. DOI: 10.5604/12314005.1216499.

[158] International Towing Tank Conference (ITTC), "ITTC recommended procedures and guidelines: Analysis of speed/power trial data, Procedure 7.5-04-01-01.2", International Towing Tank Conference (ITTC), Nantes, France, Tech. Rep., 2005. [Online]. Available: https://ittc.info/media/1363/75-04-01-012.pdf.

[159] A. Aijjou, L. Bahatti and A. Raihani, "Wind energy for shipboard electric power needs", *International Journal of Advanced Trends in Computer Science and Engineering*, vol. 9, no. 1.5, pp. 168–177, 2020. DOI: 10.30534/ijatcse/2020/2491.52020.

[160] International Maritime Organization (IMO), "Guidelines for determining minimum propulsion power to maintain the manoeuvrability of ships in adverse conditions, (MEPC.1/Circ.850/Rev.3)", International Maritime Organization, London, Tech. Rep., 2021. [Online]. Available: https://www.classnk.or.jp/hp/pdf/activities/statutory/eedi/13_MEPC.1-CIRC.850-Rev.3.pdf.

[161] M. Mittendorf, U. D. Nielsen, H. B. Bingham and S. Liu, "Towards the uncertainty quantification of semi-empirical formulas applied to the added resistance of ships in waves of arbitrary heading", *Ocean Engineering*, vol. 251, 2022, Art. no. 111040. DOI: 10.1016/j.oceaneng.2022.111040.

[162] J. Wang, S. Bielicki, F. Kluwe, H. Orihara, G. Xin, K. Kume, S. Oh, S. Liu and P. Feng, "Validation study on a new semi-empirical method for the prediction of added resistance in waves of arbitrary heading in analyzing ship speed trial results", *Ocean Engineering*, vol. 240, 2021, Art. no. 109959. DOI: 10.1016/j.oceaneng.2021.109959.

[163] Y. R. Kim, E. Esmailian and S. Steen, "A meta-model for added resistance in waves", *Ocean Engineering*, vol. 266, 2022, Art. no. 112749. DOI: 10.1016/j.oceaneng.2022.112749.

[164] D. M. Park, J. H. Lee, Y. W. Jung, J. Lee, Y. Kim and F. Gerhardt, "Experimental and numerical studies on added resistance of ship in oblique sea conditions", *Ocean Engineering*, vol. 186, 2019, Art. no. 106070. DOI: 10.1016/j.oceaneng.2019.05.052.

[165] X. Liu, Z. Yan and J. Wu, "Optimal coordinated operation of a multi-energy community considering interactions between energy storage and conversion devices", *Applied Energy*, vol. 248, pp. 256–273, 2019. DOI: 10.1016/j.apenergy.2019.04.106.

[166] N. Vahabzad, B. Mohammadi-Ivatloo and A. Anvari-Moghaddam, "Modeling hybrid energy systems for marine applications: Hybrid electric ships", *Hybrid Technologies for Power Generation: Hybrid Energy Systems*, M. Lo Faro, O. Barbera and G. Giacoppo, Eds., Academic Press, 2022, pp. 419–437. DOI: 10.1016/B978-0-12-823793-9.00012-7.

[167] D. Zhang, Y. Song, J. Gao, Z. Shen, L. Li and A. Yao, "Research on ship engine fuel consumption prediction algorithm based on adaptive optimization generative network", *Journal of Marine Science and Engineering*, vol. 13, no. 6, 2025, Art. no. 1140. DOI: 10.3390/jmse13061140.

[168] T. Kopka, F. Mylonopoulos, A. Coraddu and H. Polinder, "Decentralized power sharing with frequency decoupling for a fuel cell–battery DC shipboard power system", *Proceedings of the Modelling and Optimisation of Ship Energy Systems (MOSES)*, 2023. DOI: 10.59490/moses.2023.670.

PUBLICATIONS

Journal articles

• *As part of this thesis:*

(1). F. Mylonopoulos, H. Polinder and A. Coraddu, "A comprehensive review of modeling and optimization methods for ship energy systems", *IEEE Access*, vol. 11, pp. 32697 –32 707, 2023. DOI: 10.1109/ACCESS.2023.3263719

(2). F. Mylonopoulos, S. Durgaprasad, A. Coraddu and H. Polinder, "Lifetime design, operation, and cost analysis for the energy system of a retrofitted cargo vessel with fuel cells and batteries", *International Journal of Hydrogen Energy*, vol. 91, pp. 1262–1273, 2024. DOI: 10.1016/J.IJHYDENE.2024.10.235

(3). F. Mylonopoulos, A. Coraddu and H. Polinder, "A holistic framework for optimal ship energy system design, including operational requirements, lifetime cost, and vessel stability", *Energy Conversion and Management: X*, vol. 30, 2026, Art. no. 101685. DOI: 10.1016/j.ecmx.2026.101685

(4). F. Mylonopoulos, A. Coraddu, H. Polinder and A. Orlandi, "Design and lifetime cost optimization of ship energy systems including weather-driven speed profile variability", *Ocean Engineering*, vol. 356, 2026, Art. no. 125220. DOI: 10.1016/j.oceaneng.2026.125220

Conferences attended with papers

(5). F. Mylonopoulos, T. Kopka, A. Coraddu and H. Polinder, "Model-based parametric study for comparison of system configurations and control of a hydrogen hybrid cargo vessel", *in Proceedings of the Modelling and Optimisation of Ship Energy Systems (MOSES)*, 2023. DOI: 10.59490/moses.2023.671

Other studies

(6). T. Kopka, F. Mylonopoulos, A. Coraddu and H. Polinder, "Decentralized power sharing with frequency decoupling for a fuel cell–battery DC shipboard power system", *Proceedings of the Modelling and Optimisation of Ship Energy Systems (MOSES)*, 2023. DOI: 10.59490/moses.2023.670

ACKNOWLEDGMENTS

I would like to thank my supervisors Henk and Andrea, for their guidance, constructive feedack, and continuous support throughout this PhD. Their expertise, insights, and availability were invaluable in shaping both the direction and quality of this work.

I would also like to thank my colleagues for the discussions, collaboration, and support during these four years. I am deeply grateful to my friends and family for their constant encouragement, understanding, and support throughout this journey.

Finally, I would like to sincerely thank the project partners of SH2IPDRIVE for the valuable discussions and collaboration. In particular, I thank Van Dam Shipping and Jurrien Baretta for providing the data required for the case study vessel.

Foivos Panagiotis Mylonopoulos
Delft, June 2026

CURRICULUM VITAE

Foivos Panagiotis Mylonopoulos was born in Athens, Greece in 1999. He completed his secondary education in Athens in June 2017. He received the MEng degree in Naval Architecture and Marine Engineering from the University of Strathclyde in Glasgow, Scotland in May 2022, graduating with distinction. During his studies, he was awarded the Archibald Denny Prize and received third place in the 2021 RINA – BAE Systems-Strathclyde University 4th Year Student Project Presentations.

In June 2022, he commenced his doctoral research under the supervision of Dr Andrea Coraddu and Dr Henk Polinder. The outcomes of this research are presented in this thesis.

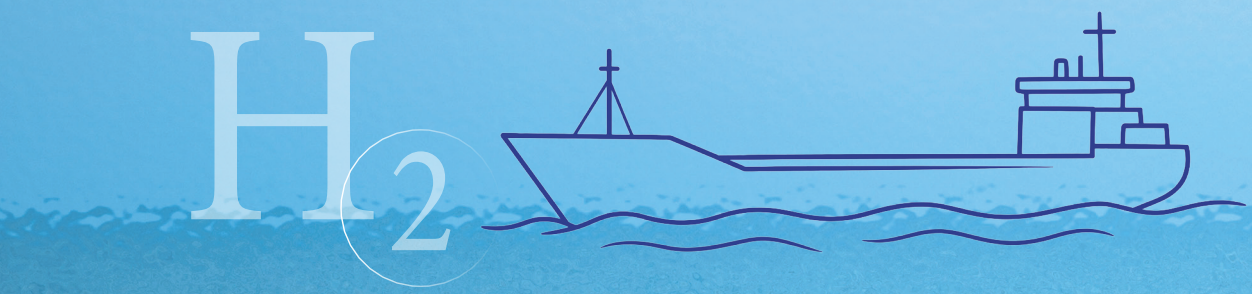
H2